NON-NASA
7N-90
209855
85P.

Effects of main-sequence mass loss on stellar and galactic chemical evolution

by

Joyce Ann Guzik

A Dissertation Submitted to the
Graduate Faculty in Partial Fulfillment of the
Requirements for the Degree of
DOCTOR OF PHILOSOPHY

Department: Physics
Major: Astrophysics

Approved:

(NASA-CR-185325) EFFECTS OF MAIN-SEQUENCE MASS LOSS ON STELLAR AND GALACTIC CHEMICAL EVOLUTION Ph.D. Thesis (Iowa State Univ. of Science and Technology) 85 p N90-70106
Unclas
00/90 0209855

In Charge of Major Work

For the Major Department

For the Graduate College

Iowa State University
Ames, Iowa

1988

Effects of main-sequence mass loss on stellar and galactic chemical evolution

Joyce Ann Guzik

Under the supervision of Lee Anne Willson and Curtis Struck-Marcell
From the Department of Physics
Iowa State University

Iowa State faculty members L. A. Willson, G. H. Bowen and C. Struck-Marcell have proposed that stars of 1 to 3 solar masses may experience mass loss of evolutionary significance during the early part of their lives on the main sequence. The suggested mass-loss mechanism is pulsation, facilitated by rapid rotation. Initial mass-loss rates may be as large as several times 10^{-9} $M_\odot$/yr, diminishing during the first several times 10^8 years. The goal of this dissertation is to test the main-sequence mass loss hypothesis via a comparison of theoretical implications to observations. Three specific areas are addressed: Solar models, cluster HR diagrams, and galactic chemical evolution.

Mass-losing solar models were evolved that match the solar luminosity and radius at the present solar age. The most extreme viable models have initial mass about 2.0 $M_\odot$, and exponentially decreasing mass-loss rates with timescales 2-3 x 10^8 years. Compared to a standard constant-mass model, these models require a reduced initial ^{4}He abundance and increased mixing length, have deeper envelope convection zones, higher ^{8}B neutrino fluxes, and shorter main-sequence lifetimes. Early exposure of additional material to higher interior temperatures increases the final surface ^{3}He abundance, completely destroys Li and Be, and decreases the surface C/N ratio during and after first dredge-up.

Evolution calculations incorporating main-sequence mass loss were completed for a grid of models with solar metallicity, initial masses 1.25 to 2.0 $M_\odot$, and exponentially decreasing mass-loss rates with timescales 0.2 to 2.0 Gyr. Comparisons between cluster HR diagrams synthesized with these models and those of young clusters confirm the potential for

the main-sequence mass loss hypothesis to explain features such as spreads or bifurcations in the upper main sequence, blue stragglers, anomalous giants, and poor fits of main-sequence turnoffs by standard isochrones.

A simple closed model of galactic chemical evolution was employed to test the effects of main-sequence mass loss on the distribution of F and G dwarfs. Stars of initial mass between 3.0 $M_\odot$ and a metallicity-dependent lower mass are assumed to undergo mass loss. The models produce a 30 to 60% increase in the ratio of dwarfs to dwarfs plus remnants, a depletion of early-F dwarfs and a large enhancement in the number of late-F dwarfs remaining on the main sequence at the present disk age, relative to models without mass loss. The ratio of main-sequence stars to stellar remnants and the age distribution of white dwarfs may prove valuable in distinguishing between proposed explanations for the observed bimodality of the present-day stellar mass function.

TABLE OF CONTENTS

	Page
PREFACE	1
I. INTRODUCTION	2
A. Overview	2
B. Historical Background	6
II. SOLAR MODELS	11
A. Introduction	11
B. Modeling	12
C. Discussion	30
1. ^{4}He	30
2. ^{3}He	32
3. Lithium, beryllium and boron	38
4. Carbon and nitrogen	42
5. Neutrino fluxes	47
6. Convection zones	49
D. Conclusions	50
E. Topics for Further Investigation	51
III. CLUSTER HR DIAGRAMS	52
A. Evolution Modeling	52
B. Cluster Synthesis Procedures	54
C. Discussion of Synthesized Clusters	66
D. Comparison to Observed Clusters	78
1. Group I	80
a. The Hyades	80
b. Praesepe	86
c. M39	86
d. NGC 2567	87

	Page
2. Group II	87
a. NGC 5822	87
b. NGC 2360	91
c. NGC 6192	92
3. Group III	93
a. NGC 7789	93
b. NGC 752	100
c. NGC 3680	100
4. Group IV	101
a. NGC 2158	101
b. NGC 2204	106
c. NGC 2420	106
d. NGC 2506	106
e. Discussion	106
5. Group V	107
a. Melotte 66	107
b. M67	112
c. NGC 188	114
D. Conclusions	115
E. Topics for Further Investigation	118
IV. GALACTIC CHEMICAL EVOLUTION	120
A. Introduction	120
B. Modeling	122
C. Results	130
D. Discussion	146
E. Conclusions	150
F. Topics for Further Investigation	152

Page

V. REFERENCES 153
VI. ACKNOWLEDGEMENTS 162

PREFACE

The problem of stellar evolution unquestionably numbers as one of the fundamental problems in astronomy . . . . This problem by its very nature is complex. . . after all, just by looking at stars it is not possible at once to say how they are situated in genetic relationship. In general, this problem turned out to be very difficult, and after a few decades hasn't quite yielded to solution. Moreover, until comparatively recently, the efforts of researchers frequently were directed in completely wrong directions. For example, the very presence of the main sequence on the Hertzsprung-Russell diagram "inspired" many naive researchers to imagine that stars evolved along this diagram from hot white giants to red dwarfs. But when the mass-luminosity relation was discovered, according to which the masses of stars situated along the main sequence should continuously decrease, the mentioning researchers stubbornly considered that the evolution of stars in the indicated direction should be accompanied by continuous and furthermore highly significant loss of their mass. . . . All of this turned out to be erroneous.

–I. K. Shklovskii, in *Stars: Their Birth, Life and Death*, 1970
(translated from Russian by J. A. Guzik)

It is to be pointed out that all these arguments are only indirect ones and not all of them have the necessary precision. Nevertheless, direct arguments against the corpuscular theory of stellar evolution apparently do not exist at all.

–V. G. Fesenkov and G. M. Idlis, in *The Hertzsprung Russell Diagram*, 1958.

I. INTRODUCTION

A. Overview

Iowa State faculty members L. A. Willson, G. H. Bowen and C. Struck-Marcell (1987, hereafter WBS) have advanced the hypothesis that stars arriving on the main sequence at its intersection with the Cepheid pulsation instability strip may lose a substantial portion of their mass during the early part of their lives on the main sequence. The affected stars include those of spectral types A through early G, with initial masses of about 1 to 3 solar masses. The mass loss is pulsation-driven, and facilitated by rapid rotation. Mass-loss rates may be as large as several times 10^{-9} solar masses per year, diminishing over timescales of the order of several times 10^8 years. Mass loss ceases as envelope convection zones develop, channeling mechanical energy away from pulsation, and as magnetic fields develop, transferring angular momentum to the outflow and braking rotation. In this manner a star of initial mass 2 to 3 $M_\odot$ may evolve "down" the main sequence toward a final mass of ~1 to 1.4 $M_\odot$, to become a star of spectral type mid-F to early-G.

Willson, Bowen and Struck-Marcell began investigating the feasibility of such mass loss by checking for predictions or implications that are in obvious conflict with observations. While direct evidence in the form of observed mass loss at the proposed rate from main-sequence stars, and/or theoretical modeling establishing a mechanism for pulsation/rotation-driven winds from these stars is lacking at present, they have found no consequences that *a priori* rule out the hypothesis. A significant impetus for continued investigation has been the potential impact of these ideas on a number of problems that have eluded explanation in the framework of standard stellar evolution theory. WBS and collaborators have concurrently been working out the details of alternative explanations for some of these problems in the context of the main-sequence mass loss hypothesis.

Mass loss by A to early-F stars at rates large enough to affect evolution are quite plausible, given energy requirements and conditions in these stars (WBS 1987). The rotation velocities of the majority of these stars are already a substantial fraction of the velocity at which the centripetal force balances the gravitational force at the stellar surface. The energy required to remove material from the star at escape velocity, without the assistance of rotation, is only a few percent of the total luminous energy flux. The δ Scuti pulsating variables are found among main-sequence stars of mid-A to mid-F spectral type (Hoffmeister, Richter and Wenzel 1985). Theoretical calculations suggest that strong damping mechanisms (Stellingwerf 1979) and/or partitioning the mechanical energy between a number of destructively interfering radial/nonradial modes (Dziembowski 1979) may be required to prevent large amplitude pulsations among A and F main-sequence stars. The simultaneous presence of several pulsation modes may improve the efficiency of converting mechanical energy to kinetic and potential energy required to drive mass loss.

Mass loss from main-sequence A-F stars at the proposed rate has not been observed to date, or at least not recognized as mass loss from main-sequence objects. Such mass loss is difficult to detect, for several reasons (WBS 1987). The column density and the emission measure of material around a star can be derived from observations and used to estimate mass-loss rates; these quantities are functions of $\dot{M}/v_{wind}$ and $(\dot{M}/v_{wind})^2$, respectively. Since the surface gravity of main-sequence stars is relatively high, the wind velocity is expected to be high. Only mass-loss rates in excess of 10^{-8} $M_\odot$/yr are detectable by these methods. Second, the phase of rapid mass loss, with rates in excess of 10^{-9} $M_\odot$/yr, is expected to be short-lived. Main-sequence stars undergoing such mass loss may still be imbedded in the nebulosity of a region of star formation. Third, early estimates indicated that the wind temperature may be quite high, 10^5 to 10^6 K; at this temperature, spectral line signatures in the form of P Cygni profiles are scarce in the observable visual and ultraviolet regions of the spectrum. Fourth, if the

mass flux is sufficiently high, and the wind temperature sufficiently low, the mass loss may be detectable, but the atmospheric density structure of the star may lead to its classification as a pre-main sequence object. For example, the Herbig Ae stars, classified as pre-main sequence objects, exhibit P Cygni line profiles indicative of mass loss; however, the Herbig Ae star AB Aur has mass, luminosity, and radius characteristic of a main-sequence star.

Modeling the proposed mass-loss mechanism may prove exceptionally difficult, requiring perhaps decades of effort and the use of new generations of supercomputers. The pulsation is likely to be non-radial, and the winds non-isotropic; the role of differential rotation in enhancing mass loss and selecting pulsation modes, and the roles of convection and magnetic fields in transferring angular momentum, braking rotation, and redistributing mechanical energy will require investigation. It quickly becomes evident that one-dimensional plane-parallel models are completely inadequate; two- or three-dimensional hydrodynamic models incorporating radiative transfer, a detailed theory of convection, effects of magnetic fields, and non-radial, non-adiabatic pulsation theory may be necessary. Some relevant theoretical work has been begun, mainly for application to non-radially pulsating B stars, for example by Osaki (1974), Ando (1981), and Lee and Saio (1986) in investigating the roles of rotation and convection in producing pulsation instabilities.

The hypothesis has widespread implications for stellar evolution theory. For example, the main-sequence lifetime of a star located at the apparent main-sequence turnoff becomes an invalid indicator of cluster age, as stars situated at the apparent turnoff may have evolved down the main sequence; hence clusters may actually be younger than they appear. Globular cluster ages (estimated from the main-sequence turnoff to be as large as 18 Gyr) may thus be reconciled with ages of the galaxy and universe determined from other methods, such as white dwarf cooling rates, the Hubble constant and nuclear cosmochronology, which all arrive at an age $\leq$ 12 Gyr (WBS 1987). The hypothesis also

explains the relative paucity of clusters with main-sequence turnoffs at spectral types A-early F (WBS 1987; Willson and Guzik 1988). "Blue stragglers", apparently normal stars that are situated on the main sequence above the turnoff in many clusters may be explained as stars that have lost mass slowly or not at all due to slow rotation and/or lack of pulsation (WBS 1987; Willson and Guzik 1988). The hypothesis may account for gaps in the A-F star range and bumps at ~3 $M_\odot$ and ~1.4 $M_\odot$ in stellar distributions (WBS 1987; Willson, Bowen and Titus 1988; Guzik and Struck-Marcell 1988). Implications for galactic chemical evolution include changes in timescales of stellar returns from intermediate-mass stars, differences in the expected metallicity and spectral-type distributions of F and G main-sequence stars, and decreased production of stellar remnants (Guzik and Struck-Marcell 1988). Surface abundances and returns of light elements, including isotopes of He, Li, Be, B, C and N, are substantially altered as material is processed in the interior during the high mass/luminosity phase, then exposed by mass loss or dredge up (WBS 1987; Guzik, Willson and Brunish 1987). Such changes affect the interpretation of observed stellar and interstellar abundances, and consequently the derived primordial abundances, thereby having an impact on cosmological models. Finally, if the Sun itself experienced an epoch of early main-sequence mass loss, solar evolution calculations (Guzik, Willson and Brunish 1987) and models of solar system formation (Bowen 1988) require revision.

The objective of my dissertation work is to test the main-sequence mass loss hypothesis, via a theoretical exploration of some implications that can be compared to observations. Section II describes the evolution of solar models including an epoch of early main-sequence mass loss, and resulting differences in interior structure and composition compared to standard constant-mass models. Section III presents the evolutionary tracks of a series of stellar models with a variety of initial masses and mass-loss timescales. Cluster HR diagrams are synthesized for several cluster ages, and qualitatively compared with

observed clusters. Section IV discusses results of simple "closed box" models of galactic chemical evolution incorporating main-sequence mass loss, quantifying predictions for the metallicity and spectral-type distributions of F and G stars, and the proportion of stellar remnants.

B. Historical Background

The earliest interpretation of the main sequence was as an evolutionary sequence, with stars evolving from hot O-B giants to cool M dwarfs as gravitational contraction supplied the luminosity (Russell 1914). With the discovery of the mass-luminosity relation for main-sequence stars (Eddington 1924), retaining this interpretation required that stars lose mass during their evolution. Proposals for the method of mass loss included annihilation of matter, necessarily in excess of the small amount of mass converted to energy when 4 H nuclei fuse to become a He nucleus (Eddington 1927); and removal of material by "corpuscular emission", e.g., in a stellar wind (Fesenkov 1949). Soon afterward, it was discovered that the conversion of H into He via the pp and CNO cycles could provide the luminosity of main-sequence stars; this energy source allowed stellar lifetimes compatible with the geologic age of the Earth and the Hubble age of universe. The concept of the main sequence as evolutionary was gradually abandoned in favor of star formation with a distribution of initial masses (Struve and Zebergs 1962).

The possibility of restricted, but evolutionarily significant main-sequence mass loss via "corpuscular emission" was advocated as recently as the late 1950s by Soviet astronomers A. G. Masevich and P. P. Parenago of Sternberg Astronomical Institute in Moscow, and V. G. Fesenkov and G. M. Idlis of the Astrophysical Institute of Alma Ata, and was debated in the astrophysical literature until the mid-1960s. In contrast to the WBS theory, stars more massive than 2-3 $M_\odot$ evolve "down" the main sequence, losing mass with rates proportional to their luminosity, and evolution proceeds with complete mixing, i.e. homogeneous composition.

with complete mixing, i.e. homogeneous composition.

Masevich (1958) cites a number of reasons for preferring homogeneous evolution. High-mass stars evolving inhomogeneously rapidly exhaust hydrogen in their convective cores. Subsequent evolution cannot be calculated analytically, since the stars do not remain in hydrostatic equilibrium; on the other hand, useful insight could be gained through studying completely-mixed stars. Furthermore, several researchers concluded from both theory and observation that mean molecular weight (μ) increases continuously with decreasing stellar mass. Homogeneous evolution with mass loss would naturally produce this result. Severnyi (1954) even derived a semi-empirical relation, assuming CN-cycle reactions are the energy source: $\mu/\mu_\odot \sim (M/M_\odot)^{-0.225}$. However, Stothers (1966) noted that Severnyi's relation was based upon abundance determinations from only three stars; more recent observations indicated that μ is more likely constant or even increasing with increasing stellar mass. Masevich (1958) also claimed that a sequence of inhomogeneous (not completely-mixed) stars of the same age with varying convective core sizes fails to reproduce the high-mass end of the empirical main sequence, although she allowed that the discrepancy may be due to uncertainties in bolometric corrections, or neglect of radiation pressure in stellar interior calculations. The main-sequence lifetimes of massive stars evolving inhomogeneously at constant mass are very short; the fact that they exist today implies that they are produced continuously. The supernovae rate cannot account for the deaths of these massive stars. Alternatively, the stars could be transformed to white dwarfs via mass loss during the brief red giant phase; however, Masevich concluded that the required mass-loss rates were unacceptably high. The combination of mass loss and complete mixing greatly prolongs the main-sequence lifetime of massive stars, reducing the number that have had time to evolve off of the main sequence over the lifetime of the Galaxy. Masevich (1958) believed that complete mixing was at least plausible, given the substantial convective cores and rapid rotation rates of

high-mass stars.

For mass loss to significantly alter evolution, the mass-loss timescale must be comparable to the nuclear-burning timescale. A simple parametrization of the mass-loss rate was first proposed by Fesenkov (1949): $dM/dt = -kL$, with k as a constant of order $1/\alpha$, where α is the thermonuclear energy released by conversion of 1 g of H into He, 6×10^{18} erg/g. The proportionality constant k can be derived more rigorously, assuming homogeneous evolution (Masevich 1958). The rate of H depletion in a completely mixed star is given by

$$\frac{d(XM)}{dt} = M\frac{dX}{dt} + X\frac{dM}{dt} = -\frac{L}{\alpha} - qX$$

where q is the rate of mass loss via stellar wind. The total rate of mass loss is

$$\frac{dM}{dt} = -q - \frac{L}{c^2}$$

where L/c^2 is the mass excess converted to energy in nuclear reactions. Neglecting L/c^2 compared to q, and substituting into the first expression,

$$\frac{dX}{dt} = -\frac{L}{\alpha}M$$

Then

$$\frac{dM}{dt} = \frac{dM}{dX}\frac{dX}{dt} = -\frac{1}{\alpha}\frac{d(\ln M)}{dX}L$$

which identifies k:

$$k = \frac{1}{\alpha}\frac{d(\ln M)}{dX}$$

Since X varies slowly during main-sequence evolution, k=constant is an acceptable approximation. For $k = 10^{-18}$ g/erg, and $L \sim M^4$,

$dM/dt = 6.3 \times 10^{-11} (M/M_\odot)^4\ M_\odot/yr$. For a 20 $M_\odot$ O9 star, $dM/dt \sim 10^{-5}\ M_\odot/yr$; for a 10 $M_\odot$ B2 star, $dM/dt \sim 6 \times 10^{-7}\ M_\odot/yr$; for a 2 $M_\odot$ A1 star, $dM/dt \sim 10^{-9}\ M_\odot/yr$. Note that the latter is of the same order of magnitude as the estimated initial mass-loss rate of a 2 $M_\odot$ star in the WBS theory.

Roberts (Henyey 1960) and Usher (1963) attempted to test the Soviet hypothesis by theoretically evolving luminosity functions using the Fesenkov mass-loss rate; they found that the predicted pileup of stars at late-B spectral type is not observed in Galactic clusters; however, the uncertainties in the initial luminosity function and the paucity of clusters with the earliest member at late B spectral type make this test inconclusive. Stothers (1966), after evolving luminosity functions with a generalized Fesenkov law $dM/dt = -kL^n$, concluded that "cluster luminosity functions *per se* may not be used to decide for or against the theory of homogeneous evolution with mass loss, since any observed function may be reasonably well reproduced on this theory. Moreover, it does not seem possible to determine k and the age uniquely, by using such functions. On the other hand, the theory of inhomogeneous evolution without mass loss makes definite predictions of the luminosity function. Good evidence exists that this theory predicts correctly." Weymann, in his 1963 review on stellar mass loss, stated that most recearchers were in agreement that constant-mass evolution with no mixing reproduced the observed main sequence acceptably well, given the uncertainties in bolometric corrections.

To credit Masevich and colleagues, it is now known that O-B main-sequence stars do lose mass on the main sequence via radiatively-driven winds (Abbott 1982), with mass-loss rates $\sim 10^{-5}\ M_\odot/yr$, over timescales comparable to their main-sequence lifetimes; however, these stars are not completely mixed, and do not exactly evolve "down" the main sequence, but more generally to the right. Only recently have calculations of evolution of upper main-sequence stars accounting for this mass loss been undertaken (Maeder 1981; Brunish and Truran 1982). Also, the mass-loss rates of red giants and

supergiants are observed to be ~ 10^{-5} to 10^{-6} $M_\odot$/yr, high enough to allow evolution toward white dwarf masses in the brief AGB and subsequent phases (Cassinelli 1979). It appears that the primary arguments both for and against the Soviet theory of "corpuscular emission" from main-sequence stars were based upon *underestimates* of mass-loss rates of both red giants/supergiants and O-B stars.

The consensus in the 1950s was that the Soviet theory of "corpuscular emission" did not apply to the Sun. Even in 1958, estimates of the solar mass-loss rate were very low (10^{-15} $M_\odot$/yr; Mustel 1958). Fesenkov and Idlis (1958) estimate that a mass-losing star would have time to evolve "down" to 1.1 $M_\odot$ during the lifetime of the Galactic disk (5 x 10^9 yr). They also point out that the mass–luminosity relation changes slope for low-mass stars, implying fundamentally different behavior. Another Soviet astronomer, V. Krat (1958), remarks, "It is difficult to imagine that stars similar to the Sun, with rotational velocities of the order of 1-2 km/s could have been formed from the diffuse matter with such a small angular momentum. There are reasons to suppose that the present slow rate of rotation of the Sun can be explained by the loss of a considerable part of its mass in the past. Of course the decrease in stellar mass cannot be considered as a uniform process, leading to the evolution of the star along the main sequence." Main-sequence mass loss as proposed by WBS may plausibly account for the Sun's slow rotation rate, as well as other features of its structure and composition; this is the subject of Section II.

II. SOLAR MODELS

A. Introduction

The main-sequence mass loss mechanism is postulated to operate among stars in the pulsation instability strip, between spectral types A0 and mid-F. If the development of convective envelopes is important in bringing an end to the rapid mass-loss phase, then stars moving down the main sequence may potentially overshoot the red edge of the instability strip, to become stars of late-F and early-G spectral type. This implies that the Sun may be a candidate for early main-sequence mass loss. We found that it is possible to evolve solar models with initial mass ≤ 2 $M_\odot$, reasonable composition, and plausible mass-loss rates that match the Sun's observed luminosity and radius at its present age (Guzik, Willson and Brunish 1987). The constraints on initial mass and mass-loss rates obtained from solar modeling, conditions in the inner solar system (Bowen 1988), and stellar evolution (WBS 1987) are consistent. Such an alternative scenario for solar evolution may prove advantageous in resolving problems encountered with solar structure and solar system formation.

Bowen (1988) examined the effects of a more massive and luminous early Sun and strong solar wind on the formation of the terrestrial planets. The decrease in size of the planet accretion region due to smaller semi-major axes would have increased collision rates and shortened the accretion timescale. The larger early solar tidal torques (Torque ~ M^2/semi-major axis^6) would have been sufficient to stop the rotation of Venus, so that atmospheric circulation alone would suffice to produce the very slow retrograde rotation observed today. Solar tidal effects would also have been important in selecting the 3:2 spin-orbit resonance mode of Mercury. Earth would have avoided spindown due to its larger semi-major axis. The impact of the solar wind on smaller planetesimals would change their angular momentum, and cause them to spiral toward the Sun (pseudo Poynting-Robertson effect), resulting in intense cratering of the larger planetesimals spiraling outward as the

Sun's gravitational attraction decreased. A constraint on the e-folding time for the decrease in mass loss rate (~200 Myr) is derived from the observed decrease in lunar cratering rate that would have occured with the diminished effectiveness of the solar wind in causing small planetesimals to spiral toward the Sun.

Standard solar models predict that the Sun's initial luminosity was 70% its present value; a strong greenhouse effect is generally invoked to explain evidence for a warmer climate on Earth, and the presence of liquid water on Mars during the first billion years after the formation of the solar system. A modest greenhouse effect would suffice if the early Sun was more luminous. A luminous early Sun and strong solar wind would also be capable of vaporizing and carrying away much of the mantle of Mercury, thereby explaining Mercury's unusually high density and thin mantle compared to the other terrestrial planets. The sensitivity of the vaporization rate to the solar luminosity constrains the initial mass of the Sun to very nearly 2.0 $M_\odot$; an initial mass > 2.1 $M_\odot$ would have destroyed Mercury, while an initial mass < 1.9 $M_\odot$ would have had little effect.

This section focuses on the effects of main-sequence mass loss on the evolution, interior structure, and surface composition of the Sun. Three mass-losing solar models, each of initial mass 2 $M_\odot$, having exponentially decreasing mass-loss rates with e-folding times of a few times 10^8 yr are compared with a standard 1 $M_\odot$ model.

B. Modeling

The models were calculated using the evolution code developed by Iben (1965) and modified to incorporate mass loss by Brunish and Truran (1982). Stellar atmospheres are not modeled; instead, the amount of mass in a surface mass reservoir can be specified, and serves to determine the pressure boundary condition for inner layers. Mass loss is treated by subtracting the product of the mass-loss rate and the evolution time step from this mass reservoir after each time step. The model is rezoned frequently to ensure that evolution proceeds smoothly

and that there is enough mass left in the surface reservoir to allow continued mass loss.

The nuclear reaction rates are from Fowler, Caughlan and Zimmerman (1975). The opacities used are analytical fits to the Cox-Stewart (1970) opacity tables as described by Iben (1975). Convection is treated using standard mixing-length theory, applying the Schwarzschild criterion for convective stability. The ratio of the mixing length to pressure scale height, which will be called simply the "mixing length" and designated by the symbol "α", is held constant throughout the evolution. Convective overshoot is not included. Variable parameters that must be chosen or constrained for these models are: 1) M_0, the initial mass; 2) τ, the mass-loss timescale in the parametrization of M(t); 3) Y_0, the initial ^{4}He mass fraction; 4) Z_0, the initial metal abundance; and 5) α, the mixing length.

The initial mass of the mass-losing models presented is $M_0 = 2\ M_\odot$. We restricted our considerations to models with initial mass-loss rates $M_0 \leq 10^{-8}\ M_\odot$/yr (see WBS 1987) and initial helium abundances $0.20 \leq Y_0 \leq 0.30$. Solar models with higher initial mass would require a higher initial mass-loss rate and/or a lower initial helium abundance to satisfy constraints on the present solar luminosity, radius and mass. Higher initial mass-loss rates may not be plausible, as mass loss from 2 $M_\odot$ stars should then be observable; lower initial helium abundances may be in conflict with estimates of the primordial ^{4}He abundance. Models with lower initial mass can be evolved which satisfy observational constraints; the effects on the solar interior are similar to, but less extreme than those of the models presented here.

The three mass-losing models use the following parametrizations of *mass* as a function of time: (See Table 1 for values of τ, τ_1 and τ_2.)

Models 1, 3 $\quad M(t) = (1.0 + e^{-t/\tau})\ M_\odot$

Model 2 $\quad M(t) = (1.0 + 0.75\ e^{-t/\tau_1} + 0.25\ e^{-t/\tau_2})\ M_\odot$

Mass-loss rates are parametrized as exponentially decreasing, and

characterized by the decay timescale τ. The exponential parametrization was chosen because it is simple and decreases smoothly with time. It is in principle physically plausible in terms of the mass-loss mechanism, as the mass-loss rate should be highest when a rapidly-rotating star arrives on the main-sequence within the instability strip, where pulsation and rotation can facilitate mass loss, and should decrease as the star moves out of the instability strip, ceases to pulsate, spins down, and develops an envelope convection zone. The two-part exponential of Model 2 allows more rapid loss of the first 0.75 $M_\odot$, and slow loss of the remaining 0.25 $M_\odot$, which may be a natural refinement if the development of the surface convection zone, after the star reaches about 1.25 $M_\odot$, is effective in channeling energy away from pulsation.

Zero-age main-sequence models of 2 $M_\odot$ with Population I metal abundance ($Z = 0.02$) were constructed with the range of initial ^{4}He abundances $0.20 < Y_0 < 0.24$ (since our "standard model" requires $Y_0 = 0.24$; see discussion below). For a given zero-age model, the mass-loss timescale(s) and the mixing length (α) are chosen so that the model has luminosity 1 $L_\odot$ and radius 1 $R_\odot$ at age 4.6 ± 0.1 billion years. Decreasing the mass-loss timescale decreases the final luminosity; decreasing α increases the radius while slightly decreasing the luminosity. The standard model was constructed by choosing the initial ^{4}He abundance and α in a constant 1 $M_\odot$ model, again to match the Sun's observed luminosity and radius at its present age. Finally, all of the models were evolved through the ascent of the red-giant branch to compare their main-sequence lifetimes and surface abundances of CN-processed material following the first dredge-up phase.

Table 1 summarizes the fitting parameters used in the three models plus the standard model. Tables 2 and 3 summarize some characteristics of the interiors and envelopes of the mass-losing models for ease of comparison with the standard model. Tables 4a through 4d present the radius, temperature, cumulative luminosity, density, X(H), and X(^{3}He) of thirty mass zones for each model at age 4.6 Gyr. Tables 5a through 5d present the luminosity, effective temperature, radius,

Table 1. Model parameters

	Standard	Model 1	Model 2	Model 3
M_0 ($M_\odot$)	1.00	2.00	2.00	2.00
Y_0	0.238	0.220	0.210	0.200
τ (Gyr)	...	0.13	0.17/0.50[a]	0.33
$\dot{M}_0$ (10^{-9} $M_\odot$/yr)	...	7.69	4.91	3.03
α[b]	1.00	1.10	1.15	1.25

[a]Two-part exponentially decreasing mass-loss rate. Model loses 0.75 $M_\odot$ with timescale 0.17 Gyr, and 0.25 $M_\odot$ with timescale 0.50 Gyr.

[b] α is the mixing length/pressure scale height ratio.

Table 2. Interior comparison

	Standard	Model 1	Model 2	Model 3
$X(H)_{central}$	0.391	0.344	0.312	0.285
$\rho_{central}$ (g/cm^3)	156.9	173.6	186.4	198.2
$T_{central}$ (10^6 K)	14.95	15.24	15.43	15.63
Neutrino Flux (SNUs)				
^8B	5.3	7.7	9.5	11.6
other[a]	1.3	1.6	1.8	2.1
Total	6.6	9.3	11.3	13.7
Main-Sequence Lifetime (Gyr)[b]	9.91	9.52	9.24	8.97

[a]Includes ^7Be, ^{13}N, and ^{15}O neutrinos, plus an estimated 0.26 SNUs from pep reactions.

[b]Based on central X(H) depletion to 10^{-5}.

Table 3. Envelope comparison

	Standard	Model 1	Model 2	Model 3
Surface Convection Zone Depth ($R_\odot$)	0.245	0.264	0.277	0.282
Convective Envelope Mass ($M_\odot$)	0.0125	0.0176	0.0210	0.0246
T at Base of Convection Zone (10^6 K)	1.724	1.889	1.988	2.051
Surface $X(^3He)$ (10^{-4})	0.659[a]	4.83	6.39	7.83
Surface $X(^{12}C)$ (10^{-3})	2.82	2.77	2.77	2.75
Surface $X(^{14}N)$ (10^{-4})	9.20	9.81	9.82	10.1

[a] Reflects initial $X(^3He) = 0.650 \times 10^{-4}$.

Table 4a. Standard model structure

M_r ($M_\odot$)	r ($R_\odot$)	L_r ($L_\odot$)	T (10^6 K)	ρ (g/cm^3)	X(H)	X(^{3}He)
0.0000	0.0000	0.0000	14.95	156.9	0.391	1.18E-05
0.0006	0.0017	0.0049	14.86	156.9	0.399	1.27E-05
0.0010	0.0209	0.0085	14.81	152.5	0.404	1.31E-05
0.0050	0.0362	0.0400	14.55	143.4	0.429	1.60E-05
0.0104	0.0468	0.0805	14.31	135.3	0.451	1.92E-05
0.0198	0.0589	0.1448	13.48	125.2	0.480	2.42E-05
0.0412	0.0775	0.2738	13.97	109.4	0.528	3.58E-05
0.0610	0.0903	0.3747	12.93	98.82	0.561	4.78E-05
0.0994	0.1103	0.5330	12.21	83.21	0.608	7.59E-05
0.1467	0.1306	0.6762	11.46	69.65	0.647	1.23E-04
0.1962	0.1494	0.7819	10.78	58.83	0.676	1.94E-04
0.2499	0.1683	0.8608	10.12	49.49	0.698	3.07E-04
0.2996	0.1850	0.9099	9.563	42.16	0.711	4.63E-04
0.3411	0.1918	0.9386	9.129	37.10	0.720	6.53E-04
0.3968	0.2172	0.9648	8.580	30.52	0.728	1.04E-03
0.4519	0.2357	0.9811	8.063	25.16	0.733	1.67E-03
0.5035	0.2538	0.9907	7.595	20.73	0.736	2.70E-03
0.5518	0.2716	0.9961	7.167	17.08	0.737	3.62E-03
0.6050	0.2927	0.9987	6.700	13.51	0.739	2.85E-03
0.6533	0.3137	0.9996	6.275	10.67	0.740	1.72E-03
0.6969	0.3347	1.0000	5.885	8.410	0.741	1.01E-03
0.7481	0.3628	1.0003	5.411	6.104	0.742	5.00E-04
0.8021	0.3987	1.0004	4.880	4.067	0.742	2.28E-04
0.8503	0.4392	1.0004	4.360	2.584	0.742	1.19E-04
0.9004	0.4972	1.0004	3.732	1.374	0.742	7.68E-05
0.9504	0.5932	1.0003	2.909	0.5062	0.742	6.67E-05
0.9752	0.6820	1.0003	2.290	0.2105	0.742	6.60E-05
0.9902	0.7818	1.0003	1.516	0.0850	0.742	6.59E-05
0.9990	0.9140	1.0003	0.5076	0.0164	0.742	6.59E-05
1.0000	1.0044	1.0003	0.0058	0.0000	0.742	6.59E-05

Table 4b. Model 1 structure

M_r ($M_\odot$)	r ($R_\odot$)	L_r ($L_\odot$)	T (10^6 K)	ρ (g/cm^3)	X(H)	X(^{3}He)
0.0000	0.0000	0.0000	15.24	173.6	0.344	8.58E-06
0.0005	0.0161	0.0045	15.15	173.6	0.352	9.28E-06
0.0010	0.0203	0.0087	15.09	168.4	0.358	9.75E-06
0.0048	0.0345	0.0391	14.83	158.0	0.383	1.22E-05
0.0102	0.0449	0.0799	14.56	148.4	0.407	1.49E-05
0.0204	0.0579	0.1514	14.17	135.6	0.441	1.99E-05
0.0403	0.0747	0.2716	13.58	118.5	0.488	2.97E-05
0.0617	0.0885	0.3813	13.07	105.1	0.527	4.17E-05
0.1067	0.1113	0.5610	12.18	85.50	0.588	7.42E-05
0.1551	0.1316	0.6987	11.40	70.28	0.632	1.24E-04
0.1980	0.1479	0.7863	10.79	59.50	0.666	1.89E-04
0.2556	0.1685	0.8688	10.06	49.27	0.702	3.21E-04
0.3008	0.1841	0.9125	9.542	41.46	0.717	4.75E-04
0.3483	0.2002	0.9442	9.033	35.51	0.729	7.14E-04
0.4023	0.2186	0.9678	8.490	29.50	0.738	1.14E-03
0.4542	0.2368	0.9823	7.993	24.08	0.744	1.82E-03
0.5002	0.2534	0.9905	7.570	20.23	0.748	2.82E-03
0.5552	0.2745	0.9963	7.074	16.07	0.751	3.94E-03
0.5944	0.2906	0.9982	6.725	13.47	0.753	3.53E-03
0.6545	0.3175	0.9994	6.191	10.08	0.755	2.25E-03
0.7018	0.3414	0.9998	5.764	7.747	0.757	1.52E-03
0.7483	0.3683	1.0000	5.332	5.771	0.757	1.07E-03
0.7994	0.4036	1.0000	4.830	3.847	0.758	7.81E-04
0.8493	0.4472	1.0001	4.294	2.413	0.759	6.34E-04
0.9006	0.5093	1.0000	3.656	1.246	0.759	5.55E-04
0.9504	0.6091	1.0000	2.841	0.4683	0.759	5.10E-04
0.9746	0.6976	1.0000	2.223	0.2035	0.759	4.94E-04
0.9898	0.7940	1.0000	1.393	0.0898	0.759	4.83E-04
0.9990	0.9261	1.0000	0.4193	0.0148	0.759	4.83E-04
0.9998	1.0033	1.0000	0.0058	0.0000	0.759	4.83E-04

Table 4c. Model 2 structure

M_r ($M_\odot$)	r ($R_\odot$)	L_r ($L_\odot$)	T (10^6 K)	ρ (g/cm^3)	X(H)	X(^{3}He)
0.0000	0.0000	0.0000	15.43	186.4	0.312	6.78E-06
0.0005	0.0157	0.0045	15.33	183.0	0.320	7.41E-06
0.0010	0.0199	0.0089	15.27	180.2	0.326	7.85E-06
0.0049	0.0341	0.0403	14.99	168.2	0.353	1.01E-05
0.0096	0.0431	0.0757	14.75	158.9	0.375	1.23E-05
0.0208	0.0571	0.1543	14.29	143.0	0.415	1.74E-05
0.0407	0.0737	0.2744	13.69	123.7	0.466	2.68E-05
0.0601	0.0860	0.3738	13.20	110.5	0.504	3.72E-05
0.1061	0.1094	0.5591	12.26	88.13	0.570	6.90E-05
0.1460	0.1265	0.6767	11.58	73.50	0.617	1.09E-04
0.1962	0.1459	0.7843	10.84	61.26	0.662	1.82E-04
0.2523	0.1663	0.8664	10.11	48.84	0.700	3.11E-04
0.2957	0.1815	0.9096	9.596	42.57	0.717	4.58E-04
0.3548	0.2020	0.9487	8.951	34.32	0.734	7.68E-04
0.4097	0.2211	0.9711	8.394	28.25	0.744	1.25E-03
0.4513	0.2359	0.9821	7.993	23.80	0.750	1.83E-03
0.4969	0.2528	0.9903	7.566	19.96	0.755	2.83E-03
0.5472	0.2723	0.9958	7.109	16.24	0.758	4.01E-03
0.5977	0.2934	0.9982	6.656	12.94	0.761	3.76E-03
0.6461	0.3154	0.9991	6.225	10.17	0.763	2.80E-03
0.6941	0.3398	0.9958	5.791	7.801	0.765	2.00E-03
0.7471	0.3708	0.9998	5.299	5.466	0.766	1.41E-03
0.7989	0.4074	0.9998	4.791	3.689	0.767	1.06E-03
0.8494	0.4527	0.9998	4.249	2.294	0.768	8.68E-04
0.9014	0.5174	0.9998	3.605	1.170	0.769	7.51E-04
0.9491	0.6146	0.9998	2.829	0.4617	0.769	6.84E-04
0.9749	0.7090	0.9998	2.157	0.1959	0.769	6.57E-04
0.9903	0.8059	0.9998	1.296	0.0873	0.769	6.39E-04
0.9990	0.9284	0.9998	0.4144	0.0157	0.769	6.39E-04
0.9998	1.0058	0.9998	0.0058	0.0000	0.769	6.39E-04

Table 4d. Model 3 structure

M_r ($M_\odot$)	r ($R_\odot$)	L_r ($L_\odot$)	T (10^6 K)	ρ (g/cm^3)	X(H)	X(^{3}He)
0.0000	0.0000	0.0000	15.63	198.2	0.285	5.36E-06
0.0005	0.0153	0.0045	15.52	194.3	0.294	5.92E-06
0.0010	0.0195	0.0090	15.46	191.4	0.300	6.32E-06
0.0051	0.0337	0.0421	15.15	177.5	0.329	8.44E-06
0.0096	0.0423	0.0773	14.90	167.2	0.351	1.05E-05
0.0191	0.0544	0.1450	14.50	152.2	0.387	1.45E-05
0.0405	0.0724	0.2760	13.81	129.4	0.444	2.39E-05
0.0625	0.0861	0.3879	13.24	113.0	0.488	3.52E-05
0.1060	0.1080	0.5616	12.32	90.24	0.557	6.50E-05
0.1477	0.1258	0.6833	11.60	75.28	0.605	1.06E-04
0.1977	0.1453	0.7888	10.84	60.81	0.659	1.82E-04
0.2506	0.1647	0.8663	10.13	49.64	0.701	3.06E-04
0.2954	0.1807	0.9113	9.593	42.18	0.720	4.60E-04
0.3413	0.1969	0.9431	9.079	35.47	0.735	6.94E-04
0.3950	0.2159	0.9675	8.517	29.31	0.747	1.13E-03
0.4456	0.2341	0.9820	8.018	23.81	0.756	1.80E-03
0.5022	0.2554	0.9919	7.484	19.05	0.762	3.09E-03
0.5529	0.2757	0.9967	7.021	15.40	0.766	4.05E-03
0.5971	0.2946	0.9986	6.623	12.52	0.769	3.66E-03
0.6454	0.3171	0.9995	6.190	9.859	0.772	2.75E-03
0.7046	0.3483	0.9999	5.653	7.048	0.774	1.89E-03
0.7512	0.3768	1.0001	5.218	5.097	0.775	1.47E-03
0.8024	0.4144	1.0001	4.714	3.428	0.777	1.18E-03
0.8523	0.4610	1.0001	4.177	2.124	0.777	1.01E-03
0.9010	0.5234	1.0001	3.573	1.148	0.778	9.00E-04
0.9509	0.5982	1.0001	2.755	0.4262	0.778	8.26E-04
0.9751	0.7177	1.0001	2.051	0.1960	0.779	7.83E-04
0.9897	0.8042	1.0001	1.267	0.0950	0.779	7.83E-04
0.9990	0.9255	1.0001	0.3938	0.0164	0.779	7.83E-04
0.9998	0.9993	1.0001	0.0058	0.0000	0.779	7.83E-04

Table 5a. Standard model evolution

Age (Gyr)	Log($L/L_\odot$)	Log T_{eff} (K)	R ($R_\odot$)	X_c	T_c (10^6 K)	ρ_c (g/cm^3)	Convective Envelope Mass[a]
0.00	-0.1582	3.7511	0.8771	0.741	13.26	84.05	0.0177
0.50	-0.1292	3.7527	0.9004	0.706	13.17	91.15	0.0170
1.00	-0.1141	3.7538	0.9113	0.669	13.35	96.41	0.0164
1.50	-0.0998	3.7549	0.9218	0.633	13.52	102.0	0.0158
2.00	-0.0851	3.7560	0.9329	0.596	13.70	108.1	0.0152
3.00	-0.0535	3.7582	0.9575	0.519	14.12	123.3	0.0140
4.00	-0.0203	3.7603	0.9856	0.440	14.62	142.5	0.0130
4.60	0.0001	3.7613	1.0044	0.391	14.95	156.9	0.0125

[a] Convective envelope masses are accurate to ±0.0003, which is half the zone spacing at the base of the envelope convection zone.

Table 5b. Model 1 evolution

Age (Gyr)	Mass ($M_\odot$)	Log ($L/L_\odot$)	Log T_{eff} (K)	R ($R_\odot$)	X_c	T_c (10^6 K)	ρ_c (g/cm^3)	Convective Core Mass	Convective Envelope Mass[a]
0.00	2.0000	1.1794	3.9648	1.5293	0.753	20.68	73.48	0.2238	...
0.05	1.6821	0.8903	3.9040	1.4507	0.732	19.24	85.30	0.1315	...
0.10	1.4622	0.6888	3.8593	1.4129	0.717	18.08	91.98	0.0696	...
0.20	1.2154	0.3074	3.7995	1.1999	0.697	15.76	97.56	0.0047	...
0.30	1.0993	0.1055	3.7795	1.0426	0.683	14.59	98.05	...	...
0.50	1.0212	-0.0775	3.7595	0.9261	0.665	13.66	98.56	...	...
0.75	1.0029	-0.1120	3.7548	0.9095	0.645	13.51	101.0	...	0.0194
1.00	1.0002	-0.1127	3.7544	0.9104	0.627	13.55	103.8	...	0.0206
1.50	0.9998	-0.0991	3.7553	0.9210	0.589	13.72	110.2	...	0.0201
2.00	0.9998	-0.0845	3.7564	0.9319	0.552	13.92	117.3	...	0.0201
3.00	0.9998	-0.0534	3.7585	0.9563	0.474	14.36	134.6	...	0.0188
4.00	0.9998	-0.0208	3.7604	0.9842	0.394	14.88	156.7	...	0.0176
4.59	0.9998	0.0000	3.7615	1.0033	0.344	15.24	173.6	...	0.0176

[a] Convective envelope masses are accurate to ±0.0003, which is half the zone spacing at the base of the envelope convection zone.

Table 5c. Model 2 evolution

Age (Gyr)	Mass ($M_\odot$)	Log ($L/L_\odot$)	Log T_{eff} (K)	R ($R_\odot$)	X_c	T_c (10^6 K)	ρ_c (g/cm^3)	Convective Core Mass	Convective Envelope Mass[a]
0.00	2.0000	1.1589	3.9596	1.5300	0.764	20.52	73.89	0.2125	...
0.05	1.7852	1.0106	3.9272	1.4973	0.743	19.82	79.88	0.1674	...
0.10	1.6217	0.8307	3.8880	1.4577	0.725	18.88	87.19	0.1092	...
0.20	1.3981	0.5477	3.8289	1.3818	0.698	17.25	96.21	0.0362	...
0.30	1.2659	0.3955	3.8082	1.2756	0.679	16.35	99.93	0.0112	...
0.50	1.1317	0.1302	3.7817	1.0619	0.649	14.85	103.4	...	...
0.75	1.0646	0.0285	3.7707	0.9935	0.621	14.34	106.7	...	...
1.00	1.0358	-0.0377	3.7631	0.9533	0.599	14.06	109.8	...	0.0167
1.50	1.0122	-0.0630	3.7593	0.9424	0.557	14.04	117.0	...	0.0143
2.00	1.0043	-0.0684	3.7579	0.9426	0.518	14.14	124.9	...	0.0192
3.00	1.0003	-0.0491	3.7586	0.9609	0.438	14.55	144.2	...	0.0203
4.00	0.9998	-0.0185	3.7602	0.9880	0.359	15.08	168.8	...	0.0211
4.55	0.9997	-0.0001	3.7609	1.0058	0.312	15.43	186.4	...	0.0210

[a] Convective envelope masses are accurate to ±0.0007, which is half the zone spacing at the base of the envelope convection zone.

Table 5d. Model 3 evolution

Age (Gyr)	Mass ($M_\odot$)	Log ($L/L_\odot$)	Log T_{eff} (K)	R ($R_\odot$)	X_c	T_c (10^6 K)	ρ_c (g/cm^3)	Convective Core Mass	Convective Envelope Mass[a]
0.00	2.0000	1.1383	3.9541	1.5323	0.774	20.38	74.18	0.2043	...
0.05	1.8586	1.0591	3.9354	1.5248	0.752	20.02	77.37	0.1836	...
0.10	1.7378	0.9852	3.9181	1.5163	0.732	19.68	80.91	0.1579	...
0.20	1.5467	0.7801	3.8721	1.4798	0.701	18.65	90.35	0.0946	...
0.30	1.4036	0.6038	5.8358	1.4280	0.675	17.69	97.67	0.0493	...
0.50	1.2191	0.2861	3.7977	1.1803	0.637	15.86	106.3	0.0039	...
0.75	1.1032	0.1100	3.7806	1.0426	0.603	14.91	111.2	...	...
1.00	1.0484	-0.0238	3.7664	0.9542	0.577	14.30	114.7	...	...
1.50	1.0104	-0.0685	3.7601	0.9333	0.534	14.15	122.4	...	0.0213
2.00	1.0021	-0.0764	3.7583	0.9322	0.494	14.24	130.9	...	0.0257
3.00	0.9999	-0.0504	3.7598	0.9540	0.414	14.70	151.8	...	0.0260
4.00	0.9998	-0.0182	3.7615	0.9824	0.331	15.27	179.4	...	0.0246
4.53	0.9998	0.0000	3.7624	0.9993	0.285	15.63	198.2	...	0.0246

[a] Convective envelope masses are accurate to ±0.0007, which is half the zone spacing at the base of the envelope convection zone.

Figure 1. Luminosity vs. time for the standard model and three mass-losing models. The mass-losing models have initial mass 2 $M_\odot$ and mass-loss rates that decrease exponentially with time. See Table 1 for a summary of model parameters, including mass-loss timescales

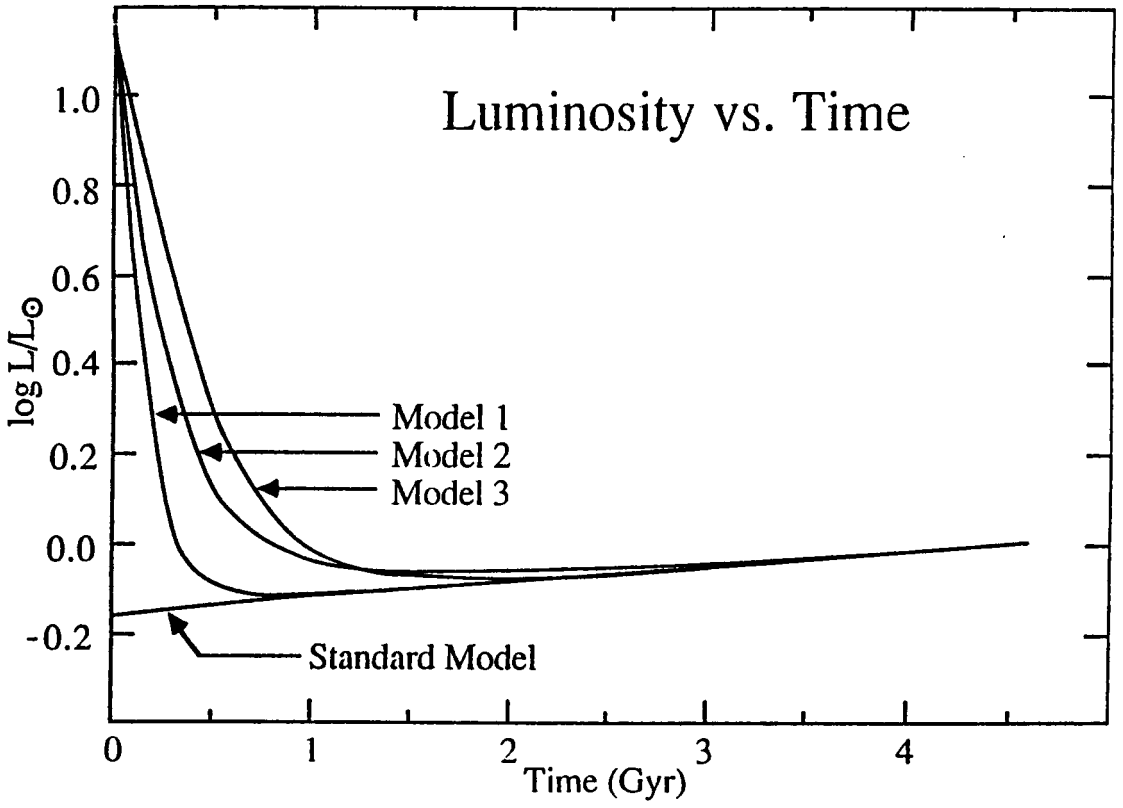

Figure 2. Hydrogen mass fraction vs. mass zone for the standard model and mass-losing models at age 4.6 Gyr. The curve for Model 2 (not shown) lies between those of Models 1 and 3. The mass-losing models have lower interior H abundance due to early main-sequence burning at high luminosity, and have higher surface H abundance due to lower initial He abundance required to achieve 1 $L_\odot$ at age 4.6 Gyr

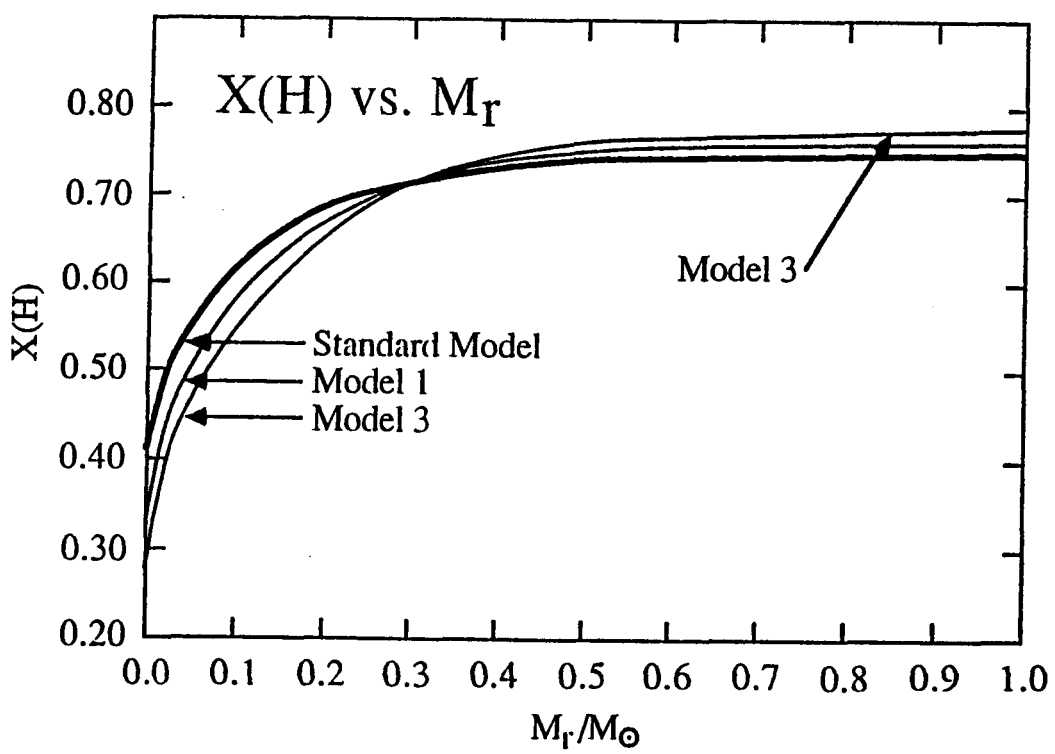

core hydrogen mass fraction, central temperature, central density, and convective envelope masses for the models during their evolution. In addition, Tables 5b through 5d follow the shrinking of the convective cores in the mass-losing models from an initial ~ 0.21 $M_\odot$ to their disappearance after 3-5 x 10^8 yr.

C. Discussion

Figure 1 shows the luminosity of the models as a function of age. The mass-losing models begin hydrogen burning with luminosity ~15 $L_\odot$, and rapidly decrease in luminosity as they lose mass; they follow the luminosity track of the standard model when their masses reach ~1 $M_\odot$. Model 2, with a long timescale for loss of its final 0.25 $M_\odot$, has the shallowest luminosity minimum of the mass-losing models; its luminosity becomes greater than that of Model 3 after the first 1.25 Gyr of evolution.

Figure 2 shows the hydrogen mass fraction as a function of $M(r)/M_\odot$ for Model 1, Model 3, and the standard model at age 4.6 Gyr. The differences can be understood with a simple explanation based on polytropes. The luminosity of a star is proportional to $\mu^{7.5}$, where μ is the mean molecular weight (Clayton 1968). Since the mass-losing models have depleted more core hydrogen than the standard model, they require lower initial ^{4}He abundances to decrease the molecular weight of the envelope; the mass-losing models thus attain the same *mean* molecular weight, and hence the same luminosity (1 $L_\odot$) as the standard model. The rapid depletion of core hydrogen during the high luminosity stage of the mass-losing models is partially offset by the lower initial ^{4}He abundances used; the net effect is a modest decrease in the main-sequence lifetimes of mass-losing models (see Table 2).

1. ^{4}He

The mass-losing models discussed here require initial ^{4}He mass fractions betweeen 0.20 and 0.22, while the standard model requires Y = 0.238. The viability of these lower Y abundances of the mass-losing

models with regard to the primordial ^{4}He abundance derived from cosmology and observations requires comment. For baryon to photon ratio η = 1-10 x 10^{-10}, three light neutrino species, and neutron half-life 10.6 minutes, standard big-bang nucleosynthesis predicts $0.225 \leq Y_p \leq 0.255$ (Boesgaard and Steigman 1985). However, a lower limit to η is obtained by requiring consistency between the primordial ^{7}Li and D + ^{3}He abundances deduced from observed solar and stellar abundances. These estimates will be irrelevant if the Sun and other stars lose even a few percent of their mass during the main-sequence phase; interior processing of Li and ^{3}He alters abundances, so that when interior layers are exposed, the surface Li and ^{3}He abundances retain little or no information on proto-stellar abundances. (See discussion below of Li and ^{3}He abundances for the mass-losing models.) Primordial ^{4}He abundances as low as 0.20 can be accommodated if η ~ 4-5 x 10^{-11}.

Lequeux et al. (1979) estimate $Y_p = 0.228 \pm 0.014$ from observations of H II regions in six blue compact and irregular galaxies, the Magellanic Clouds, and the Orion Nebula by using oxygen as a metallicity indicator and extrapolating to zero metallicity. Kunth and Sargent (1983) find no correlation between ^{16}O and ^{4}He abundances in their observations of 12 metal-poor low-luminosity galaxies, and give as their best estimate $Y_p = 0.245 \pm 0.003$. Peimbert (1983) deduces Y_p = 0.218 (+0.026, -0.037) for the three best-observed halo planetary nebulae in his sample, but this value is dependent upon ^{4}He enrichment factors estimated from stellar evolution theory. Ferland (1986) has recently pointed out that the contribution of collisional excitations to the formation of the λ5876 and λ6678 He I lines should be taken into account in determinations of the ^{4}He abundance. Neglecting this contribution can lead to overestimates of 30% in the ^{4}He abundance of low-Z extragalactic HII regions, and 50% overestimates of the ^{4}He abundance of planetary nebulae. Ferland's reanalysis of the ^{4}He abundance in a small sample of metal-deficient extragalactic H II regions gives $Y = 0.207 \pm 0.016$; one object, I Zw18,

had a very low derived Y abundance of 0.186. Bame et al. (1977) estimated from measurements of the high speed wind from coronal holes that $^4He/H = 0.048 \pm 0.005$, or $Y = 0.158 \pm 0.013$. Given that the measured value does not vary significantly with time and is reproducible for different coronal holes, Bame et al. are unwilling to discount their very low solar ^4He abundance determination. We conclude that solar Y abundances of 0.20-0.22, as required for the mass-losing solar models, are consistent with standard big-bang cosmological determinations, and with solar, stellar, and galactic observational estimates.

Moreover, determinations of Y from standard solar evolution modeling vary from Y = 0.23 to 0.29, depending upon the equation of state, treatment of opacities, and reaction rates. Cox, Guzik and Kidman (1988) have recently completed a comparison between the opacity and equation of state obtained analytically with the Iben evolution code and tables from the Los Alamos Opacity Library for solar interior conditions. After adjusting the Iben analytical fits within limits of uncertainty to provide better agreement with the table values and solar p-mode frequencies, the standard solar model required an initial Y of 0.291, as compared to the previous value of 0.238. Mass-losing models evolved with updated opacities and equation of state will then require initial Y of 0.25 to 0.27; alternatively, the mass-loss timescales and/or initial mass could be increased slightly without requiring unreasonable initial Y abundance to match the solar luminosity. Therefore, it is most important to consider the relative ^4He requirements between the standard and mass-losing models evolved with the same evolution code, rather than absolute Y abundances.

2. ^3He

Figure 3 shows ^3He mass fraction as a function of $M(r)/M_\odot$ for Model 1, Model 3, and the standard model at age 4.6 Gyr. In order to account for the deuterium processed into ^3He during the pre-main sequence convective phase, the initial ^3He abundance by mass, 6.50×10^{-5}, represents the proto-solar abundance of D + ^3He. The surface

Figure 3. ^3He mass fraction vs. mass zone for the standard model and mass-losing models at age 4.6 Gyr. The curve for Model 2 (not shown) lies between those of Models 1 and 3. The high surface ^3He abundances of the mass-losing models reflect the equilibrium ^3He abundance attained in earlier processing of present surface layers at high interior temperatures. The surface abundance of the standard model reflects the initial ^3He abundance

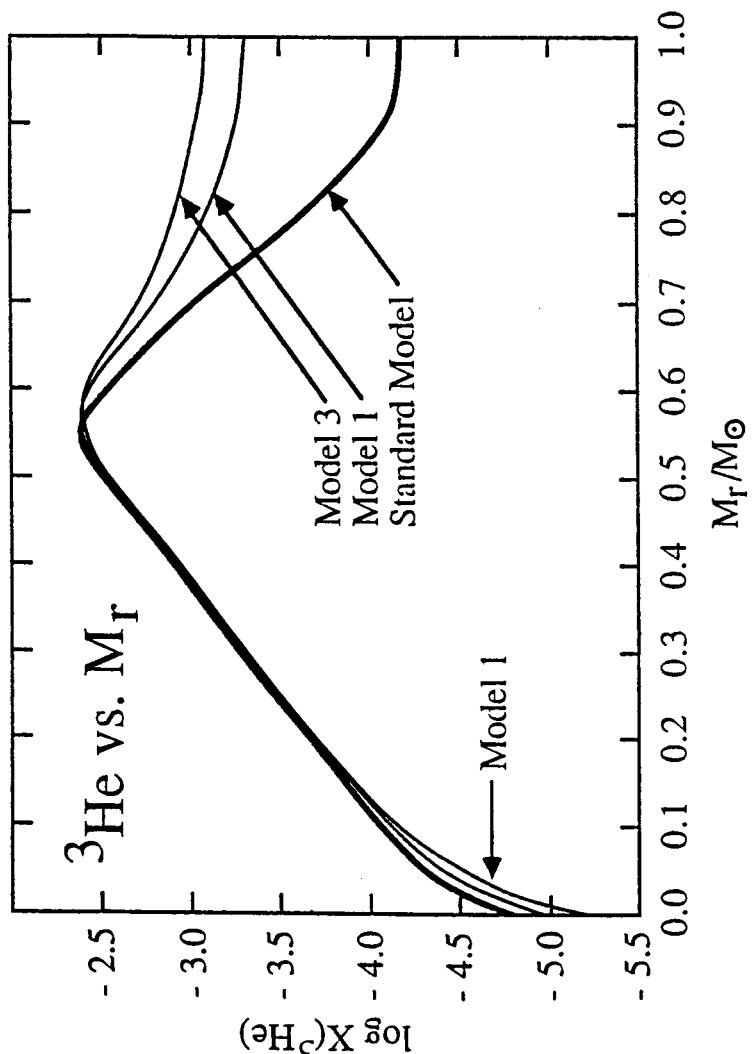

^{3}He abundance of the standard model at age 4.6 Gyr reflects this choice of initial value. However, the layers at the surface of the mass-losing models at age 4.6 Gyr were originally at a temperature of nearly 11 million K, and remained at temperatures above 8 million K for 1-3 x 10^8 years, sufficient for ^{3}He to achieve equilibrium abundances independent of the choice of initial abundance (Clayton 1968). The mass-losing models have surface ^{3}He mass fractions of 4.8-7.8 x 10^{-4}, seven to twelve times that of the standard model. Figure 3 also shows the slightly higher central ^{3}He abundance of the standard model compared to the mass-losing models. This reflects the standard model's lower central temperatures and resulting higher equilibrium ^{3}He concentration.

The solar surface ^{3}He abundance can be estimated from solar wind measurements and spectra of solar prominences. Geiss et al. (1972), from analysis of the solar-wind collection foil taken to the Moon by the Apollo astronauts, estimate that the solar surface $^3He/^4He$ ratio by number is $4.3 \pm 0.3 \times 10^{-4}$. Black (1972) estimates $^3He/^4He = 3.9 \pm 0.3 \times 10^{-4}$ from solar-wind implanted ^{3}He in gas-rich meteorites, lunar fines, and breccias. Black finds a larger range of ^{3}He abundances in the wind component associated with low energy solar flares: $^3He/^4He = 4.1 \pm 1.0 \times 10^{-4}$, although individual flare measurements sometimes show large deviations from average. Hall (1975) determined $^3He/^4He = 4 \pm 2 \times 10^{-4}$ from solar prominence spectroscopy. Taking this latter estimate, and assuming a range for the solar ^{4}He mass fraction $0.20 \leq Y \leq 0.30$, the mass fraction of ^{3}He would then be in the range 0.3-1.4 x 10^{-4}, at least a factor of three less than the surface ^{3}He abundances of the mass-losing models.

A direct determination of the photospheric ^{3}He abundance is preferrable, since fractionation, non-thermal equilibrium, and radiative transfer effects complicate the interpretation of coronal and prominence spectra, and since some ^{3}He is likely to have diffused out of the gas-rich meteorites. The observed strength of the 2.223 MeV gamma-ray line from the capture of flare-produced neutrons by

photospheric hydrogen can be used to gauge the the photospheric ^{3}He abundance since the ^{3}He(n,γ)^{4}He reaction, with a cross section 1.6 x 10^4 times larger than the ^{1}H(n,γ)^{2}H reaction, effectively competes for the capture of neutrons (Hua and Lingenfelter 1987). Using this method, Ramaty (1986) places a "safe" upper limit on the photospheric ^{3}He abundance: ^{3}He/H < 2 x 10^{-4}, or X(^{3}He) < 5 x 10^{-4}, comparable to the surface ^{3}He abundances of the mass-losing models. Hua and Lingenfelter (1987) model the time-dependence of the 2.223 MeV gamma-ray emission from the June 3, 1982 solar flare which was well-observed by the *Solar Maximum Mission* to obtain a solar photospheric ^{3}He/H ratio of 2.3 ± 1.2 x 10^{-5}, or X(^{3}He) <~ 6 x 10^{-5} at the 90% confidence level. Hua and Lingenfelter caution that this value is model-dependent and derived from measurements of only one flare; in particular, the ion angular distribution and acceleration mechanism will require more detailed modeling. However, most plausible modifications in the assumed ion angular distribution *reduce* the derived ^{3}He abundance, and measurements of other flares are consistent with those of the June 3, 1982 flare. If Hua and Lingenfelter have indeed determined the photospheric ^{3}He abundance, solar models with initial mass and mass-loss duration discussed here overproduce ^{3}He by a factor of 10. Either these particular solar models are not viable, or we do not fully understand the production, depletion, or destruction of ^{3}He.

There is actually a good deal of evidence to suggest that the production/destruction of ^{3}He is poorly understood. Rood, Steigman and Tinsely (1976) note that ^{3}He + D is produced primordially in the standard big bang models in quantities already within a factor of two of the solar system abundance. Yet low-mass stars should be producing copious amounts of ^{3}He in their envelopes and returning it to the interstellar medium during the red giant phase. Dearborn, Schramm and Steigman (1986) find that even massive stars do not completely destroy their initial ^{3}He + D during evolution. Unenriched infall into the solar neighborhood would dilute produced ^{3}He, but evidence for

such infall is inconclusive (see Section IV). Bania, Rood and Wilson (1987; see also Rood, Bania and Wilson 1984) measured the strength of the 8.7 GHz hyperfine line of ^{3}He$^+$ to determine ^{3}He/H abundances in nine Galactic HII regions. They obtain values ranging from 1.2 x 10^{-5} to 14.7 x 10^{-5}, and find no apparent correlation between Galactocentric distance or other indicators of stellar processing; rather, they find a marginal tendency for sources outside the solar circle to have *larger* abundances, in contradiction with the expectation that stellar processing produces ^{3}He.

Fractionation in the solar wind is unlikely to deplete ^{3}He relative to ^{4}He by the necessary amount. Fractionation processes should depend upon the relative mass, charge, or charge-to-mass ratio of the ionic species involved. The charge, mass, and charge-to-mass ratio of ^{3}He is the same as, or intermediate to that of H and ^{4}He; since solar wind measurements do not show an order of magnitude depletion of H relative to ^{4}He (Bame et al. 1977), ^{3}He would be even less likely to be depleted relative to ^{4}He. Similarly, gravitational and thermal diffusion are unable to deplete ^{3}He by a factor of ten during the lifetime of the Sun (Cox, Guzik and Kidman 1988).

The ^{3}He abundance in mass-losing solar models following the mass-loss phase could be lowered somewhat by more rapid mass loss and/or lower initial mass. However, such alterations of initial assumptions perhaps would not be as favorable for explaining formation of the inner solar system. Willson (1987, private communication, Department of Physics, Iowa State University) has pointed out that, if a resonance reaction exists between ^{3}He and some other abundant isotope (e.g., ^{12}C, ^{14}N, or ^{16}O), the expected ^{3}He equilibrium abundances may be reduced; such a reaction may have the additional advantage of competing with the ^{3}He + ^{4}He reaction leading to the ppIII chain, thereby decreasing the predicted flux of ^{8}B neutrinos. Struck-Marcell (1987, private communication, Department of Physics, Iowa State University) suggested that the effect of the envelope ^{3}He abundance peak, higher predicted abundances of ^{3}He for

stars that experienced main-sequence mass loss, or removal of ^{3}He via resonance reactions may be discernible in products of s-process nucleosynthesis in asymptotic giant branch stars, as ^{3}He is an effective neutron absorber.

3. Lithium, beryllium and boron

Because isotopes of the elements Li, Be, and B are easily destroyed at temperatures characteristic of stellar interiors, their abundance at stellar surfaces can provide constraints on the operation of processes such as mass loss, diffusion, and convection. Boesgaard (1976) reviewed abundance determinations, and summarized the best estimates of stellar, solar, solar system, and terrestrial abundances of these fragile elements. These are given below; see Boesgaard's review for individual references. In a 1 $M_\odot$ star, ^{7}Li can survive only in the outer 2.5% by mass, ^{9}Be in the outer 4.8%, ^{10}B in the outer 18.8%, and ^{11}B in the outer 17.8%. The solar photospheric abundance of ^{7}Li/H is 1.2×10^{-11}, while the abundance found in meteorites is two orders of magnitude larger, ^{7}Li/H = 2×10^{-9}. The meteoritic value is also typical of that found for upper main-sequence stars in young clusters, indicating that the Sun has depleted ^{7}Li. The ^{6}Li/^{7}Li isotopic ratio for materials on Earth is 0.08; ^{6}Li seems to be depleted relative to ^{7}Li by solar processes, as the solar ratio is ~ 0.04. The solar ^{9}Be abundance is ^{9}Be/H = 1.2×10^{-11}, nearly a factor of two less than the meteoritic value of 2.0×10^{-11}, but typical of F and G stars. ^{7}Be and ^{10}Be are unstable, with half-lives of 54.5 days and 2.7 million years, respectively, so are not observed. The solar boron abundance, measured from the B I line at 2497 Å is ^{10}B/H = 1.6×10^{-10}. Measurements of the B abundance of Vega yield a similar result: ^{10}B/H = 1×10^{-10}. Since boron compounds are volatile when gaseous, and refractory when solid, present meteoritic abundances do not reflect the initial abundance, but the ^{11}B/^{10}B ratio of ~ 4 may still be representative.

The finite abundances of these elements on the solar surface pose a potential problem for the solar main-sequence mass loss hypothesis.

Early exposure of present surface layers to temperatures greater than 8 million K would certainly have destroyed all of the protosolar Li, Be, and B. In fact, at least the surface Li and Be would be destroyed in any star that loses more than a few percent of its mass on the main sequence. On the other hand, the standard picture of solar structure and evolution also fails to account for depletion of Li and possible depletion of Be, relative to meteoritic values. The temperature at the base of the surface convection zone in most standard constant-mass solar models is not much above 2 million K, too low to destroy either Li or Be during the lifetime of the Sun. Pre-main sequence convective mixing may be able to deplete Li by only as much as a factor of five (Soderblom 1983). A mechanism such as convective overshoot or turbulent diffusion is generally invoked to mix material in the convection zone to layers where T ~ 2.5 million K, deep enough to destroy ^{7}Li, but not deeper than layers where T ~ 3.2 million K in order to preserve most of the ^{9}Be (Boesgaard and Lavery 1986). Thus, while standard constant-mass models must account for the destruction of nearly all of the protosolar Li and up to half, but not more, of protosolar Be, a viable mass-losing model must first account for the presence of any surface Li and Be.

A possible resolution to the dilemma for the mass-losing models is production of the necessary light elements in conjunction with and/or following the rapid mass-loss phase. High-energy spallation reactions in the solar atmosphere and in solar flares may be able to replenish the surface convection zone with observed abundances of Li, Be, and B. Ryter et al. (1970) calculated the typical plasma energies necessary to produce one L-nucleus (i.e., one Li, Be, or B nucleus) for various astrophysical conditions. The necessary energy depends upon the gas temperature and the energy spectrum of the particles which collide with heavy nuclei to create an L-nucleus. The hardness of the spectrum can be parametrized in terms of the a power of the kinetic energy, a power of the total particle energy (appropriate to galactic cosmic rays), or as an exponential in particle rigidity (appropriate to solar flares). Ryter et al. (1970) state that some stellar X-ray sources have

temperatures up to 5 x 10^7 K, and that solar flares occasionally show temperatures slightly in excess of 10^8 K. At 10^8 K, for spectra with particle rigidity 50-200 MV, the energy required to form one L-nucleus is 10 to 100 ergs. However, the large enrichments of spallation-produced ^{21}Ne and ^{38}Ar found in meteorites with solar flare heavy ion tracks suggest that the proton flux from flares in the early Sun was several orders of magnitude higher, and the energy spectrum harder than for contemporary solar flares (Caffee et al. 1987). Using a slightly harder energy spectrum, and/or a somewhat higher gas temperature (between 10^8 and 10^9 K) reduces the energy requirement to 1-10 ergs per L-nucleus.

Most of this plasma energy is expected to emerge in the form of X-rays. To contaminate the solar convection zone, which contains roughly 2% of the Sun's mass, with 10^{-11} Li and Be atoms and 10^{-10} B atoms per H atom would require (4 x 10^{31} g) x (1.6 x 10^{-24} g/H atom)$^{-1}$ x (10^{-11} Li/H + 10^{-11} Be/H + 10^{-10} B/H) x (1 or 10 ergs/L-nucleus) ~ 10^{45} to 10^{46} ergs. Typical X-ray fluxes of F and G type stars of age ≤ 10^9 yr are 10^{29}-10^{31} ergs/s (Rosner, Golub, and Vaiana 1985). The production rate of L-nuclei is expected to be largest when the Sun was younger and more massive, and the X-ray flux larger. Assuming that the particle energy spectrum remained hard and particle flux remained high for about 1 billion years, the total plasma energy available to make the observed solar Li, Be, and B can be estimated at 10^{29}-10^{31} ergs/s x (3 x 10^7 s/yr) x (10^9 yr) ~10^{45}-10^{47} ergs, sufficient to account for the present estimated solar L-nuclei abundance. Production at the surface would at first be offset by losses in the outflowing mass of the solar wind. Later, as mass-loss rates decrease, the X-ray flux and production rate would also decrease. The expected preferential loss in the solar wind of lighter elements relative to L-nuclei, and possible effects of diffusion would further complicate the situation. More detailed calculations are planned to determine the feasibility of this suggestion.

The observed solar ^{6}Li/^{7}Li ratio could be explained for the

mass-losing models in a similar manner as for the constant-mass models, i.e. by convective depletion of ^{6}Li relative to ^{7}Li. Since solar flare processes are expected to produce roughly equal amounts of ^{6}Li and ^{7}Li (Hultqvist 1977), a slightly deeper convection zone would be required (and is expected from the evolution modeling) for the mass-losing models to reduce the ratio from ~1 to 0.04.

Whether or not the Sun has experienced main-sequence mass loss as proposed, recent observations of Li and Be abundances in A-G stars suggest that the simple explanation of convective depletion is inadequate. Boesgaard and Tripicco (1986) found that Hyades dwarfs with T_{eff} ~ 6600 K are depleted in ^{7}Li/H by over two orders of magnitude relative to stars with T_{eff} 300 K hotter or cooler. The minimum corresponds to mid-F spectral type, where the transition from rapid to slow rotation occurs (Boesgaard 1987a), and in the spectral-type region where main-sequence mass loss is proposed to operate. Li-deficient F stars are also present at the same T_{eff} in the Coma cluster (Boesgaard 1987b) and NGC 752 (Pilachowski and Hobbs 1988), but not in the Pleiades (Pilachowski, Booth and Hobbs 1987), suggesting that the deficiency develops after the stars are at least 10^8 years old. Boesgaard (1987b) also reports an Am star in the Coma cluster with ^{7}Li enhanced by a factor of 4.

Suggested explanations for this Li "gap" have included differential rotation and/or meridional circulation, convective overshoot, mass loss, and diffusion. These processes would have to operate in a narrow range of effective temperature. Michaud (1986) has shown that diffusion combined with mass loss at the low rate of 10^{-15} $M_\odot$/yr can produce a narrow Li-abundance gap. However, Boesgaard and Lavery (1986) find that Be-deficient stars are also Li-deficient, and that these deficiencies do not correlate with anomalies in other element abundances, which suggests that diffusion is not responsible. The ultimate resolution may require some combination of mass loss, diffusion, mixing, and production of Li.

4. Carbon and nitrogen

The carbon and nitrogen profiles of the mass-losing models differ markedly from the standard model. Figure 4 shows the log of the ^{12}C abundance by mass as a function of $M(r)/M_{\odot}$ for Model 1, Model 3 and the standard model at age 4.6 Gyr. The models presented have initial envelope abundance ratio $X(^{12}C)/X(^{14}N) = 3.07$, consistent with recent observational determinations (Bahcall et al. 1982). The surface ^{12}C and ^{14}N abundances of the mass-losing models at age 4.6 Gyr are only slightly different from their initial values. However, early partial CN-cycle processing in the mass-losing models causes substantial ^{12}C depletion and ^{14}N enhancement in the inner 0.50-0.60 $M_{\odot}$, while only the inner 0.15 $M_{\odot}$ is affected in the standard model. As the models begin their ascent of the red giant branch, CN-processed material is dredged to the surface earlier and affects the surface composition more dramatically in the mass-losing models. Table 6 lists the surface mass fractions of ^{12}C and ^{14}N, and the $X(^{12}C)/X(^{14}N)$ ratios before and after the first dredge-up phase. When the convective envelope reaches its maximum depth, mixing the upper three-fourths of the star's mass, the $X(^{12}C)/X(^{14}N)$ ratio decreases by a factor of 7-8 in the mass-losing models, but only by a factor of 1.6 in the standard model.

Early main-sequence mass loss may, in this manner, provide a viable explanation for the apparent mixing of more CN-processed material than predicted to the surface of some low-mass G and K giants Standard stellar models predict that mixing during first dredge-up in typical giants of mass $\geq 1\ M_{\odot}$ will lower the observed $^{12}C/^{13}C$ isotope (number) ratio from initial values of 40-90 to about 15-30, decrease the ^{12}C abundance by a factor of ~2, and increase the ^{14}N abundance by a factor of ~2.5 (Sneden and Pilachowski 1986). However, some cluster and field giants in both Population I and Population II exhibit anomalously low C/N ratios, and $^{12}C/^{13}C$ ratios approaching the CN-cycle equilibrium value of 3.4 (Dearborn, Eggleton and Schramm 1976; Lambert and Ries 1981; Sneden, Pilachowski and VandenBerg 1986).

Figure 4. ^{12}C mass fraction vs. mass zone for the standard model and mass-losing models at age 4.6 Gyr. The curve for Model 2 (not shown) lies between those of Models 1 and 3. The extension of the region of partial CN-cycle processing to mass 0.6 $M_{\odot}$ in the mass-losing models enables earlier and more pronounced dredge-up of CN-processed material, and may explain the low surface $^{12}C/^{14}N$ ratios observed in some low-mass G and K giants

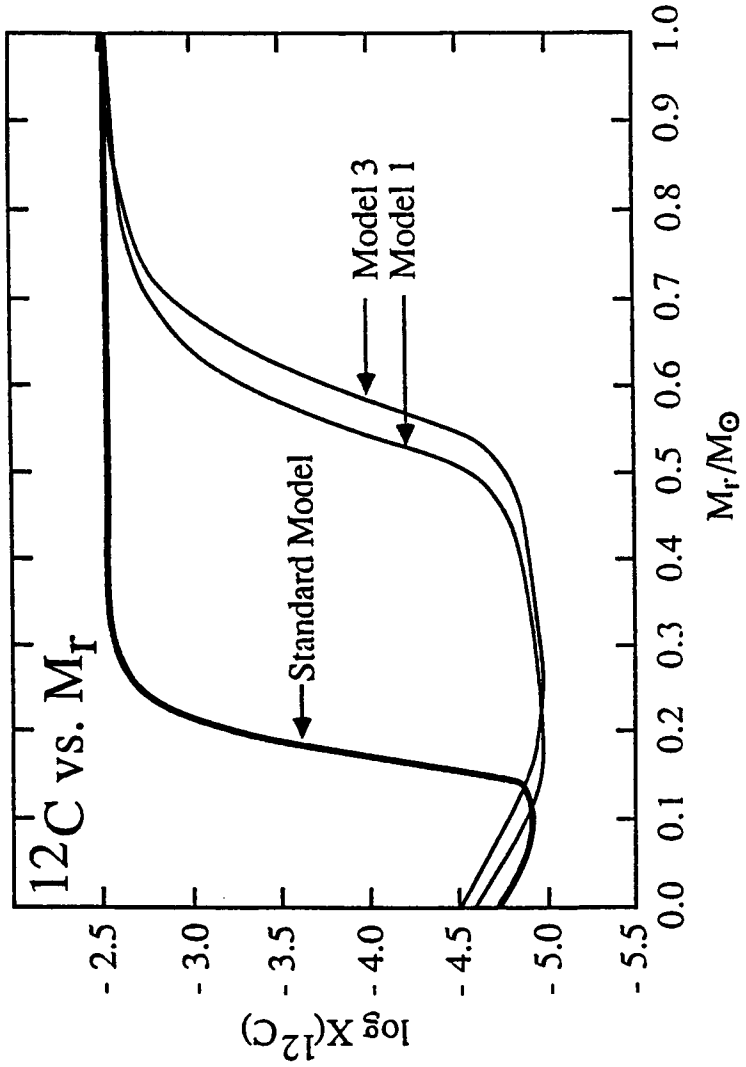

Table 6. Post main-sequence surface ^{12}C and ^{14}N abundances

	End of Main Sequence			End of First Dredge-Up		
	$X(^{12}C)$	$X(^{14}N)$	Ratio	$X(^{12}C)$	$X(^{14}N)$	Ratio
Standard	2.82	0.920	3.07	2.50	1.29	1.94
Model 1	2.76	0.989	2.79	1.12	2.90	0.386
Model 2	2.76	0.994	2.78	1.09	2.94	0.371
Model 3	2.73	1.02	2.68	1.00	3.04	0.329

Many explanations have been advanced to explain these anomalies. Dearborn, Eggleton and Schramm (1976) explored several causes, including hydrogen shell-burning instability, core He-flash, initial composition gradients, and mass loss during or immediately following the main-sequence phase. They find that the lowest observed $^{12}C/^{13}C$ and $^{12}C/^{14}N$ ratios among ~1 $M_\odot$ giants could be explained if these stars evolved from 2 $M_\odot$ progenitors which lost mass prior to ascending the first giant branch. Lambert and Ries (1981) support the idea of mixing between the core and outer convection zone during the main-sequence phase, arguing that unusually high mass-loss rates of 10^{-10} to 10^{-11} $M_\odot$/yr throughout the main-sequence phase are required to bring observations into agreement with model predictions. Scalo and Miller (1978) suggested that meridional circulation or shear instability due to differential rotation could produce the abundance anomalies.

A consensus is emerging in favor of additional mixing to explain the giants with low $^{12}C/^{13}C$ and C/N ratios, but a satisfactory mechanism has not been identified (Sneden, Pilachowski and VandenBerg 1986). Brown (1987) finds extra CN-processed material in the envelopes of stars beginning their ascent up the well-delineated giant branch of M67, ruling out core He-flash as the source of the anomalies. Scalo and Miller (1978) used the $^{12}C/^{13}C$ abundance distribution of 42 G-K giants to constrain the giant progenitor masses. For Galaxy age 9 Gyr, they find that giants with $^{12}C/^{13}C < 15$ must have progenitor masses < 1.7 $M_\odot$; to produce the observed fraction of giants with $^{12}C/^{13}C < 20$ requires that the progenitors have masses < 1.3 $M_\odot$. Allowing for the maximum possible statistical uncertainty in the giant abundance distribution raises the maximum masses to 2.3 and 1.5 $M_\odot$, respectively. Since the allowed progenitor masses are low (probably < 2 $M_\odot$), Miller and Scalo argued that mass loss, as proposed by Dearborn, Eggleton and Schramm (1976), is not responsible for the low $^{12}C/^{13}C$ ratios. Likewise, Miller and Scalo rule out meridional circulation, which is expected to be efficient only for stars of mass > 2-3 $M_\odot$. Their

derivation of progenitor masses depends upon the assumed stellar birthrate and initial mass function (which are not independent), and upon the Galaxy age. Accounting for main-sequence mass loss in the derivation of the initial mass function may flatten the slope of the IMF, and allow higher progenitor masses. Decreasing the assumed Galaxy age also increases the maximum progenitor mass.

It may be significant that the abundance anomalies appear almost exclusively in lower-mass G-K giants (Lambert and Ries 1981). Sneden and Pilachowski (1986) find normal $^{12}C/^{13}C$ isotopic ratios in cluster stars of NGC 7769 with a turnoff mass of 1.6 $M_\odot$. It is possible that the higher-mass giants have undergone little or no mass loss. Brown's (1987) finding that in M67 stars the dredge-up is complete at lower luminosities than predicted by models may also prove valuable in distinguishing between explanations.

5. Neutrino fluxes

An original motivation for evolving solar models with main-sequence mass loss was the possibility of solving the "solar neutrino problem" encountered in standard constant-mass evolution calculations. The ppIII chain, which depends very sensitively on temperature (~T^{19}), produces high-energy neutrinos from the decay of ^8B. These neutrinos, along with a fraction of the low-energy neutrinos from the ppII and CN cycles have been detected through absorptions on ^{37}Cl (Davis et al. 1983). Standard models predict fluxes at least several times higher than the measured value of 1.8 ± 0.3 SNUs (1 σ error), where 1 Solar Neutrino Unit = 10^{-36} absorptions/target ^{37}Cl atom/s.

We speculated that an early high-mass, high-luminosity phase might completely deplete the core hydrogen in the Sun, thereby reducing the central temperature and the ^8B neutrino flux. However, we found that we could not evolve models having 1 $L_\odot$ at age 4.6 billion years with cores devoid of hydrogen using any combination of initial mass and parametrization of mass-loss rate. When the duration of the high-mass phase is prolonged, the central molecular weight increases, particle

pressure is no longer able to support the core, and the central density and temperature increase; the luminosity then becomes too high. Increasing the initial hydrogen abundance lowers the final luminosity for the same mass-loss conditions, but then of course the central hydrogen is further from depleted. Hydrogen is not burned selectively in the central core; some hydrogen is depleted as far as 40% by mass from the solar center, which creates a smooth molecular-weight profile. Core convection also mixes in fresh hydrogen while the stellar mass is $\geq 1.3\ M_\odot$. While we have succeeded in steepening the hydrogen profile using a combination of mass loss and lower initial Y, it appears that a H/He composition profile cannot be evolved that differs substantially from that of the standard model.

The predicted neutrino flux for each of our models is given in Table 2. The mass-losing models predict PPIII neutrino fluxes up to twice as high as the standard model due to their hotter and denser cores. Standard solar models evolved with the Iben code using improved opacities and equation of state have higher initial Y abundance, and consequently very high predicted ^8B neutrino fluxes of 9.3 SNUs (Cox, Guzik and Kidman 1988).

Given the problems of standard solar models in reproducing observed neutrino fluxes, the mass-losing models should not be discarded for failing this test either. Several possibilities have recently been suggested to solve the solar neutrino problem. According to Dearborn, Marx and Ruff (1987), the Debye-Huckel approximation predicts that iron should precipitate in much of the solar interior. The reduced opacity would lower the central temperature and decrease the expected number of ^8B neutrinos. Faulkner and Gilliland (1985) find that weakly interacting massive particles (WIMPs) can efficiently transport energy from the solar interior, decreasing the central temperature and ^8B neutrino production. The presence of $10^{-8}\ M_\odot$ of 4 GeV WIMPS, or 1 WIMP per 10^{12} protons, would reduce the ^8B neutrino flux by a factor of three.

Alternatively, solar interior temperatures, and the neutrino

production rates, may be correct; the excess neutrinos may be undergoing transformations to other (undetected) types of particles, for example muon or tau neutrinos, before reaching the Earth. Neutrino transformations, or "oscillations", require that neutrinos have a small rest mass. Oscillations in a vacuum require large mixing angles between the electron, muon, and tau neutrino states, but large mixing angles are ruled out in accelerator experiments and not expected theoretically (Rosen 1988, private communication, Los Alamos National Laboritory). However, small mixing angles between the electron and muon neutrino can be enhanced by interactions with matter; with minor restrictions on mixing angle and mass difference between the muon and electron neutrino, essentially all of the ^8B neutrinos can be transformed to muon neutrinos before emerging from the Sun (Bethe 1986; Rosen and Gelb 1986).

6. Convection zones

The mass-losing models have fossil convective cores of 0.20-0.22 $M_\odot$. Since the convective core shrinks rapidly as mass loss proceeds, and disappears after 2-5 x 10^8 years, its influence is not readily apparent in the hydrogen profiles of the mass-losing models at age 4.6 Gyr. Evidence of the early presence of a convective core is more obvious near the 0.2 $M_\odot$ zone in the ^{12}C and ^{14}N profiles of the mass-losing models, as can be seen in Figure 4.

Tables 5a through 5d include the convective envelope mass of each model during its evolution. The convection zones are generally largest when the luminosity is lowest. For the mass-losing models, convective envelope masses are unavailable at early ages when the convective envelope lies entirely within the surface mass reservoir. The mass per zone at the base of the convective envelope is about 0.0006 for the standard model and Model 1, and about 0.0013 for Model 2 and Model 3; therefore the convective envelope masses cited in these tables are only accurate to about half of these zone-spacings.

The convection zone depth and temperature at the base of the

convection zone are given for each model in Table 3. Due to the larger mixing lengths required to evolve mass-losing models with radius 1 $R_\odot$ at age 4.6 Gyr, the surface convection zones of the mass-losing models are deeper than for the standard model. Observations of the high-degree five minute oscillations indicate that the depth of the Sun's surface convection zone is about 0.30 $R_\odot$ (Christensen-Dalsgaard et al. 1985); the convection-zone depths of the mass-losing models are between 0.264 and 0.282 $R_\odot$, in better agreement with this value than the depth calculated for the standard model, 0.245 $R_\odot$. Standard solar models recently evolved using the Iben code with improved analytical fits to the opacities and equation of state have a convection zone depth of 0.283 $R_\odot$, but still have p-mode frequencies averaging 5-10 μHz lower than observed (Cox, Guzik and Kidman 1988). Mass-losing solar models with updated opacities and equation of state are likely to have convective envelopes somewhat deeper than 0.30 $R_\odot$, which should further improve agreement of calculated p-mode frequencies with observations.

D. Conclusions

Solar models incorporating early main-sequence mass loss can be evolved to produce present-day solar models that do not differ drastically in structure and composition from standard solar models. The mass-losing models require slightly lower initial ^{4}He abundances, and higher mixing length than the standard model to attain 1 $L_\odot$ and 1 $R_\odot$ at age 4.6 Gyr. The mass-losing models also have steeper molecular-weight gradients, shorter main-sequence lifetimes, higher ^{8}B neutrino fluxes, deeper surface convection zones, higher surface ^{3}He abundances, and earlier, more pronounced dredge-up of CN-cycle processed material in the post-main sequence phase compared to the standard model. In addition, mass-losing models predict complete destruction of protosolar Li, Be, and B, requiring a mechanism, such as production in spallation reactions or flares, for partial replenishment to observed surface abundances.

Consideration of the structure and composition of the mass-losing models shows that they do not necessarily generate inconsistencies with observations in addition to those already encountered in standard constant-mass models. Mass-losing solar models hold promise for avoiding discrepancies between theory and observations regarding the depth of the solar convection zone, frequencies of p-mode oscillations, and abundances of Li, Be, and B. Main-sequence mass loss may explain the high abundances of CN-processed material in low-mass G-K giants following the first dredge-up. A potentially fatal flaw of the mass-losing solar models is the production of envelope ^{3}He in excess of the estimated solar photospheric abundance, but a decision based on this consideration alone would be premature given current confusion regarding stellar production/destruction of ^{3}He. None of the features of the mass-losing solar models provide reason to dismiss them from consideration as a possible alternative to conventional, constant-mass models.

E. Topics for Further Investigation

If the evidence from early solar system modeling continues to show promise and yields more definite constraints on the Sun's initial mass and mass-loss rate, it may be worthwhile to rerun the evolution calculations with improved opacities and equation of state, and subsequently calculate the predicted p-mode frequencies. The problems of high predicted ^{3}He abundance and total destruction of Li and Be in the mass-losing models also need to be addressed in more detail. Modeling stellar production of Li, Be, and B isotopes via spallation reactions, and depletion via convection, mass loss, and diffusion, constrained by recent determinations of light-element abundances in cluster and field stars would be an excellent first step.

III. CLUSTER HR DIAGRAMS

A. Evolution Modeling

Stellar evolution calculations incorporating early main-sequence mass loss were performed for a grid of models with a spectrum of initial masses and mass-loss timescales for the purpose of synthesizing cluster HR diagrams. The evolution calculations were conducted on the Los Alamos Cray computers using the Iben stellar evolution code as modified by Brunish according to the procedures for the solar evolution calculations described in Section II B. The mass-losing models have initial masses (M_o) 1.25, 1.5, 1.75 and 2.0 $M_\odot$, and lose mass with exponentially-decreasing mass-loss rates of characteristic e-folding time τ, evolving toward a final mass of 1 $M_\odot$. The stellar mass as a function of time is then

$$M(t) = 1.0 + (M_o - 1.0)\, e^{-t/\tau}\ M_\odot$$

The models were evolved for each of four mass-loss timescales: 0.2, 0.4, 1.0, and 2.0 Gyr. Six constant-mass models of initial masses 1.0, 1.25, 1.5, 1.75, 2.0, and 2.25 were also evolved for comparison. All models have initial ^{4}He mass fraction Y = 0.20 and initial metal abundance Z = 0.02, and are evolved with constant mixing-length/pressure scale height ratio α = 1.25. The models were evolved from the zero-age main sequence, where they have homogeneous composition, through the beginning of their ascent of the first-giant branch, until their luminosity reached ~ 16 $L_\odot$ and their radius reached ~ 6 $R_\odot$.

Figures 5 through 8 show the evolutionary tracks of each of the mass-losing models plotted on the theoretical HR diagram (log luminosity vs. log effective temperature); evolutionary tracks for the constant-mass models with the corresponding initial mass and target final mass (1 $M_\odot$) are also plotted for comparison. The features of the evolution tracks are characterized by the length of the mass-loss timescale compared to the evolution timescale (i.e., main-sequence lifetime). For the shortest mass-loss timescales, 0.2 Gyr (Figure 5) and 0.4 Gyr (Figure 6), all of the mass-losing models, regardless of initial

mass, follow the usual constant-mass main sequence closely as they evolve down; shortly after reaching 1 $M_\odot$, their evolutionary tracks are nearly indistinguishable from the constant 1 $M_\odot$ model track for the remainder of main-sequence evolution and the first giant-branch ascent.

For mass-loss timescale 1 Gyr (Figure 7), the mass-losing models of initial mass 1.25 and 1.5 $M_\odot$ also evolve down the normal main sequence, and behave like 1 $M_\odot$ stars when their mass loss ceases. However, for the 1.75 and 2.0 $M_\odot$ models, the mass-loss timescale is approaching a significant fraction of the main-sequence lifetime, such that evolution away from the main sequence begins to compete with evolution down the main sequence; the tracks consequently veer perceptibly to the right as well as downward, and lie slightly above the 1 $M_\odot$ track during evolution across to the giant branch. The 2.0 $M_\odot$ model even retains a trace of the blueward hook present at the end of the main-sequence lifetimes of stars of mass ≥ 1.2 $M_\odot$; the leftward hook occurs due to rapid readjustment of the star's structure following core hydrogen exhaustion, in preparation for shell burning of the hydrogen left behind during the shrinking of the convective core. All of the models do manage to reach the target mass of 1 $M_\odot$ before evolving off of the main sequence.

Finally, for the longest mass-loss timescale considered, 2 Gyr (Figure 8), the 1.25 $M_\odot$ model behaves generally as before, but the 1.5 $M_\odot$ model begins to deviate to the right of the main sequence as it evolves down, and fails to join the 1 $M_\odot$ track as it evolves redward toward the giant branch. The 1.75 $M_\odot$ model has sufficient time to reach only 1.3 $M_\odot$ before it evolves off the main sequence, tracing a small blueward hook as it leaves. The 2.0 $M_\odot$ model manages to evolve down to only 1.5 $M_\odot$ before exhausting its core hydrogen, tracing a blueward hook comparable in size to that of a constant-mass 1.5 $M_\odot$ star.

Table 7 lists the main-sequence lifetimes of each model. The end of the main sequence is defined as the time corresponding to the bluest (highest effective temperature) point in evolution following mass loss

for the models without blueward hooks. For the models with blueward hooks, the table records the time at which the reddest and bluest point in the hook is reached. Figure 9 shows the main-sequence lifetimes versus initial mass for each model. The main-sequence lifetime of a 1 $M_\odot$ star that experienced a short epoch of early main-sequence mass loss ($\tau \sim 0.2$ Gyr) is reduced by $\leq 30\%$ from the lifetime of a constant-mass 1 $M_\odot$ star. The main-sequence lifetime of a star of final mass 1 $M_\odot$ can be decreased by as much as 70% due to early H-burning at higher mass if the mass-loss rates are lower (e.g., $\tau = 1$ Gyr).

B. Cluster Synthesis Procedures

In order to effectively cover the mass spectrum of stars formed in clusters, evolutionary tracks of mass-losing and constant-mass models were interpolated from the calculated models in increments of 0.05 $M_\odot$. Thus 22 models were actually evolved, and from these 64 mass-losing models and 20 constant-mass models were interpolated. The interpolation was done using Akima (shape-preserving) cubic splines. While the highest-mass star in the interpolation was still on the main sequence, the luminosity, effective temperature, and radius were interpolated at fixed time given the initial mass. Post-main sequence evolution was interpolated using reference points on the evolutionary tracks to determine the luminosity, effective temperature, radius, and time where these points were reached, given the initial mass. The points used depended upon the initial masses and the mass-loss timescales of models being interpolated, and included some combination of the main sequence luminosity minimum, the bluest point after the stars reached 1 $M_\odot$, the tips of the blueward hooks, the midpoint of the horizontal crossing to the giant branch, the base of the giant branch, or the point where $\log L/L_\odot = 1.2$ on the giant branch is reached. The mass, luminosity, effective temperature, and radius of every model was eventually obtained at fixed times spaced 0.1 Gyr apart The data were then downloaded from the NAS 9160 to a Hypercard™ program, written by Thomas Beach, on a Macintosh™ personal

Figure 5. Theoretical evolutionary tracks of mass-losing models with exponentially decreasing mass-loss rate of timescale 0.2 Gyr. The evolutionary track of the constant-mass model with the same initial mass and of the 1 $M_\odot$ model are also shown for reference

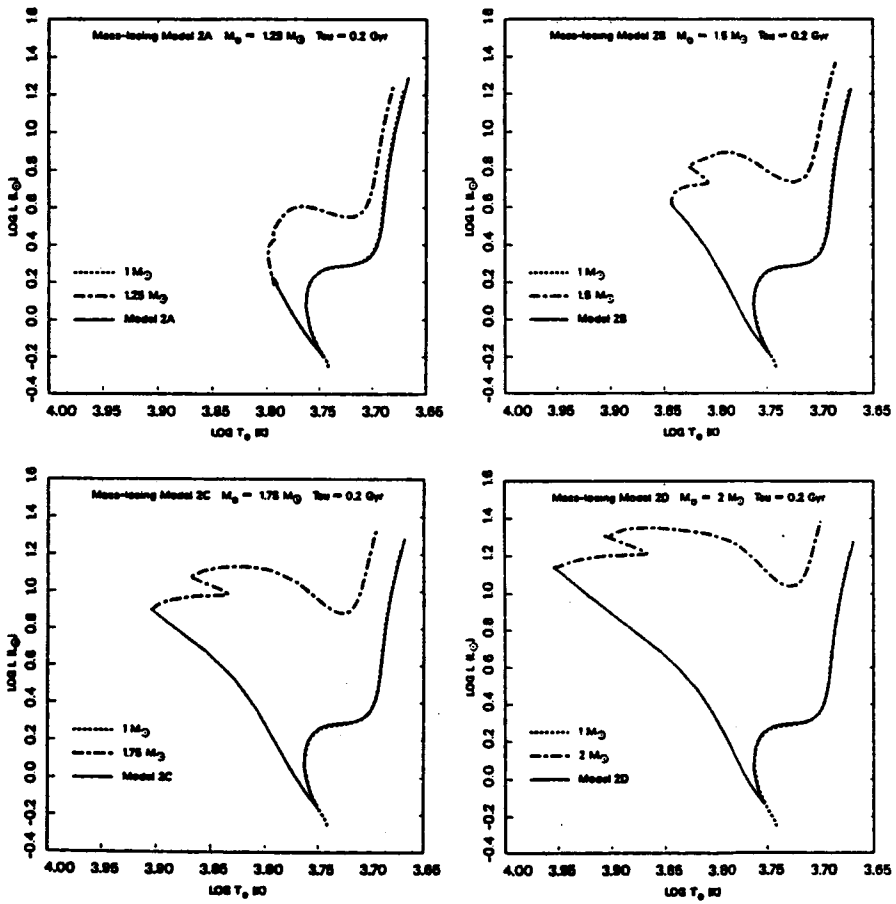

Figure 6. Theoretical evolutionary tracks of mass-losing models with exponentially decreasing mass-loss rate of timescale 0.4 Gyr. The evolutionary track of the constant-mass model with the same initial mass and of the 1 $M_\odot$ model are also shown for reference

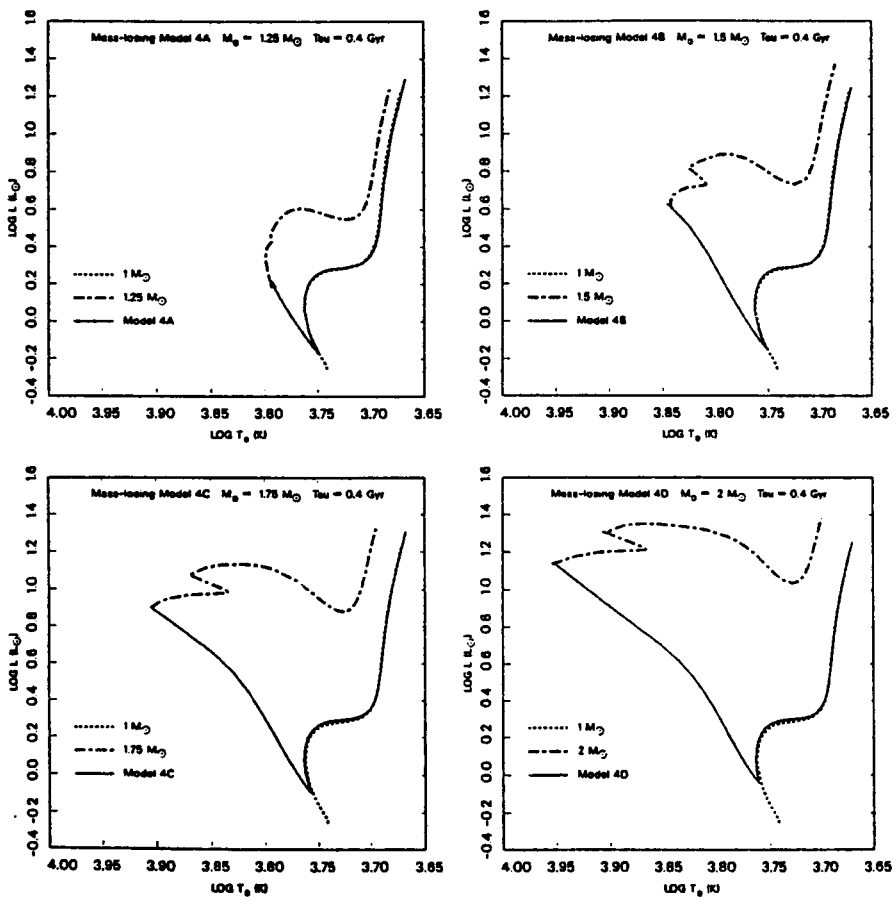

Figure 7. Theoretical evolutionary tracks of mass-losing models with exponentially decreasing mass-loss rate of timescale 1.0 Gyr. The evolutionary track of the constant-mass model with the same initial mass and of the 1 $M_\odot$ model are also shown for reference

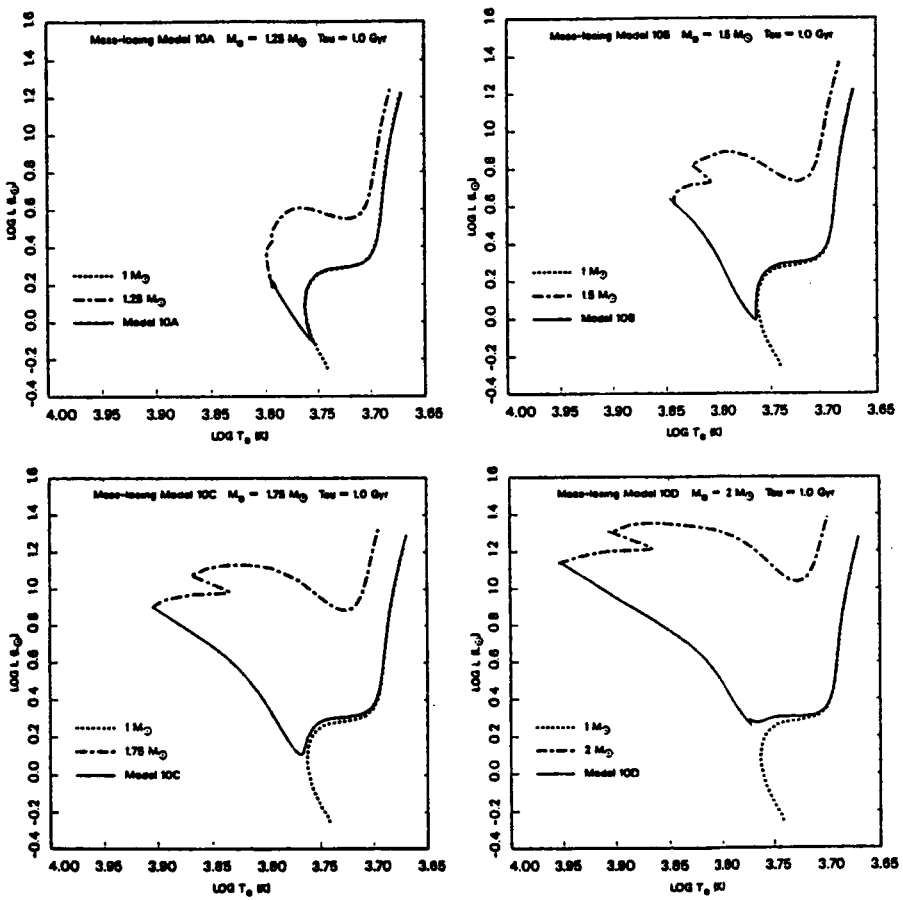

Figure 8. Theoretical evolutionary tracks of mass-losing models with exponentially decreasing mass-loss rate of timescale 2.0 Gyr. The evolutionary track of the constant-mass model with the same initial mass and of the 1 $M_\odot$ model are also shown for reference

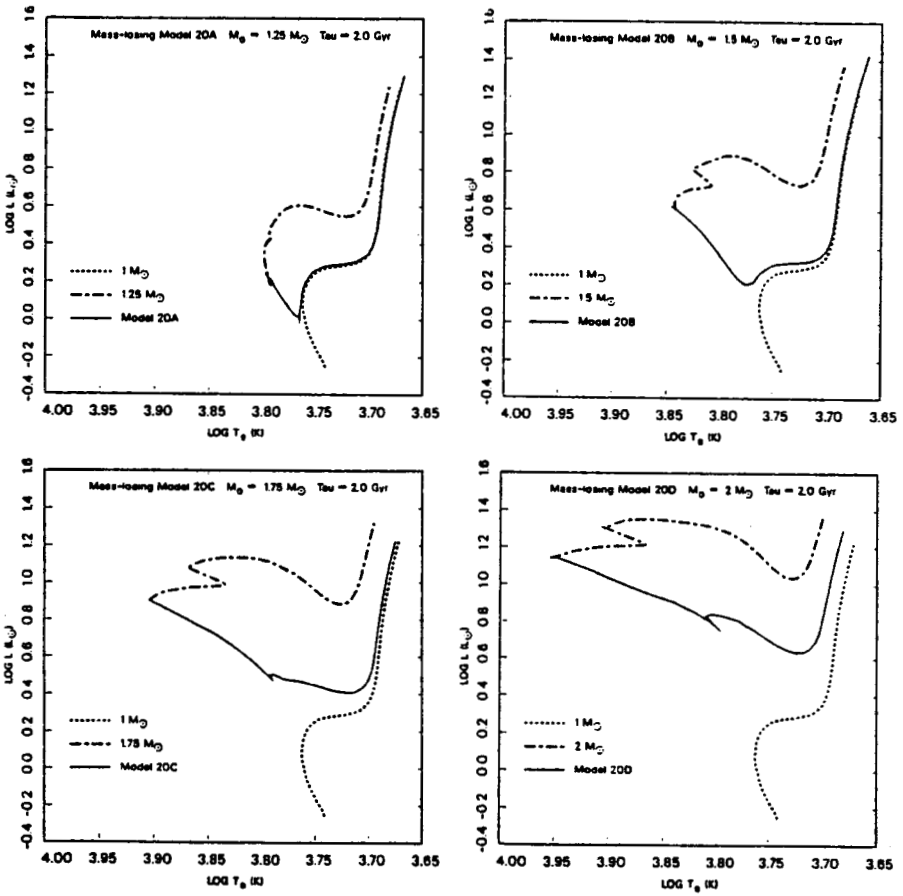

Table 7. Main-sequence lifetimes of constant-mass and mass-losing models

Initial Mass ($M_\odot$)	Mass-Loss Timescale (Gyr) 0	2.0	1.0	0.4	0.2
1.00	11.3				
1.25	R4.20 B4.42	7.89	9.19	10.2	10.5
1.50	R2.32 B2.41	E5.21	6.97	9.06	9.96
1.75	R1.41 B1.47	R2.18 B2.38	E4.35	7.48	8.93
2.00	R0.979 B1.003	R1.39 B1.45	R2.53 B2.69	5.88	7.97
2.25	R0.705 B0.723				

R Reddest point in hook at end of main-sequence evolution.
B Bluest point in hook at end of main-sequence evolution.
E Estimated reddest point at end of main-sequence evolution.

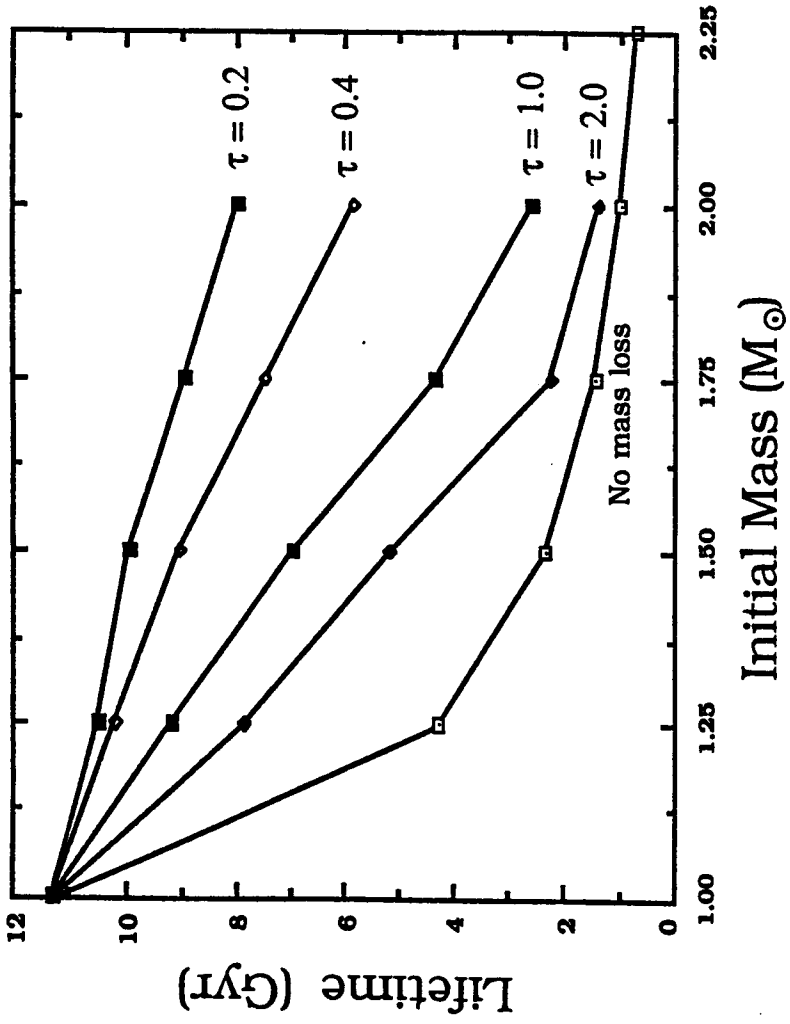

Figure 9. Main-sequence lifetimes of evolved models

computer, in which the evolutionary sequence could be previewed, and the luminosity and effective temperatures of the interpolated models adjusted slightly to correct problems at discontinuities in the interpolation. This software, and the data from the interpolated models, is available from the author.

Since observational HR-diagrams plot visual magnitude versus B-V or b-y color, rather than log L versus log T_{eff}, the theoretical data must be transferred to the color-magnitude plane. This was accomplished by using Akima bicubic splines to interpolate the bolometric correction and B-V color from tables of these quantities for solar-metallicity stars of specified surface gravity and T_{eff}. The tables were compiled from those of VandenBerg (1983) for stars with $4000 \leq T_{eff} \leq 8000$ K and of Buser and Kurucz (1978) for early-type stars of $T_{eff} \geq 8000$ K. The visual magnitude of a star is then obtained from the luminosity and bolometric correction by the formula

$$M_V = 4.72 - 2.5 \text{ Log } (L/L_\odot) - BC.$$

Once transferred to the color-magnitude plane, the points are duplicated in proportion to a Salpeter (1955) initial mass function $\phi(m) = N\, m^{-2.35}$, where m is the initial mass and N is a normalization constant. The synthesized clusters presented here use N=10, so for example 10 stars of 1 $M_\odot$, 3 stars of 1.5 $M_\odot$, and only 1 star of 2.25 $M_\odot$ are plotted per cluster. Finally, a degree of randomness is introduced into the color and magnitude values to prevent points from overlapping completely or lining up like beads-on-a-string, thus making the diagrams appear more like color-magnitude diagrams of observed clusters. Clusters exhibit intrinsic scatter for a number of reasons beyond purely photometric errors, for example varying degrees of rotation and undistinguished binaries, which scatter cluster stars to the right of the theoretical main sequence (Maeder 1974), and possibly for more exotic reasons, such as non-coeval star formation, mass transfer in binaries, mixing, mass loss, or surface composition anomalies. The B-V color in the synthesized clusters is allowed to vary by either 2 or 4%;

the smaller value is used when two or more cluster diagrams are superimposed to enhance distinguishability. M_V is allowed to vary by 3%; the scatter in this direction helps to fill in gaps between models at discrete masses. Percentage errors were used rather than absolute errors for two reasons: First, the highest luminosity stars considered would be expected to have the smallest photometric errors. These stars fortuitously have the smallest B-V and M_V, and therefore the smallest scatter calculated percentage-wise. The giants also have small M_V, but large B-V; their horizontal scatter would be expected to be large due to larger errors in bolometric correction. Second, the small-number statistics of the upper main-sequence stars due to the decreasing initial mass function make it desirable for these stars to be situated closer to their actual position.

C. Discussion of Synthesized Clusters

While looking through a time series of C-M plots for each mass-loss timescale is quite interesting, space does not permit the inclusion of so many figures. Instead, C-M diagrams at representative times showing the essential differences between cluster diagrams with and without mass loss and highlighting interesting features are presented and discussed. Where possible and informative, several cluster diagrams of different mass-loss timescales are superimposed, and some diagrams are reduced and placed side-by-side on the same page for ease of comparison. Each diagram includes stars between 1.0 and 2.25 $M_\odot$; only the stars between 1.0 and 2.0 $M_\odot$ are assumed to undergo mass loss. The zero-age main sequence is plotted as a connected solid line on each figure for reference.

Figure 10 shows the distribution of stars along the zero-age main sequence (cluster age t=0) for orientation. Despite the mass interpolations and randomness introduced, the mass intervals between points are sometimes visible, especially around B-V = +0.4, or mid-F spectral type, where the B-V color varies rapidly with mass. This sparseness around B-V = +0.4 is also visible in C-M diagrams of actual

clusters, e.g., NGC 6192 (see Figure 23).

Figure 11 shows C-M diagrams with main-sequence mass loss for each mass-loss timescale at cluster age 0.3 Gyr. The stars at the top of the clusters are the non-mass-losing stars of 2.05 to 2.25 $M_\odot$. A large main-sequence gap of width 0.3 in B-V develops by this age for cluster with the shortest mass-loss timescale τ = 0.2 Gyr. The gap is more modest, 0.2 and 0.1 in B-V for the clusters with 0.4 and 1.0 Gyr mass-loss timescales, respectively. The gap is barely noticable for the cluster with the 2.0 Gyr mass-loss timescale.

Figure 12 shows C-M diagrams with main-sequence mass loss for each mass-loss timescale at a later age, 0.6 Gyr. Gaps have appeared in the main sequence of all of the clusters, of widths 0.4, 0.3, 0.15, and 0.1 in B-V for clusters with mass-loss timescales 0.2, 0.4, 1.0, and 2.0 Gyr, respectively. The stars of mass $\geq$ 2.05 $M_\odot$ with main-sequence lifetimes of only 0.7 to 0.9 Gyr have evolved noticeably rightward. Possible giants in such a clusters would have masses $\geq$ 2.25 $M_\odot$.

Shortly after age 0.6 Gyr, the 2.05 to 2.25 $M_\odot$ stars disappear. For the clusters with the smallest mass-loss timescales, 0.2 and 0.4 Gyr, the main-sequence gaps widen further, and the stars pile up at ~ 1 $M_\odot$ near B-V = +0.65, until the stars with the highest-mass progenitors evolve off of the main sequence; this does not happen until about age 5.5 Gyr. Between ages 1 and 6 Gyr, these clusters would appear to have a truncated main sequence, with little hint of a turnoff, possibly a noticable overabundance of 1 $M_\odot$ stars, and a dearth of red giants. Stars of initial mass 1-2 $M_\odot$ that lost mass slowly or not at all may be labeled "blue-stragglers", and would be the only source for populating the giant branch. At age 6 Gyr, the cluster may develop a definite turnoff; if dated by its main-sequence turnoff assuming constant-mass stellar evolution, the cluster would appear to be over 10 Gyr old.

Figure 13 shows superimposed synthesized clusters of age 1.3 Gyr with no mass loss, and with mass-loss timescales 1.0 and 2.0 Gyr. The turnoff mass for the cluster without main-sequence mass loss is 1.95 $M_\odot$. The upper main-sequence of the clusters with mass loss curve

redward, characteristic of a cluster turnoff, but none of the mass-losing stars have had sufficient time to become red giants. The cluster with the longest mass-loss timescale would have an apparent age deduced from the false main-sequence turnoff of 2.1 Gyr, while the cluster with more rapid mass loss would have an apparent age of 3.2 Gyr. Any giants or blue stragglers associated with these clusters would arise from stars less massive than 1.95 $M_\odot$ which lost mass slowly or not at all.

Figure 14 shows the same clusters at age 2.0 Gyr. The cluster turnoff for the cluster without mass loss is now at 1.65 $M_\odot$. The gap in the main sequence between B-V = +0.3 and +0.4 is due to rapid evolution through the blueward hook as high-mass stars exhaust the hydrogen in their fossil convective cores, and reminds us to exercise caution in interpreting gaps. The cluster with mass-loss timescale 2 Gyr appears from its turnoff at 1.34 $M_\odot$ to be 3-4 Gyr old, while the cluster with mass-loss timescale 1 Gyr appears from its turnoff at 1.14 $M_\odot$ to be ~7 Gyr old. The cluster with mass-loss timescale 2 Gyr is beginning to produce giants from mass-losing stars.

By age 3.0 Gyr (Figure 15), the turnoff has shifted downward to 1.65 $M_\odot$ for the cluster without mass loss. The clusters with mass-loss timescales 2 and 1 Gyr now have respective turnoff masses of 1.18 and 1.05 $M_\odot$, yielding apparent ages of ~7 and ~10 Gyr, respectively. The cluster with τ = 2 Gyr has a well-defined giant branch, while stars of initial mass = 2 $M_\odot$ have just managed to evolve off of the main sequence for the cluster with τ = 1 Gyr. By age 6 Gyr (Figure 16), all of the clusters have well-defined turnoffs and giant branches. The turnoff mass for the cluster without mass loss is now 1.25 $M_\odot$. The clusters with mass loss have apparent turnoffs at 1.03 and 1.00 $M_\odot$, and ages deduced from these turnoffs of 9-11 Gyr.

Unfortunately, it is difficult to compare these cluster C-M diagrams to actual clusters. The majority of the mass-losing stars in these evolution calculations rapidly evolve down to final mass 1.0 $M_\odot$, producing clusters with apparent ages greater than 5 Gyr. There exist very few observable Galactic clusters of solar metallicity that appear this

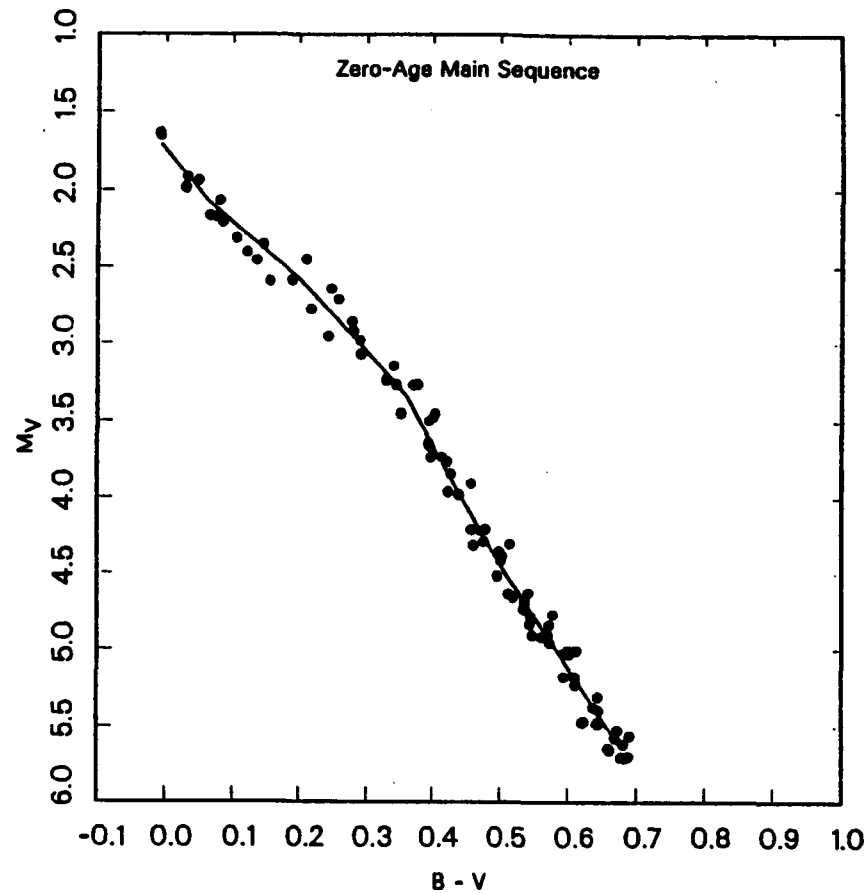

Figure 10. Color-magnitude diagram of synthesized cluster at time t = 0, including stars of mass 1.0 to 2.25 $M_\odot$

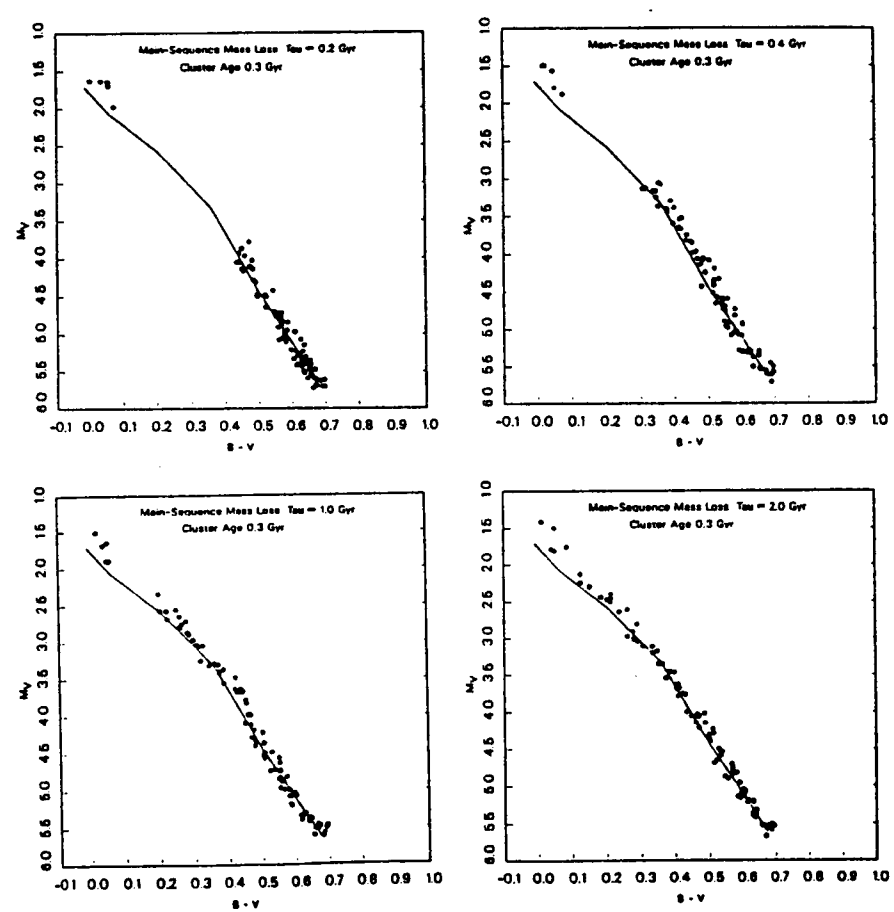

Figure 11. Color-magnitude diagrams of synthesized clusters at age 0.3 Gyr. Stars of initial mass 1.0 to 2.0 $M_\odot$ are assumed to lose mass with exponentially decreasing mass-loss rates of timescale 0.2 (upper left), 0.4 (upper right), 1.0 (lower left), and 2.0 (lower right) Gyr. Stars of initial mass 2.05 to 2.25 $M_\odot$ are assumed to evolve at constant mass. The solid line marks the position of the zero-age main sequence

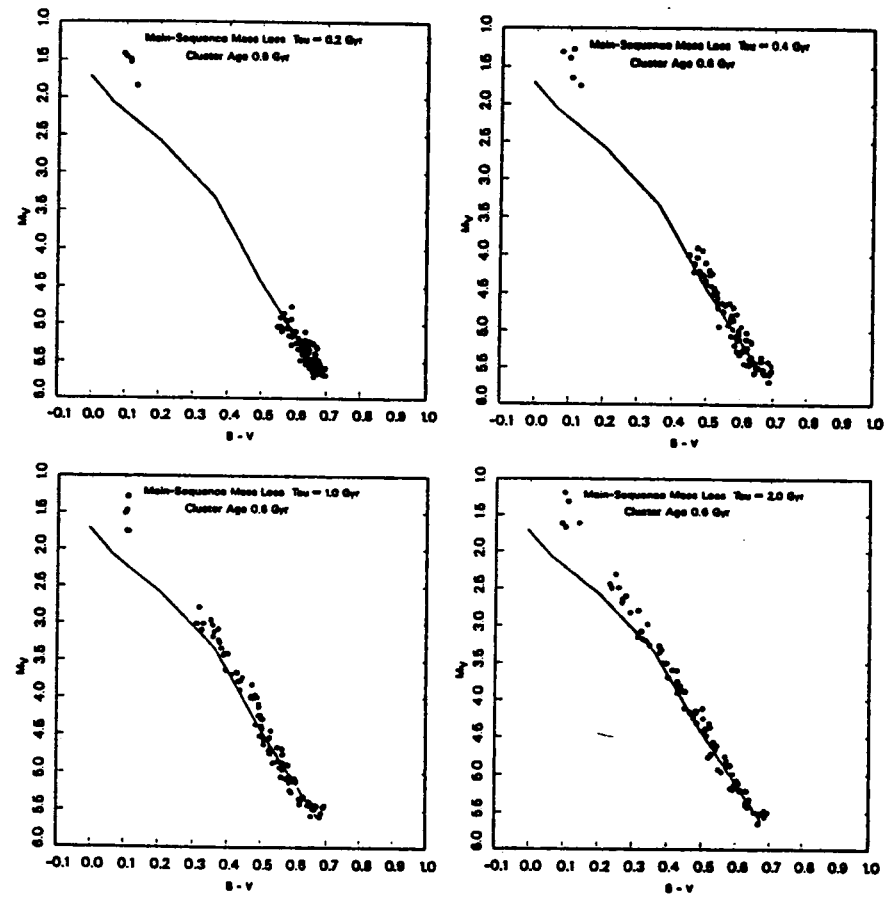

Figure 12. Color-magnitude diagrams of synthesized clusters at age 0.6 Gyr. Stars of initial mass 1.0 to 2.0 $M_\odot$ are assumed to lose mass with exponentially decreasing mass-loss rates of timescale 0.2 (upper left), 0.4 (upper right), 1.0 (lower left), and 2.0 (lower right) Gyr. Stars of initial mass 2.05 to 2.25 $M_\odot$ are assumed to evolve at constant mass. The solid line marks the position of the zero-age main sequence

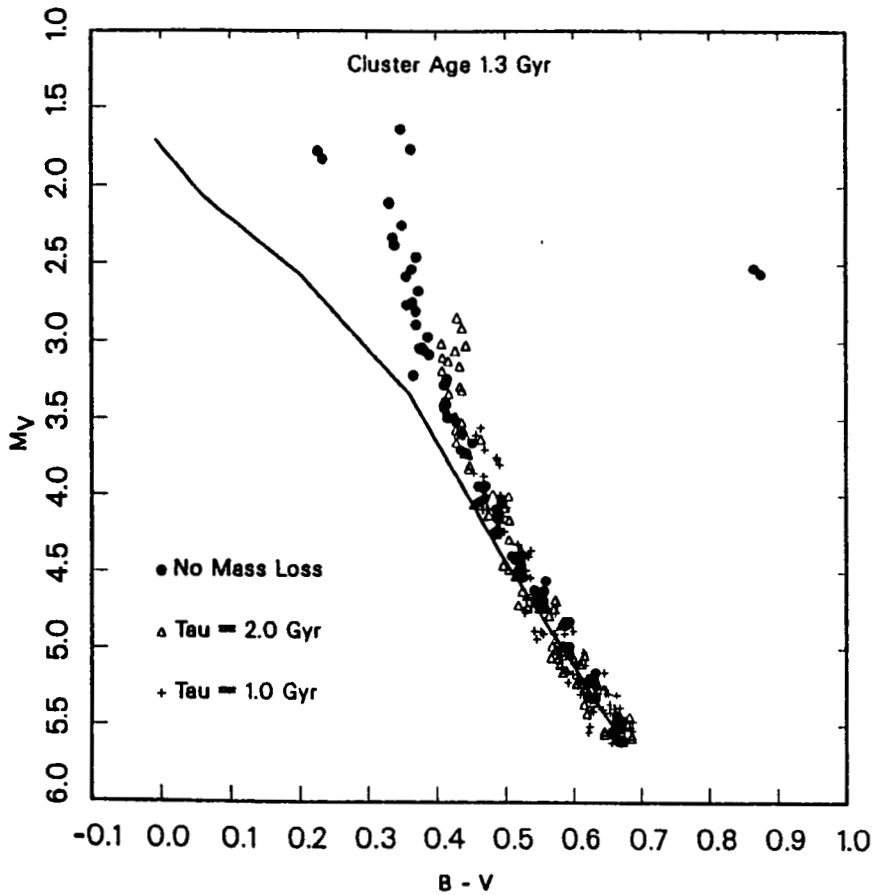

Figure 13. Color-magnitude diagram of synthesized clusters at age 1.3 Gyr. The synthesized clusters with no mass loss, and with exponentially decreasing mass-loss rates of timescale 1.0 and 2.0 Gyr are superimposed. The solid line marks the position of the zero-age main sequence

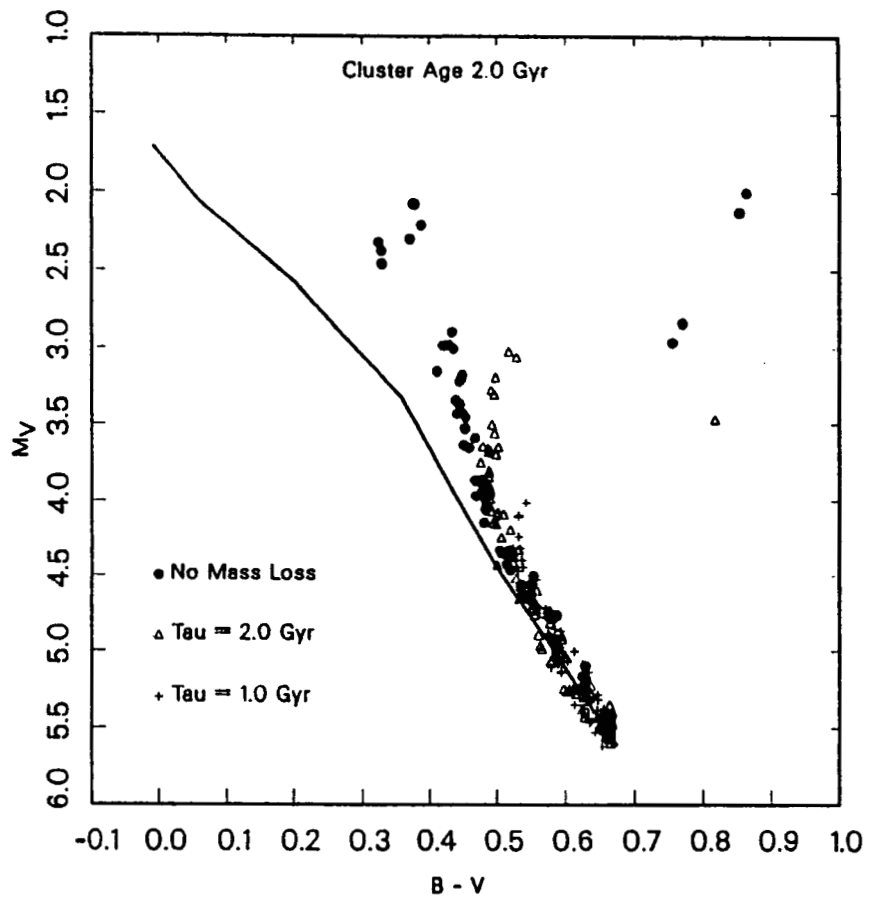

Figure 14. Color-magnitude diagram of synthesized clusters at age 2.0 Gyr. The synthesized clusters with no mass loss, and with exponentially decreasing mass-loss rates of timescale 1.0 and 2.0 Gyr are superimposed. The solid line marks the position of the zero-age main sequence

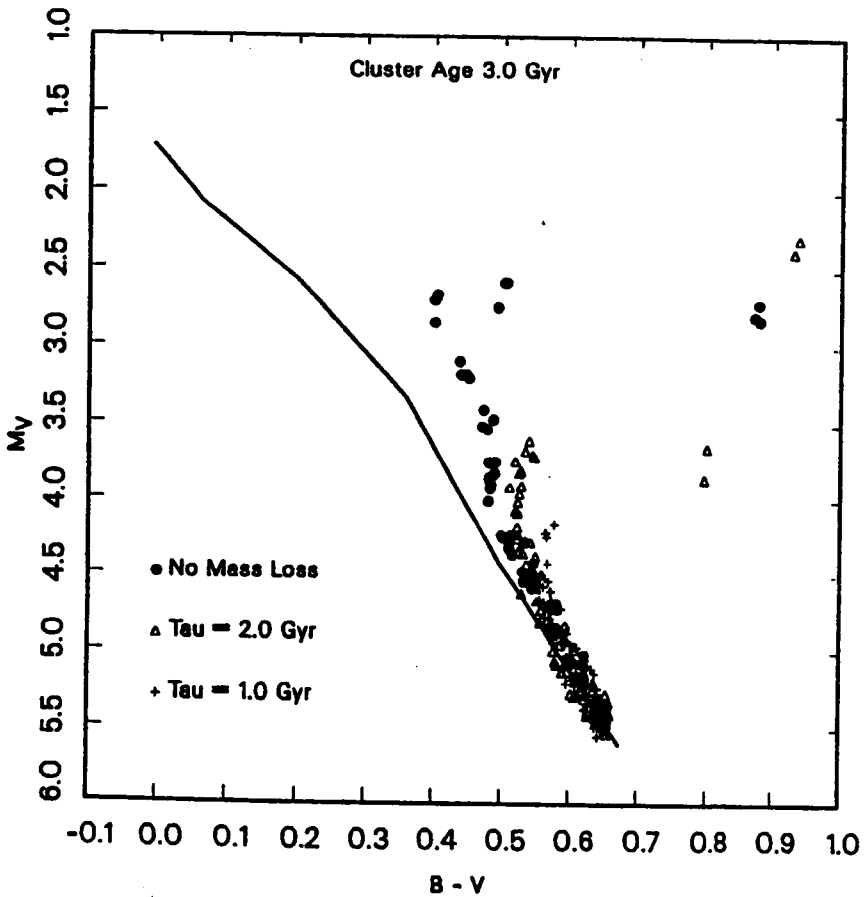

Figure 15. Color-magnitude diagram of synthesized clusters at age 3.0 Gyr. The synthesized clusters with no mass loss, and with exponentially decreasing mass-loss rates of timescale 1.0 and 2.0 Gyr are superimposed. The solid line marks the position of the zero-age main sequence

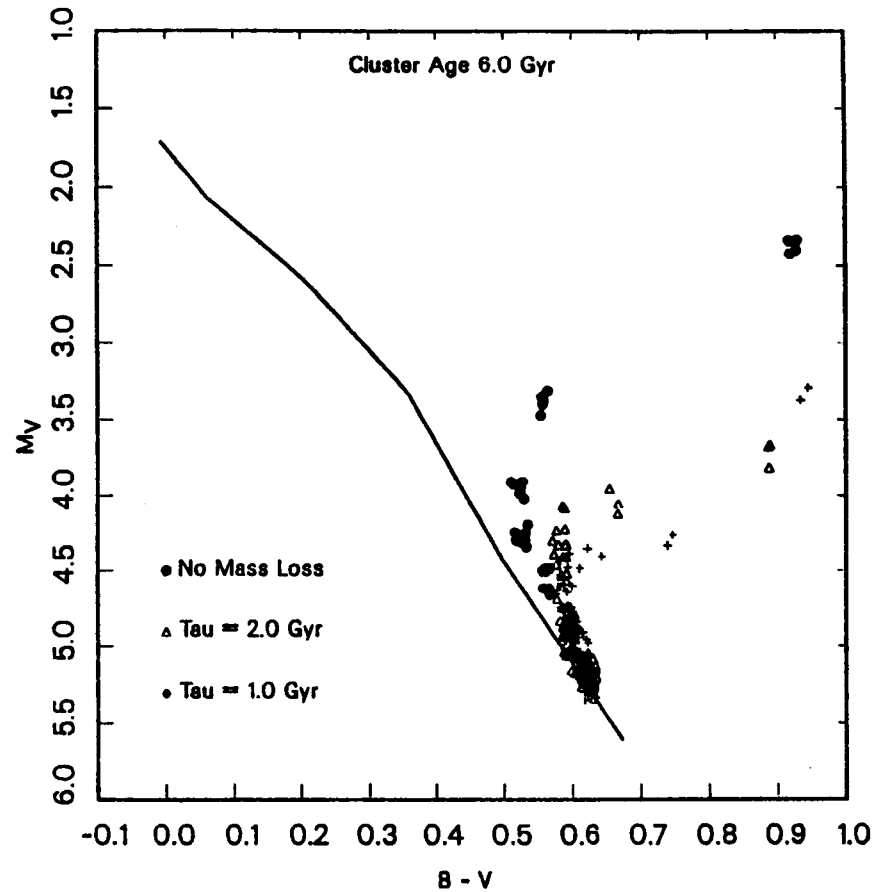

Figure 16. Color-magnitude diagram of synthesized clusters at age 6.0 Gyr. The synthesized clusters with no mass loss, and with exponentially decreasing mass-loss rates of timescale 1.0 and 2.0 Gyr are superimposed. The solid line marks the position of the zero-age main sequence

old, perhaps only two–NGC 188 and M67. In the future, it might be preferrable to calculate evolutionary tracks of Population II (low-Z) stars for comparison with globular cluster HR diagrams; solar-composition diagrams are not useful due to the very different turnoff and giant branch morphology of low-Z clusters, as well as the different mass to spectral-type correspondence, and onset points of core and envelope convection. Alternatively, it would have been useful to increase the target mass slightly, and/or increase the mass-loss timescales to produce more interesting cluster turnoffs of more-relevant apparent ages (< 5 Gyr). Most older Population I clusters have turnoff masses of 1.2-1.5 $M_\odot$. Also, the upper mass-cutoff for main-sequence mass loss could have been extended up to, or even beyond spectral type A0, which corresponds to 2.25 $M_\odot$ for solar composition. However, the cluster HR diagrams presented here do serve to illustrate qualitatively the features produced with the inclusion of main-sequence mass loss, in particular, gaps, blue stragglers, false turnoffs, and multiple turnoffs, and assist in estimating the mass-loss rates required to produce these characteristics.

D. Comparison to Observed Clusters

A search was conducted of the recent astrophysical literature (post-1980) to locate HR diagrams of clusters satisfying the following criteria: 1) Age deduced from turnoff greater than ~ 0.3 Gyr; 2) Population I metallicity; 3) Reasonably well-populated; 4) Well-defined main sequence below the turnoff. Seventeen clusters will be discussed, several in each of five age groups: several times 10^8 yr (Group I), ~10^9 yr (Group II), ~2 x 10^9 yr (Group III), ~3 x 10^9 yr (Group IV), and > 5 x 10^9 yr (Group V). Table 8 lists the distance moduli, ages and metallicities of these clusters. This list of clusters satisfying the above criteria is not exhaustive, but is intended to be representative. There is conceivably some bias toward clusters with anomalies, as these may have been studied with more interest recently.

Table 8. Distance moduli, ages, and metallicities of Galactic clusters

Cluster	m-M[a]	Age (Gyr)[b]	$[Fe/H]_\odot$[c]
Hyades	3.2	0.29-0.97	0.2
Praesepe	6.0	0.9	0.2
M39	7.4	0.2-0.4	0.2
NGC 2567	11.0	0.29	0.0
NGC 5822	9.5	1.0	0.1
NGC 2360	10.3	1.3	-0.07
NGC 6192	10.0	1.3	~0.0
NGC 7789	12.3	1.6	-0.05
NGC 752	8.2	2.2	-0.13
NGC 3680	9.5	1.5-2.5	0.0
NGC 2158	14.4	3.0	-0.46
NGC 2204	13.1	2.5	-0.4
NGC 2420	11.4	3.3	-0.3
NGC 2506	12.2	3.4	-0.35
Melotte 66	13.0	6.0	-0.7
M 67	9.6	5.0	-0.06
NGC 188	11.1	10	0.0

[a] (m-M) = 5.0 log (D/10), where D is the cluster distance in parsecs.

[b] Cluster ages deduced from isochrone fits or color of stars at main-sequence turnoff.

[c] $[Fe/H]_\odot = \log(Fe/H_{cluster} - Fe/H_{Sun})$. It is assumed that $Z_\odot$=0.017 (Ross and Aller 1976), and Z_{Hyades}=0.027.

1. Group I

This group includes the Hyades, Praesepe (NGC 2632, M44), M39 (NGC 7092), and NGC 2567, which have turnoffs at spectral type early- to mid-A.

a. The Hyades Figure 17 shows an M_V vs. b-y diagram by Eggen (1982) of the Hyades supercluster, which includes both stars associated in space and determined kinematically to be Hyades members. The diagram exhibits a very broad upper main-sequence and three blue stragglers with b-y ~ -0.1 (spectral type late B). Fitting the turnoff to the blue stragglers yields a cluster age of 2.4×10^8 yr, while the stars at the top of the main sequence could be fit by evolved 2.5 $M_\odot$ A1 stars with an age spread from 2.6 and 9.7×10^8 yr (Eggen 1982). Demarque (1980) lists the age of the Hyades as 0.7 Gyr.

Can the blue stragglers and the broad upper main-sequence be explained in terms of the main-sequence mass loss hypothesis? It should be remembered that the Hyades metallicity $[Fe/H]_\odot = 0.2$ (Demarque 1980) is greater than solar; thus stars of spectral type A have higher masses than those in the synthesized clusters with Z=0.02. The three blue stragglers are an Ap star, an eclipsing binary, and an Hg-Mn peculiar star with variable radial velocity. Eggen (1982) notes that there are abundant examples to "make it likely that the A(B)p and blue straggler phenomena are syndromes if not causata." Eggen (1982) also observes that the blue straggler in an eclipsing binary has a 1.75 $M_\odot$ companion that falls on the 1.75 $M_\odot$ evolutionary track, indicating that mass transfer is an unlikely explanation. In the context of the main-sequence mass loss hypothesis, these blue stragglers may be stars that didn't lose mass because they were born with slow rotation rates; the spectral peculiarities, and/or the presence of binary companions may be associated with this slow rotation. Alternatively, the stragglers may have failed to lose mass because they are located to the left of the blue edge of the pulsation-instability strip.

If the blue stragglers represent the true main-sequence turnoff, the Hyades age would be 2.4×10^8 yr; the gap between the stragglers and

Figure 17. Color-magnitude diagrams of the Hyades group by Eggen (1982). The open circles are members of the cluster nucleus, while the crosses are members of the extended cluster. The top diagram shows the upper main-sequence with superimposed constant-mass evolutionary tracks (solid lines) and theoretical isochrones (dashed lines). Three blue stragglers are evident near b-y = -0.1

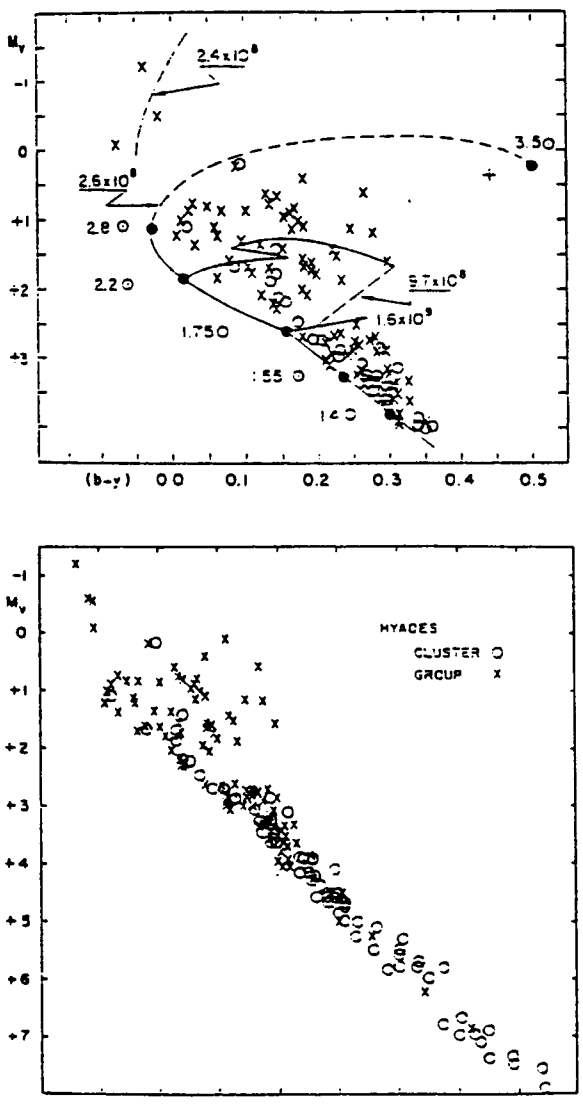

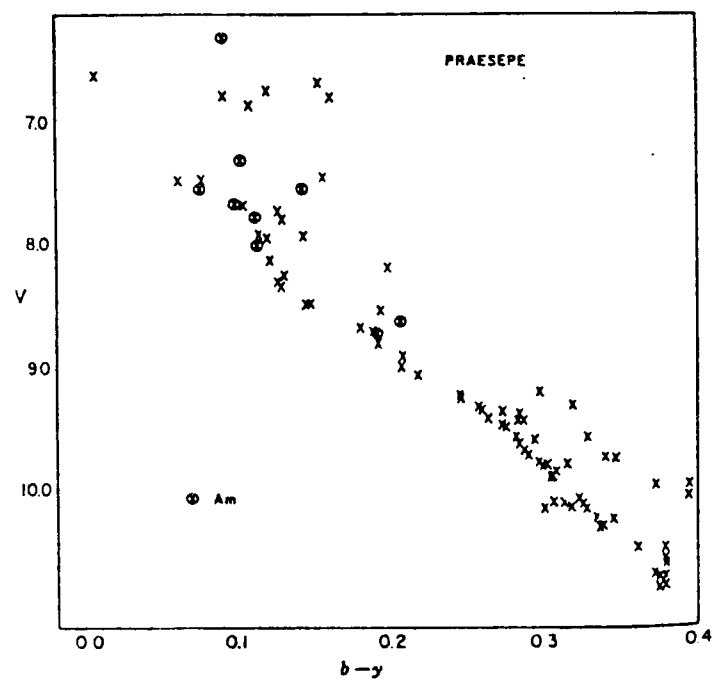

Figure 18. Praescpe color-magnitude diagram from Crawford and Barnes (1969). The circled crosses are metallic-lined Am stars. Praesepe has one blue straggler near b-y = +0.0

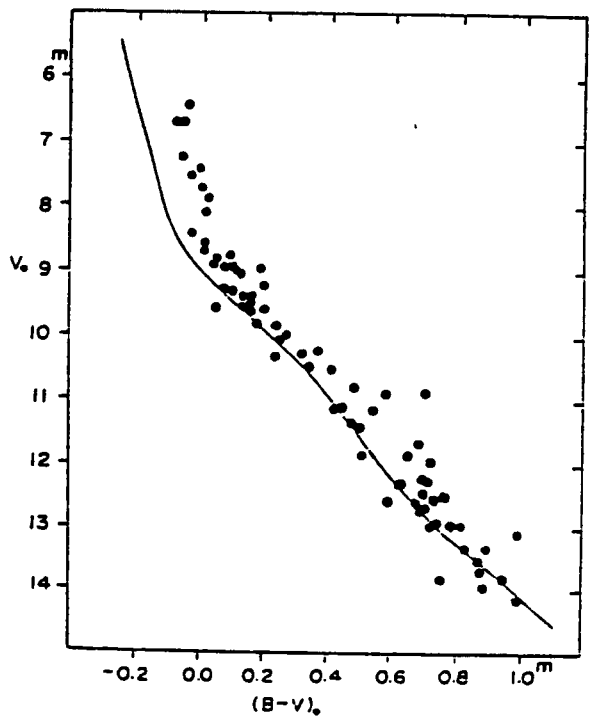

Figure 19. M39 color-magnitude diagram from Mohan and Sagar (1985). The solid line marks the zero-age main sequence

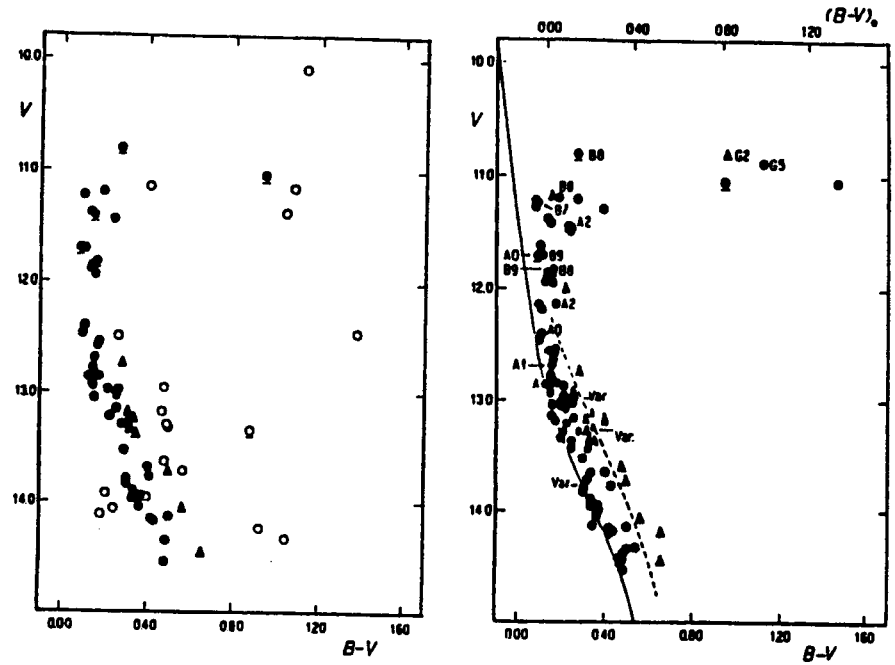

Figure 20. Color-magnitude diagrams of NGC 2567 from Claria and Lapasset (1986). Members, probable members, and field stars are marked by filled circles, triangles, and open circles, respectively. Variable stars are underlined. The solid line in the right diagram marks the zero-age main sequence. The left diagram includes only stars within 4 arc minutes of the cluster center. The main-sequence gap near $M_V = +12.2$ in the left diagram fills in when outlying cluster members are included

the apparent turnoff would have been left by early-A stars that have lost mass. If the mass-loss timescale is long compared to the main-sequence lifetime, these stars would evolve to the right as well as downward, broadening the upper main-sequence. The evolved stars in the broad upper main-sequence must have initial masses in excess of the less-evolved blue stragglers, somewhat larger than 3 $M_\odot$. The mass-loss rate required for a 3.5 $M_\odot$ star to reach 2.5 $M_\odot$ in 0.24 Gyr is a possible 4×10^{-9} $M_\odot$/yr. Keeping in mind the higher metallicity of the Hyades compared to the synthesized clusters with mass loss, the cluster with $\tau = 2$ Gyr in Figure 11 best illustrates the formation of the main-sequence gap, and Figure 13 best illustrates the spread in the upper main-sequence possible when stars of different initial masses and mass-loss rates evolve down the main sequence.

b. Praesepe The situation for Praesepe (NGC 2632, M44) is similar to that of the Hyades. Although Praesepe has a larger distance modulus than the Hyades, it is considered by many to be part of the Hyades moving group (Crawford and Perry 1966). Figure 18 shows the Praesepe M_V vs. b-y color diagram of Crawford and Barnes (1969). Praesepe has one blue straggler at b-y ~ 0.0 (spectral type A0), a 0.08 magnitude gap in color between the blue straggler and the broad upper main-sequence, and a significant number of Am stars at the top of the main sequence. VandenBerg and Bridges (1984) fit a 9×10^8 year isochrone to cluster stars, excluding the blue straggler. Given the slightly redder position of Praesepe's blue straggler and upper main-sequence compared to the Hyades, it is likely to be slightly older. The qualitative arguments for main-sequence mass loss in the Hyades can also be advanced for Praesepe. The large proportion of Am stars near the top of the main sequence is suggestive, if Am peculiarity is indeed correlated with slow rotation and slow mass loss.

c. M39 A color-magnitude diagram for M39 (NGC 7092), a sparse but relatively nearby cluster (300 pc), with brightest member at spectral type B9.5 (Mohan and Sagar 1985), is shown in Figure 19. Mohan and Sagar attempt to fit Population I isochrones to this cluster,

and derive an age between 0.2 and 0.4 Gyr. While no blue stragglers or gaps in the upper main-sequence are apparent in M39's HR diagram, there does seem to be a slight overabundance of stars at B-V = +0.15 (spectral type A5). It is possible that a few early-A stars evolved down the main sequence to create the clump, or that mass loss is proceeding too slowly to create a noticeable gap by this cluster age, or that a few stars are losing mass rapidly, but lie on the main sequence, indistinguishable from constant-mass stars; however, the features of the M39 diagram are much more consistent with standard stellar evolution than those of the Hyades and Praesepe.

d. NGC 2567 This cluster is five times as distant as M39, but more populated. The age of NGC 2567, deduced from the U-B color at the main-sequence turnoff, is 2.9×10^8 yr, the same as M39 and somewhat younger than the Hyades. Figure 20 shows the M_V vs. B-V diagrams of member B, A and F stars within 4 arc minutes and within 10 arc minutes of the cluster center, respectively (Claria' and Lapasset 1986). Membership probability is based upon photometric criteria, i. e., position in color-magnitude and color-color diagrams. There does seem to be a gap in the main sequence at early-A spectral type in the diagram including only stars near the cluster center, but the gap fills in somewhat when more outlying members are included. As is the case for M39, there is no compelling evidence for main-sequence mass loss among A stars.

2. Group II

This group includes NGC 5822, NGC 2360, and NGC 6192, which have turnoffs at mid- to late-A spectral types. It was rather difficult to locate cluster diagrams with recent photometry in this age group.

a. NGC 5822 Figure 21 shows the color-magnitude diagram of NGC 5822 by Hirshfeld, McClure and Twarog (1978), who derive an age for this cluster of 1.0 Gyr. Being only slightly older than the Hyades or Praesepe, the diagram reveals similar features, including blue stragglers at B-V ~-0.1, and a broad main sequence, although not as broad as that

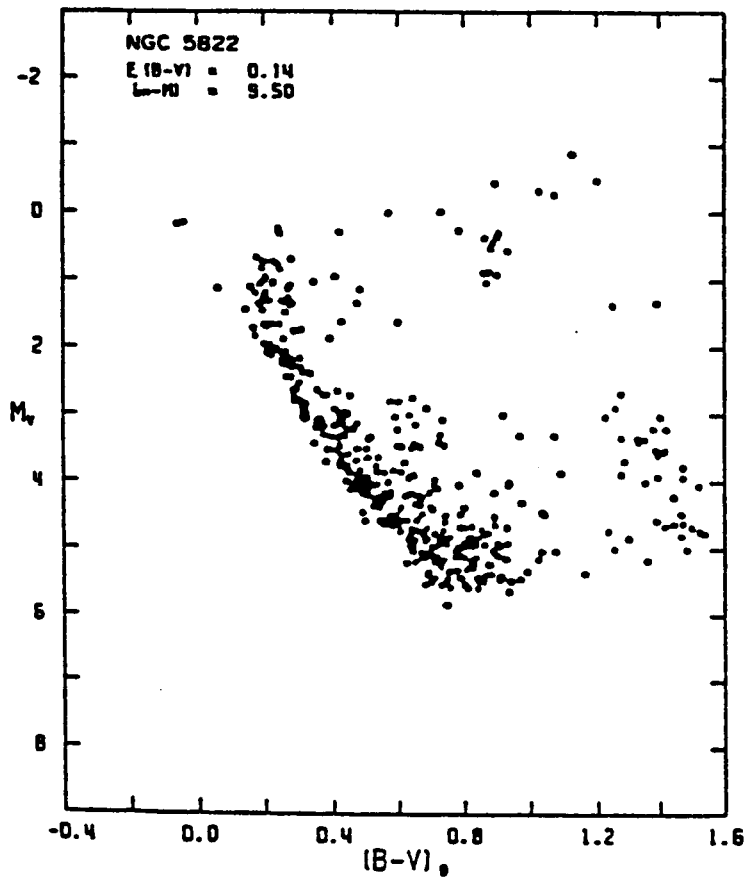

Figure 21. NGC 5822 color-magnitude diagram from Hirshfeld, McClure and Twarog (1978). Two blue stragglers are evident near B-V = -0.1

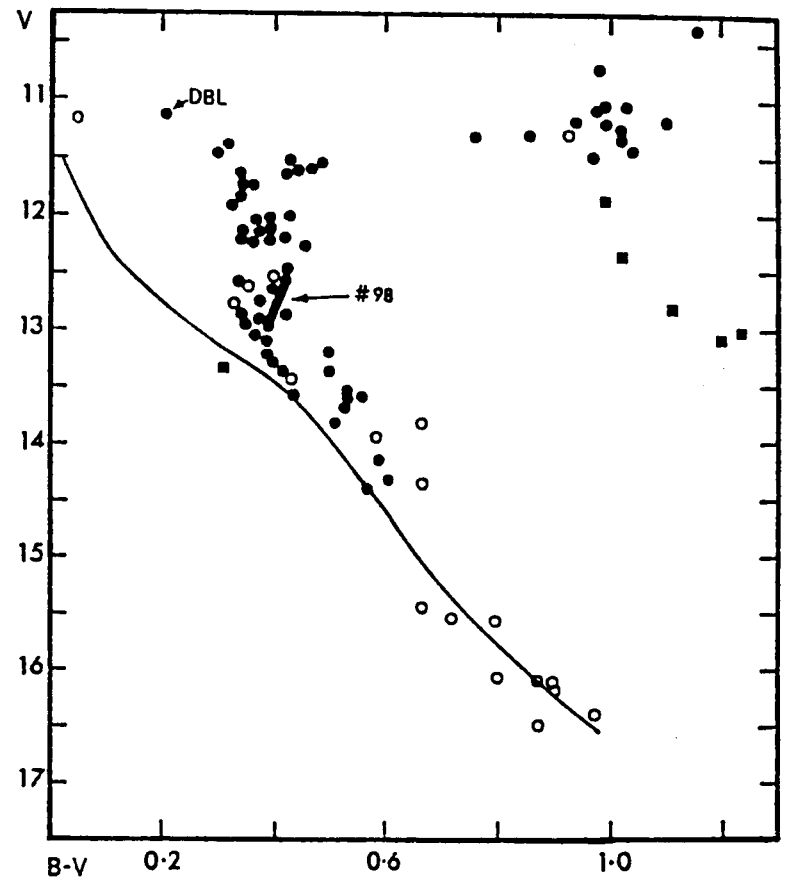

Figure 22. NGC 2360 color-magnitude diagram from Eggen (1968). Open circles represent stars with single observations, and squares represent probable field stars. #98 marks the path of a variable star. The DBL label is not explained; it may be intended to mark a possible binary

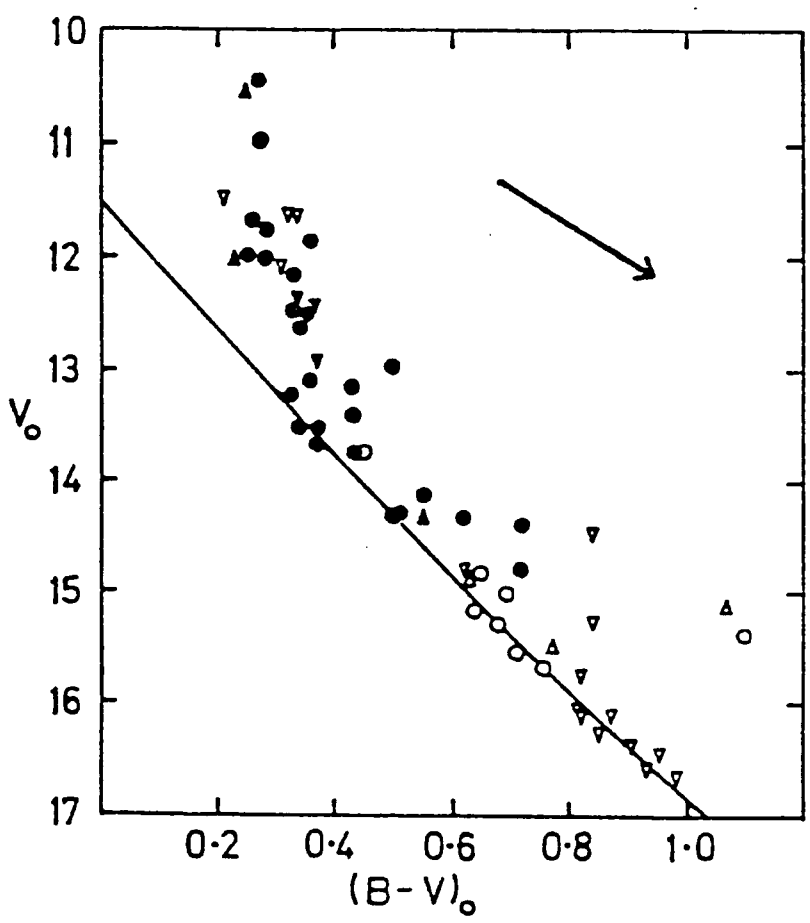

Figure 23. NGC 6192 color-magnitude diagram from King (1987). The three symbol varieties distinguish photometry from three data sets. The arrow in the upper right is the reddening vector. The solid line marks the zero-age main sequence

of the Hyades. Hirshfeld, McClure and Twarog (1978) note that the blue edge of the main sequence is well-defined, and theorize that the scatter near the main sequence is due to binaries. The metallicity of the cluster, as determined from the U-B color is $[Fe/H]_\odot = -0.07$ (Hirshfeld, McClure and Twarog 1978), significantly less than that of the Hyades, so comparison to the synthesized clusters with mass loss should be more direct. Had the mass loss in the evolution calculations extended to stars of initial mass $\geq 2.25\ M_\odot$, synthesized clusters of age a few x 10^8 years, with long (1-2 Gyr) mass-loss timescales, and giant progenitors of mass $> 2.25\ M_\odot$ may have reproduced the blue stragglers, broad turnoff, and giants of NGC 5822.

b. NGC 2360 Demarque (1978) cites an age of 1.3 Gyr and metallicity deduced from U-B color $[Fe/H]_\odot = -0.07$ for NGC 2360. Figure 22 shows NGC 2360's color-magnitude diagram from photometry of Eggen (1968). Eggen notes the presence of a somewhat evolved blue straggler at B-V ~ +0.2, and a possible blue straggler at B-V ~ 0.0. As is the case for the Hyades and Praesepe, main-sequence mass loss may be responsible for NGC 2360's broad upper main-sequence and blue straggler(s). Eggen also discusses a gap of width 0.2 in M_V near M_V = +1.9. The latter gap is expected from standard stellar evolution theory, as it corresponds to the rapid evolutionary phase of stars with convective cores through the blue hooks at the end of main-sequence evolution: the gap is visible at M_V ~ +2.0 for the 1.3 Gyr age cluster without mass loss (Figure 13).

Considering that the main sequences of NGC 2360 and of other clusters exhibit these gaps, it is questionable whether one would want to introduce main-sequence mass loss to explain the presence of one or two blue stragglers when stellar mass loss, especially with a variety of timescales, would obscure or, at best, displace the gaps. However, Maeder (1974) discusses in detail the size and location of the gaps in M67, NGC 3680, NGC 752, and Praesepe, as well as in NGC 2360, finding "clear and systematic differences" between the observed location of the gaps and those expected from standard isochrones. In

all cases, the gap on the C-M diagram is oriented *vertically* in visual magnitude, rather than slanting to the left (toward the blue) to trace the hook following the rapid core/shell-burning transition phase. In other words, the top of the gap lies too far to the right of the zero-age main sequence, or 0.05 to 0.1 magnitudes in B-V to the right of the expected location. Also, the gap is often too high relative to those of the preferred isochrones, and the subgiants are scattered above the gap in all of the above clusters except possibly M67, rather than lying with appropriate densities along the isochrones. Maeder also notes that the existence of clean gaps, with no stars present, is surprising; for M67, Maeder predicts from the length of the contraction phase that 5 to 8 stars should populate the gap.

Maeder concludes that reproducing the characteristics of the gaps in these clusters would require shortening the timescale for core hydrogen exhaustion, and inducing a vertical, rather than blueward displacement during this period. Changes in metallicity or helium content do not suppress the hook. The hook can be reduced or eliminated by smoothing the mean molecular-weight gradient in a small zone just above the convective core, for example by convective overshooting. Could early main-sequence mass loss also suppress the blue hooks? The larger convective core during the higher-mass phase would serve to smooth the mean-molecular weight gradient in the material above the subsequent convective core, and may produce the desired effect. The extra H-depletion at early times may also increase the rate of evolution through the core readjustment phase. Additional evolution calculations, with mass loss turned off before core hydrogen-exhaustion, would be useful in deciding this question.

c. NGC 6192 The relatively sparse color-magnitude diagram of NGC 6192 (Figure 23, King 1987), shows no obvious anomalies, although as always some cluster members may have been missed. There are no blue stragglers, and a well-defined main-sequence turnoff. Not plotted in the diagram are a K giant and a white dwarf. King (1987) derives an age of 1.3 Gyr for this cluster. Comparing with the

synthesized cluster of age 1.3 Gyr without mass loss (Figure 13), there seems no need to invoke mass loss to explain any features of NGC 6192. It is possible that a fraction of stars in NGC 6192 did experience mass loss, and are situated along the main sequence, indistinguishable from stars that have evolved at constant mass. Blue stragglers would also be statistically less likely to be found in a sparse cluster such as this one.

3. Group III

This group contains NGC 7789, NGC 752, and NGC 3680, three very unusual solar-metallicity clusters with turnoff ages of 1.5 to 2.5 Gyr, at spectral types early- to mid-F.

a. NGC 7789 As is obvious from its color-magnitude diagram (Figure 24; Breger 1982), NGC 7789 contains a large number of blue stragglers (at least 16 confirmed members), distributed along the main sequence above the apparent turnoff. It should be pointed out that the B-V axis of Breger's diagram has not been corrected for 0.27 magnitudes of reddening; the reddening correction was derived by Janes (1977), using DDO photometry. Twarog and Tyson (1985) derive an apparent age of 1.6 ± 0.5 Gyr, and a metallicity [Fe/H] = -0.25 relative to the Hyades, or $[Fe/H]_{\odot}$ = -0.05. Figure 24 also includes the color-magnitude diagram of Saio and Wheeler (1980) with superimposed evolutionary tracks of standard stellar models. The blue stragglers are fit by 1.7 to 3 $M_{\odot}$ models, with a strong concentration of stragglers of ~2 $M_{\odot}$. Breger used polarization to eliminate cluster non-members, and found that all of the remaining blue stragglers lay between the zero-age and the terminal-age main sequence.

The blue stragglers in this cluster have been investigated extensively. Twarog and Tyson (1985) find that the stragglers and the red giants are concentrated toward the cluster center, implying that the progenitors of both classes have similar masses. Stryker and Hrivnak (1984) conclude from their search for radial-velocity variations among the blue stragglers that it is highly improbable that all of the stragglers can be explained by binary mass-transfer. Twarog and Tyson

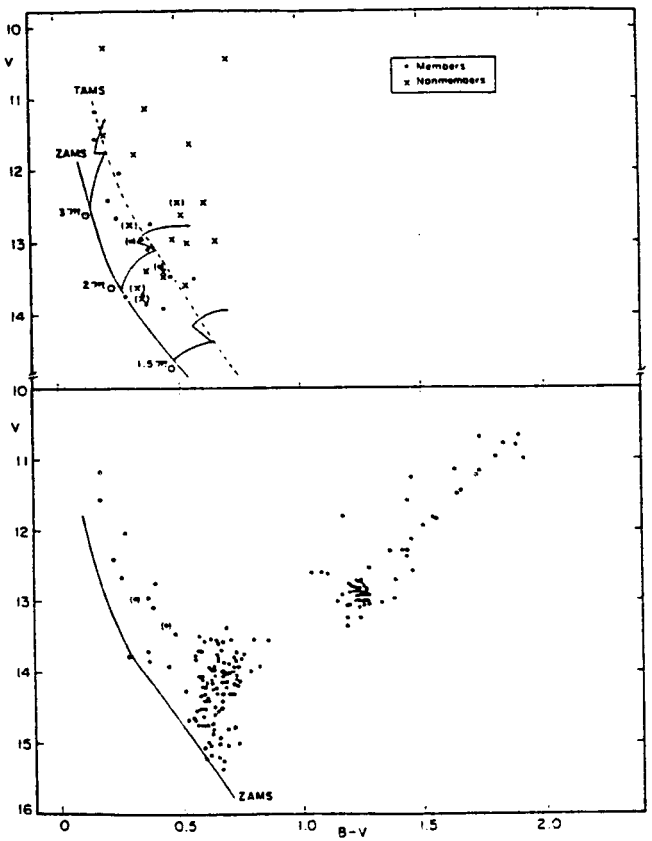

Figure 24. NGC 7789 color-magnitude diagram from Breger (1982), uncorrected for an estimated 0.27 magnitudes of reddening in B-V. The upper diagram shows the blue straggler candidates, and the standard stellar evolutionary tracks of 1.5, 2.0, and 3.0 $M_{\odot}$ stars calculated by Saio and Wheeler (1980). The solid line marks the zero-age main sequence, and the dashed line marks the terminal-age main sequence

Figure 25. Color-magnitude diagrams of NGC 752. The top diagram from Twarog (1983) shows the bifurcation of the upper main-sequence, with stars in the redward sequence marked by filled circles, stars intermediate between the two sequences marked by half-filled circles, and stars that could fall into either group marked by crosses. The sequences persist in b-y and Hβ color vs. M_V diagrams, excluding photometric errors as the source of the bimodality. The lower diagram from Maeder (1974) shows that the location and orientation of the upper main-sequence gap due to the rapid core-Hydrogen exhaustion phase is not well matched by theoretical isochrones

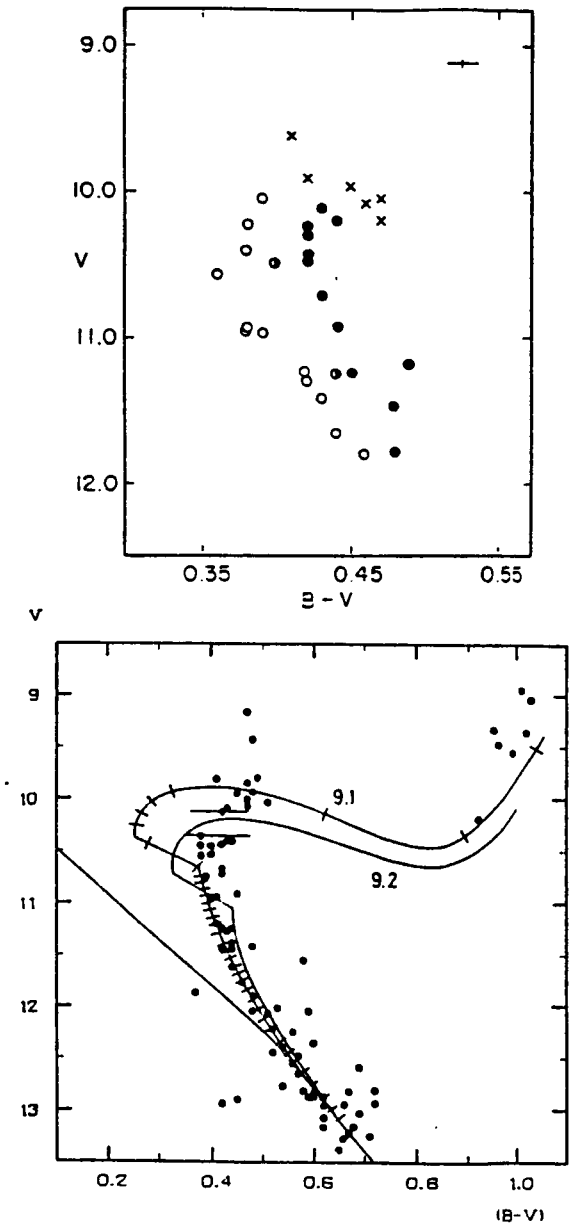

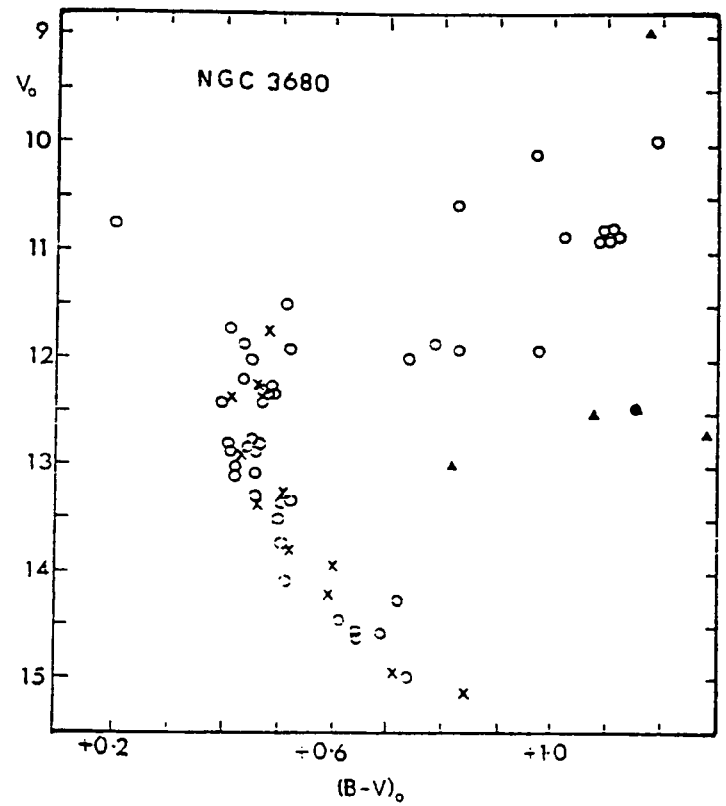

Figure 26. NGC 3680 color-magnitude diagram from Eggen (1969). Open circles mark stars with more than one observation, crosses mark stars with single observations, and triangles mark probable non-members. Nissen (1984) finds that NGC 3680 has a bimodal upper main-sequence similar to that of NGC 752

(1985) find that the only photometric clue to the nature of the blue stragglers is a tendency toward lower surface gravities (0.5 less in log g) for the stragglers compared to zero-age main-sequence stars; this may be indicative of high rotation rates. Twarog and Tyson also point out a potential deficiency of spectrally peculiar stars among the blue stragglers. From percentages of Am and Ap stars found among blue stragglers in young open clusters (Mermilliod 1982), six to eight Am or Ap stars are expected in NGC 7789; however, only one Am and one Ap star can be identified from photometric indices, although Twarog and Tyson caution that the blue stragglers should be examined spectroscopically to verify this result. The latter features–rapid rotation and deficiency of peculiar stars–are *not* typical of the blue stragglers in other open clusters discussed, and would not be expected according to the main-sequence mass loss hypothesis.

Can the features of NGC 7789 be explained by including main-sequence mass loss? Adopting Breger's mapping of Saio and Wheeler's zero-age models on the C-M plane, and accounting for reddening, the 3.0 $M_\odot$ model has spectral type B8, or B-V ~ -0.12 (Johnson 1966); the 1.5 $M_\odot$ model, near the cluster turnoff, has spectral type F0, and B-V ~ +0.3. The main-sequence lifetimes of the >3.0 $M_\odot$ stragglers (assuming these are normal stars that did not lose mass or experience extra mixing) constrain the actual age of the cluster to < 0.3 Gyr. Main-sequence mass loss by the majority of cluster stars between ~1.4 and ~4 $M_\odot$, with mass-loss rates in excess of 5×10^{-9} $M_\odot$/yr, (sufficient to decrease the mass of a 3.0 $M_\odot$ star to 1.5 $M_\odot$ in 0.3 Gyr) would possibly reproduce the main sequence and all of the blue stragglers. The evolved main-sequence stars at the cluster turnoff would require progenitors with initial mass > 3 $M_\odot$, well to the blue side of the pulsation instability strip; these stars are not necessarily expected to lose mass, according to the premises of the main-sequence mass loss hypothesis. Despite the comment of Twarog and Tyson (1985) that the blue stragglers and giants probably have the same progenitors, the well-populated giant branch and He core-burning

clump may prove very difficult to produce from the few expected blue stragglers.

If only the blue stragglers with mass ≤ 2 $M_\odot$ require explanation, the main-sequence mass loss hypothesis may be able to simultaneously accomodate these stragglers, the turnoff stars, and the giants. The cluster then could be as old as 1 Gyr. It would be necessary to invoke alternative explanations for the few high-mass blue stragglers, such as extended main-sequence lifetimes due to mixing of extra hydrogen into their cores, as discussed by Saio and Wheeler (1980). Less extensive mixing would be required if NGC 7789 was actually younger than suggested by standard isochrone fits to its turnoff.

Alternatively, the stragglers could actually be less massive; an overestimate of the reddening correction would affect the star colors and the distance modulus, leading to increased turnoff and blue straggler masses. Twarog and Tyson (1985) point out that, while Janes' (1977) derivation of the reddening correction had the advantage of excluding the potentially anomalous blue stragglers, there may be large uncertainties associated with the reddening calibration of the DDO photometric system. However, reddening determinations using UBV photometry require *a priori* knowledge of the cluster metallicity. Twarog and Tyson attempt to minimize uncertainties by using both DDO and UBV photometry to derive a consistent cluster metallicity and reddening. Their final value, 0.31 ± 0.03, is marginally larger than that of Janes, so would support an increase, rather than a decrease in the mass of the blue stragglers, as gauged from their position on the C-M diagram.

The giants themselves in NGC 7789 are unusual in several respects. Several NGC 7789 giants have ^{7}Li abundances approaching the cosmic value Li/H = 10^{-9}, whereas the Li abundance in normal field giants is far below the cosmic value due to internal destruction and dilution during first dredge-up (Pilachowski, Mould and Siegel 1984). Pilachowski (1984) finds that the Li abundances of stars near the main-sequence turnoff are consistent with the cosmic value, so NGC 7789 did not have

an abnormally high initial Li abundance. Sneden and Pilachowski (1986) find nothing unusual in the $^{12}C/^{13}C$ isotope ratios of six out of seven of NGC 7789's K giants; one giant with an abnormally low $^{12}C/^{13}C$ ratio also has a very high Li abundance. As discussed in Section II, C4, interior processing of material during a higher mass phase by mass-losing stars would produce decreased $^{12}C/^{13}C$ and C/N surface abundance ratios following first dredge-up. Possibly the processing of the additional envelope ^{3}He produced in stars with a history of early main-sequence mass loss would produce extra Li as well, but probably not until the asymptotic giant branch phase.

b. NGC 752 This sparse cluster, and the one to be discussed next (NGC 3680) exhibit bimodal main-sequence turnoffs. Figure 25 shows an older color-magnitude diagram of NGC 752 (Maeder 1974), and a closeup of the turnoff from Twarog's (1983) photometric study, with the red sequence highlighted. The bifurcation persists in color-magnitude plots with x-axes B-V, b-y, and Hβ, ruling out photometric errors as the source. Twarog (1983) derives an apparent age of 2.2 ± 0.3 Gyr, and metallicity [Fe/H] = -0.33 relative to the Hyades ($[Fe/H]_{\odot}$ = -0.13). The spacing of the sequences indicates an age difference from standard isochrones of 0.3 Gyr. Suggested explanations for the bimodality include successive generations of star formation and more-rapid rotation of the members of the redder sequence (Twarog 1983). Measured rotational velocities for five stars near the turnoff reveal that two stars in the red sequence have rotational velocities 35 km/s higher than the stars in the blue sequence (Gunn and Kraft 1963). As is evident from Figures 13 through 16, stellar main-sequence mass loss with two characteristic timescales, possibly selected by differences in initial stellar rotation velocities, can produce bimodal turnoffs. Recall that this cluster also exhibited an anomalous vertical gap in the upper main-sequence at apparent visual magnitude 10.8 (Maeder 1974) as discussed above for NGC 2360.

c. NGC 3680 Figure 26 shows the color-magnitude diagram of NGC 3680 by Eggen (1969), with the vertical gap discussed by Maeder

(1974) at M_V = 12.6. Nissen (1984) recognizes the bimodality of the early-F type stars on the upper main-sequence in this cluster using Stromgren photometry, and fits the sequences to isochrones of 1.5 and 2.5 Gyr. Nissen comments that the bimodality cannot be explained in terms of binaries alone, and affirms Twarog's suggestion for NGC 752 that rotation is the distinguishing parameter. As in the case of NGC 752, main-sequence mass loss could also produce the bifurcation.

4. Group IV

This group includes four very similar clusters with main-sequence turnoffs at early- to mid-F spectral type, but with lower metallicities than the clusters of Group III: NGC 2158, NGC 2204, NGC 2420, NGC 2506. The relevance of main-sequence mass loss to the morphology of the cluster diagrams in these groups will be discussed after describing the properties of each cluster.

a. NGC 2158 This is the most distant cluster discussed so far (4000 pc). Christian, Heasley and Janes (1985) have extended the cluster diagram into the main sequence using CCD photometry (Figure 27); they derive an age for NGC 2158 of 3.0 ± 1.0 Gyr, and a metallicity $[Fe/H]_{\odot}$ = -0.46. The diagram is uncorrected for an estimated 0.55 magnitudes of reddening. The cluster may have some blue stragglers, although there are spurious points to the lower left of the main sequence that make membership questionable for a small fraction of the stars included. NGC 2158 has a gap near the top of the main sequence at M_V = +17.5 that may correspond to the rapid core hydrogen exhaustion phase of stars with convective cores, but as is the case for the clusters discussed earlier, is not fit well by standard isochrones. Lattanzio (1984) finds that chemical inhomogeneities in the cores of intermediate-mass stars, caused perhaps by grain sedimentation during star formation, can produce at least one, and, for certain cluster age and metallicity ranges, two gaps in the main sequence; NGC 2420 and 2506, with ages and compositions similar to NGC 2158, exhibit two gaps, while NGC 2158 has only one.

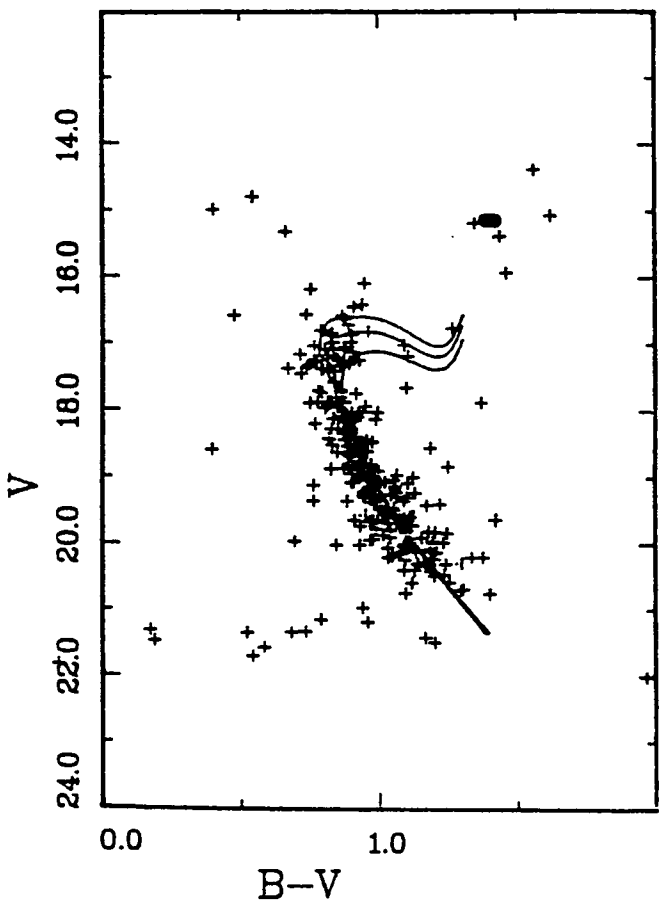

Figure 27. NGC 2158 color-magnitude diagram from Christian, Heasley, and Janes (1985), uncorrected for an estimated 0.55 magnitudes of reddening in B-V. VandenBerg's (1985) 2.5, 3.0, and 4.0 Gyr theoretical isochrones for Z = 0.006 are superimposed

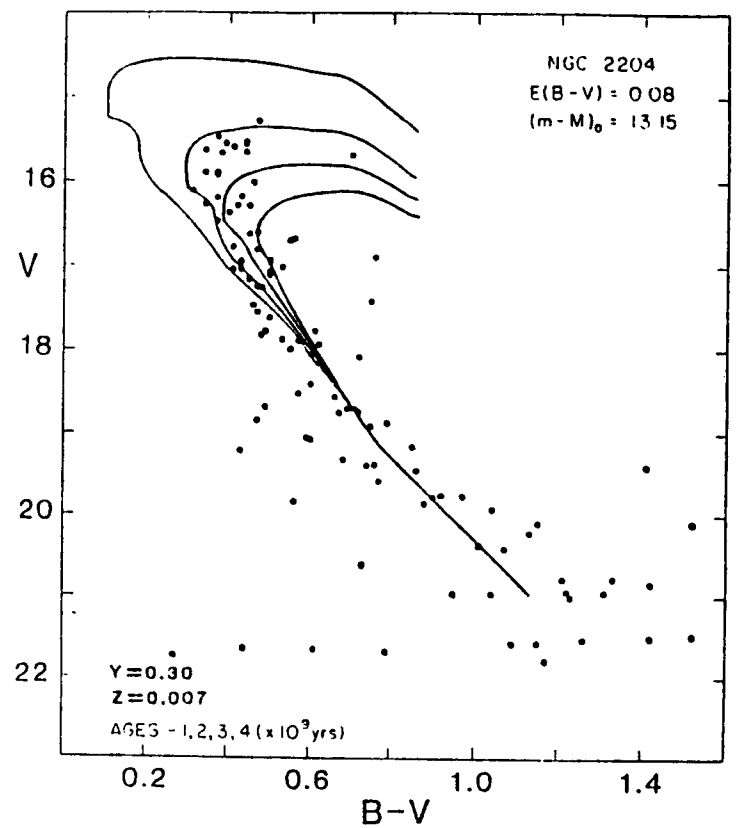

Figure 28. NGC 2204 color-magnitude diagram from Frogel and Twarog (1983). Theoretical isochrones of Ciardullo and Demarque (1977) are superimposed

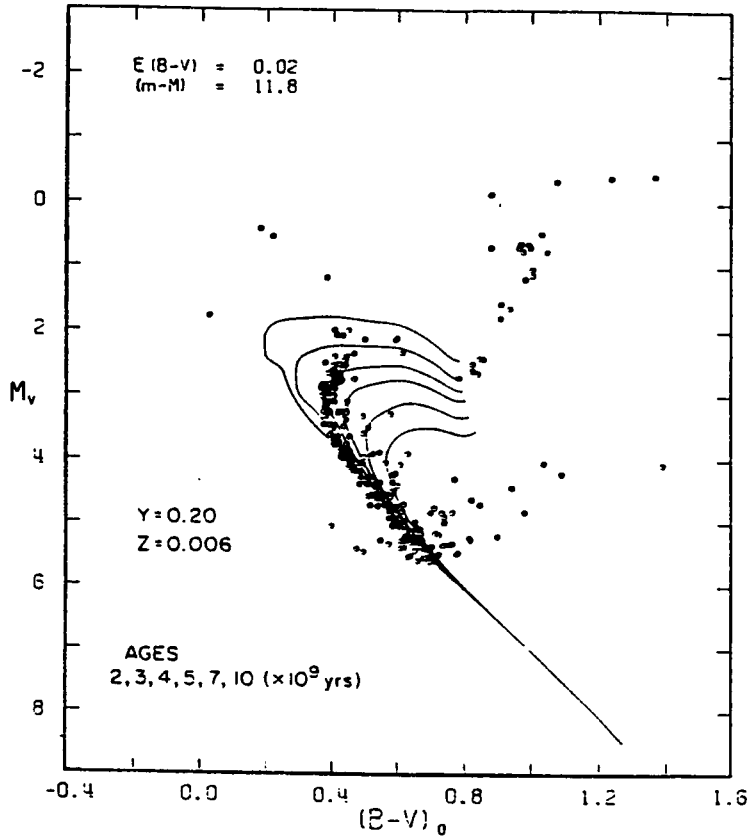

Figure 29. NGC 2420 color-magnitude diagram from McClure, Newell, and Barnes (1978). Theoretical isochrones of Ciardullo and Demarque (1977) are superimposed. Several blue stragglers are evident

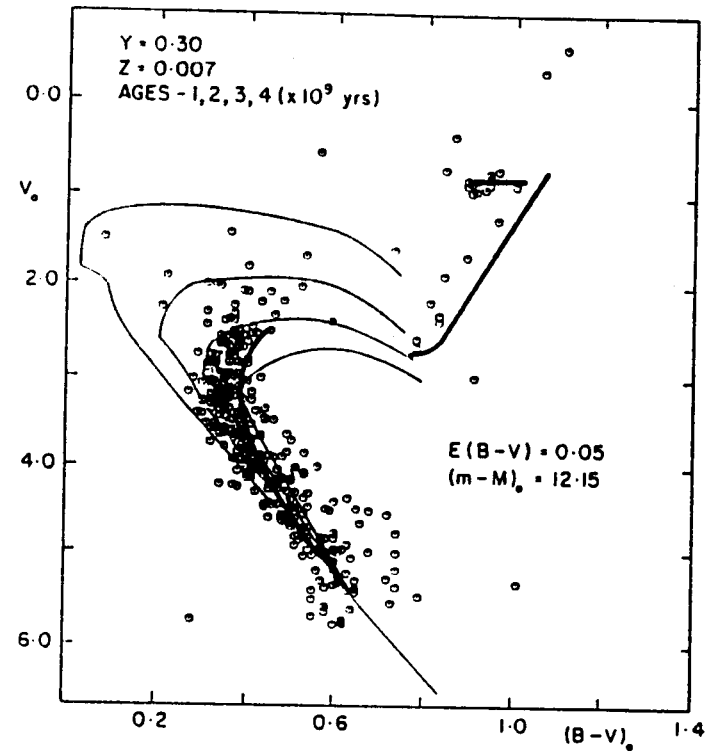

Figure 30. NGC 2506 color-magnitude diagram from McClure, Twarog, and Forrester (1981). The heavy curve is a schematic representation of NGC 2420, intended to highlight similarities. Theoretical isochrones of Ciardullo and Demarque (1977) are superimposed. Several blue stragglers are evident

b. NGC 2204 The color-magnitude diagram of this sparse cluster is shown in Figure 28 (Frogel and Twarog 1983). NGC 2204, with turnoff age 2.5 ± 0.3 Gyr, is only slightly older than NGC 752 in Group III; the dispersed upper main-sequence is reminiscent of NGC 752's bimodal turnoff. However, the metallicity of NGC 2204, $[Fe/H]_{\odot} = -0.4$, is nearly the same as that of the other three clusters in Group IV. The cluster HR diagram doesn't reveal any blue stragglers, nor upper main-sequence gaps that are present in NGC 752 and NGC 2158.

c. NGC 2420 Figure 29 shows the C-M diagram of McClure, Newell and Barnes (1978) for NGC 2420. The derived metallicity of NGC 2420 is $[Fe/H]_{\odot} = -0.3$, and the age derived from standard isochrones is 3.3 ± 0.5 Gyr (McClure, Forrester and Gibson 1974). The four blue stragglers are confirmed cluster members (McClure, Forrester and Gibson 1974). As mentioned earlier, the upper main-sequence exhibits two gaps, one at $M_V \sim 2.3$, and another at $M_V \sim 3.6$. Neither gap corresponds well with the blueward hooks of the superimposed theoretical isochrones.

d. NGC 2506 The C-M diagram of NGC 2506, shown in Figure 30 (McClure, Twarog and Forrester 1981), is almost identical to that of NGC 2420. NGC 2506 has an age derived from the turnoff of 3.4 Gyr, and metallicity $[Fe/H]_{\odot} = -0.35$. NGC 2506 has numerous blue stragglers that are confirmed members from proper motion studies. NGC 2506 also has two main-sequence gaps in the same locations as in NGC 2420; the gaps are more evident when only stars with > 90% probability of cluster membership are included.

e. Discussion The mass of stars at the main-sequence turnoff of each of these clusters is 1.2-1.3 $M_{\odot}$. The blue stragglers do not appear particularly far from the main-sequence turnoff; many appear somewhat evolved. Standard isochrones do not fit the main-sequence turnoff well for any of the clusters. The isochrones predict turnoffs that turn sharply rightward (redward), with little increase in luminosity following the turnoff until the ascent of the first giant branch; the turnoffs of the actual clusters curve rightward gently, with continued increase in

luminosity. The questions could be raised as to why these (and several other) Galactic clusters with low metallicity have similar turnoff ages, and why the number of clusters with these characteristics is so numerous. An obvious reason for the similarity in metallicity is the similar location of the clusters several kiloparsecs beyond the solar orbit (McClure, Twarog and Forrester 1981), where the metallicity is expected to be less than solar; the similar ages could be explained by a Galactic age-metallicity relation, except that for young clusters, cluster age deduced from the main-sequence turnoff is uncorrelated with cluster metallicity (Cameron 1985). Perhaps formation of multiple star clusters was triggered 2-3 Gyr ago. An alternative explanation is that the clusters are really of different ages, but for metallicity $[Fe/H]_{\odot} \sim$ 0.3-0.4, cluster stars lost mass to form the apparent turnoff at 1.2-1.3 $M_{\odot}$. Such mass loss would produce more gently curving apparent turnoffs (Figures 13-16). Blue stragglers could be produced from normal stars of mass 1.2-2.5 $M_{\odot}$ that experienced slower (or no) mass loss. The clusters could then be as young as ~1 Gyr, or as old as their apparent turnoff ages. The stars at the apparent turnoff, as well as the blue stragglers, could be the source of the giants. These clusters fit the scenario of main-sequence mass loss better than any of the clusters discussed to this point.

5. Group V

The final group contains the oldest Galactic clusters: Melotte 66, with very low metallicity, and NGC 188 and M67, with almost solar composition.

a. Melotte 66 Gratton (1982) derives an age of 6 Gyr, and a metallicity of only $[Fe/H]_{\odot} = -0.7$ for Melotte 66. Anthony-Twarog, Twarog and McClure (1979) confirm a number of anomalies found earlier by Hawarden (1976) in the morphology of Melotte 66's C-M diagram. Among these anomalies are a gap in the upper main-sequence, with the turnoff stars dispersed in luminosity; a significant number of blue stragglers; lack of a definite subgiant branch; a substantial number

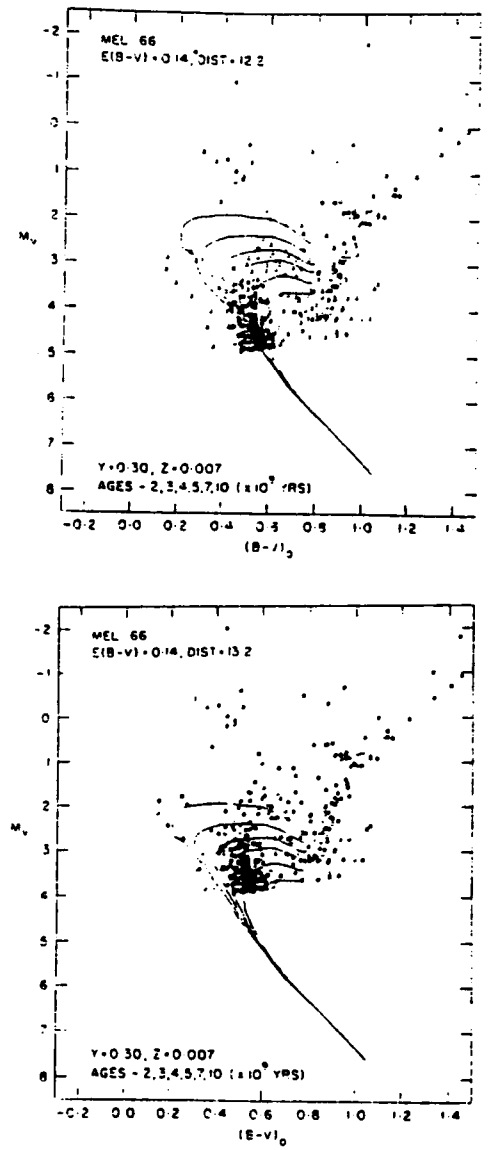

Figure 31. Color-magnitude diagrams of Melotte 66 from Anthony-Twarog, Twarog, and McClure (1979). In the first diagram, the distance modulus is chosen to fit the main-sequence turnoff by the superimposed theoretical isochrones of Ciardullo and Demarque (1977). In the second diagram, the distance modulus is chosen such that the red-giant clump falls at the expected magnitude $M_V = +1.0$. The blue stragglers are then well matched by the 2 Gyr isochrone

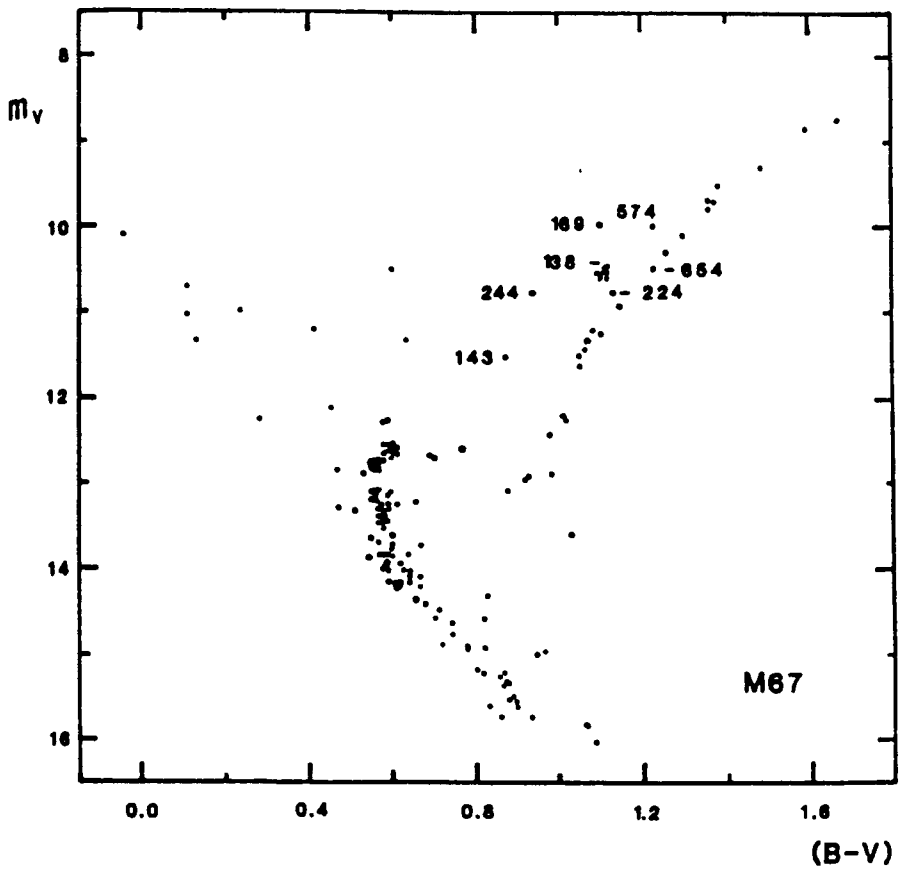

Figure 32. M67 color-magnitude diagram from Janes and Smith (1984). M67 has a well-delineated subgiant and giant branch, and numerous blue straggers. The numbered stars are anomalous giants (see text)

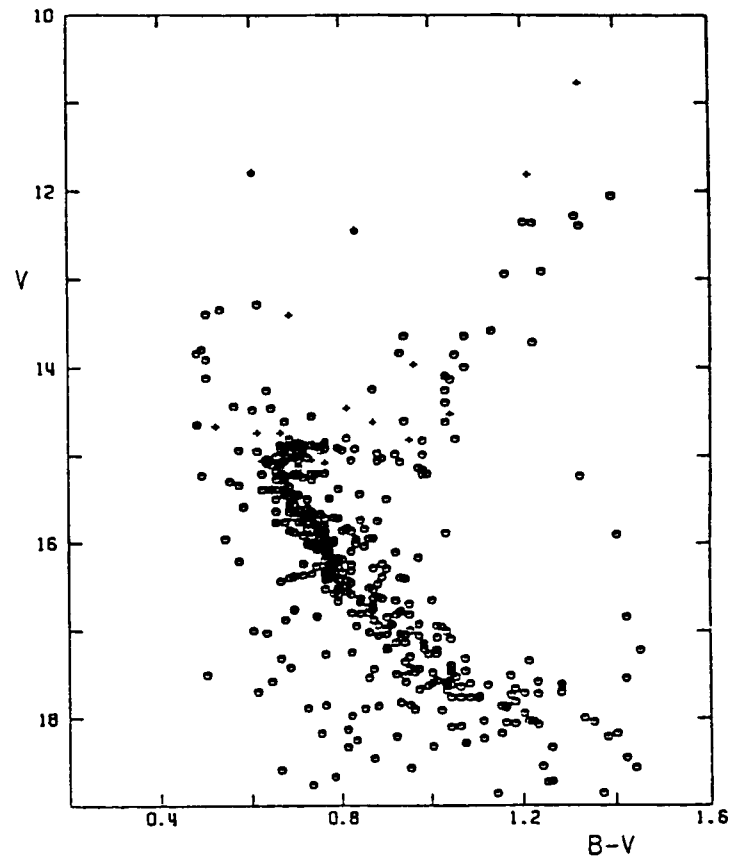

Figure 33. NGC 188 color-magnitude diagram from McClure and Twarog (1977). Unlike M67, NGC 188 has an ill-defined giant branch. Recent age estimates of 10 Gyr from main-sequence turnoff fitting to the isochrones of VandenBerg (1983) make NGC 188 the oldest Galactic open cluster

of giants in the cluster halo that are also above and blueward of the principal giant sequence; and a He-burning giant clump that is too faint for the cluster's metallicity and apparent turnoff. Anthony-Twarog, Twarog and McClure (1979) suggest that a variety of metal abundances among cluster stars could account for the blue stragglers, dispersed turnoff, and ill-defined giant branch. Anthony-Twarog et al. also attribute the presence of giants in the cluster halo to dynamical relaxation following mass loss during first giant branch evolution.

Figure 31 shows two color-magnitude diagrams of Melotte 66 from Anthony-Twarog, Twarog and McClure (1979), with superimposed theoretical isochrones. In the first diagram, the distance modulus is chosen so that the clump of main-sequence stars lies at the turnoff predicted by the isochrones. The second diagram is displaced relative to the first in M_V to force the He-burning clump giants to expected magnitude +1.0; the blue stragglers then line up remarkably well along the 2 Gyr isochrone. The bluest stragglers of this metal-poor cluster, with B-V ~ +0.15, have mid-A spectral type and mass ~1.5 $M_\odot$; they appear significantly less-evolved than the turnoff stars at B-V ~ +0.55 (late-F spectral type) with mass ~1.05 $M_\odot$. Assuming that the blue stragglers define the maximum age of the cluster (2 Gyr), simultaneously fitting the blue stragglers and producing an evolved turnoff requires that the turnoff stars have initial mass somewhat larger than 1.5 $M_\odot$, and very modest mass-loss rates of $< 5 \times 10^{-10}$ $M_\odot$/yr. The scattered giants above the turnoff could be produced from stars with a variety of initial masses > 1.6 $M_\odot$ and mass-loss histories. This cluster is rich enough that it would be very worthwhile to obtain fainter photometry of the lower main-sequence and to compare observations with the number and distribution of giants expected from the population of main-sequence stars.

b. M67 The color-magnitude diagram of M67 (Figure 32, Janes and Smith 1984) exhibits a narrow main-sequence turnoff, and a well-delineated subgiant and giant branch, and tight formation of clump giants; a number of anomalous giants are also indicated on the C-M

diagram. The age estimated from the turnoff is 5.0 ± 0.5 Gyr, and the metallicity $[Fe/H]_\odot$ = -0.06 ± 0.07 (Nissen, Twarog and Crawford 1987). M67 also contains 10 blue stragglers with membership probability from proper-motion plus radial velocity studies > 88% (Mathieu and Latham 1986); Mathieu and Latham find that the blue stragglers are concentrated toward the cluster center, indicating they are more massive than the turnoff stars of 1.2 $M_\odot$. Dynamical evolution modeling (Mathieu and Latham) as well as the position of the stragglers on the C-M diagram (Eggen 1981) point to a mass for the stragglers of about 2 $M_\odot$. Eggen (1981) compares the luminosity function of M67 with that of the younger Hyades and Pleiades clusters, and finds that there are as many 2 $M_\odot$ blue stragglers as original 2 $M_\odot$ main-sequence stars. Eggen raises two questions: Why have nearly all of the original 2 $M_\odot$ stars become blue stragglers, and why have the 1.5-2.0 $M_\odot$ stars produced so few stragglers? Eggen (1981) finds that the tight clump of three giants above M67's actual giant clump coincides in luminosity and temperature with the giant clump in the Hyades and Praesepe, suggesting that some of the blue stragglers have formed "red stragglers."

Among the giants that stray from the giant branch, Janes and Smith (1984) find that stars 224 and 654 are CN-strong, 244 and 143 are binaries, 138 has unusually low surface gravity, and 169 and 574 are probably AGB stars, binaries, or non-members. Brown (1987) finds from his study of nineteen M67 giants that the C/N ratio decreases during first dredge-up at a lower luminosity and by a larger total amount than predicted by standard evolution calculations.

Many anomalies in M67 would appear at first sight to invite explanation in terms of main-sequence mass loss, particularly Eggen's puzzles regarding the blue stragglers. The maximum age for M67 suggested by the 2 $M_\odot$ stragglers is only 1 Gyr; to form the well-delineated giant branch, stars of initial mass ~2-3 $M_\odot$ would have had to lose mass rapidly enough to reach the turnoff at 1.2 $M_\odot$ in under a billion years, yet slowly enough to evolve neatly off of the main sequence, behaving like normal 1.2 $M_\odot$ stars. The tight main-sequence

turnoff and giant branch are quite surprising from this viewpoint, given the potential for stars with varying mass-loss rates to produce scatter. It is more likely that at least the 2 $M_\odot$ stragglers are explained by mass transfer in binaries. Peterson, Carney and Latham (1984) find that two of the five bluest stragglers have post-main sequence companions, and that the radial velocities of the others are strongly suggestive that they also have companions. However, well-delineated giant branches are producible from main-sequence stars with a distribution of initial masses that lose mass with a relatively short timescale, and reach nearly the same final mass (see e.g., Figures 15-16). Early main-sequence mass loss from giant progenitors remains a viable explanation for the low C/N ratios found among M67 giants (see Section II, C4).

c. NGC 188 The age of NGC 188 as estimated from its turnoff has recently doubled from 5 to 10 Gyr due to the persuasive fit of VandenBerg's (1983) solar-metallicity isochrones. The color-magnitude diagram of NGC 188 (Figure 33, McClure and Twarog 1977) reveals an ill-defined giant branch, especially compared to that of M67. Suggested explanations for the scatter include differences in chemical composition (McClure 1974), and mass loss on the subgiant branch amounting to 0.2-0.3 $M_\odot$, followed by additional mass loss at the tip of the giant branch (Twarog 1978). The excess of giants compared to main-sequence stars found in the outlying regions of the cluster supports the suggestion of mass loss (McClure and Twarog 1977), whereas Norris and Smith (1985) find no evidence of a heavy-element abundance spread for stars near the main-sequence turnoff.

NGC 188 contains at least 10 blue stragglers (van 't Veer 1984); the stragglers are concentrated toward the cluster center, indicating that either they are more massive than the giants, or are binaries (McClure and Twarog 1977). Four late-type W UMa contact binaries are members of NGC 188, which is highly surprising, given that the lifetime of such binary systems is only several times 10^8 years, although lifetimes of up to a few times 10^9 years have been proposed (van 't Veer 1984). The presence of not one, but four of these contact binaries, as well as the

blue stragglers, leads van 't Veer to suggest that one or more rather recent episodes of star formation, possibly triggered by passages of the Galactic density wave, have occurred in NGC 188.

Evidence for pre-giant mass loss and the presence of young objects in addition to the blue stragglers lends credibility to the suggestion that main-sequence mass loss has occurred among NGC 188 cluster members. The bluest stragglers at B-V ~ +0.4 (mid-F spectral type) impose a maximum age of approximately 4 Gyr; the contact binaries may impose a more severe constraint. There seems to be no obvious obstacle to explaining the turnoff, anomalous giants, and blue stragglers in the context of the main-sequence mass loss hypothesis.

D. Conclusions

Of the seventeen clusters discussed, main-sequence mass loss may help to explain a number of features in at least fourteen, including the broad main sequence and blue stragglers the Hyades, Praesepe, NGC 5822, and NGC 2360; the bifurcated turnoffs of NGC 752 and NGC 3680; the poor fits of standard isochrones to the gently-curving turnoffs of NGC 2158, NGC 2204, NGC 2420, NGC 2506; the blue stragglers and anomalous giant branches of Melotte 66 and NGC 188, the unexpectedly early first dredge-up and large decrease in surface C/N ratio of M67 giants; and possibly the orientation and placement of the expected main-sequence gaps marking core-hydrogen exhaustion of stars with convective cores, as discussed for NGC 2360, NGC 3680, and NGC 752. While the synthesized cluster HR diagrams including main-sequence mass loss address most directly the anomalous features of the clusters in Group IV, with apparent turnoff ages ~3 Gyr, the main-sequence mass loss hypothesis could potentially explain a wide variety of features for clusters in each age group.

It may be difficult to find consistent mass-loss parameters that can account simultaneously for all of the blue stragglers and the anomalous giants in NGC 7789 and M67. The blue stragglers are relatively massive, and would imply young ages for these clusters (< 0.3 Gyr for

NGC 7789, and < 1 Gyr for M67), yet the giant branches are well-populated and well-delineated. Alternative explanations for at least the most massive stragglers, e.g., binary mass transfer, as proposed for the 2 $M_\odot$ stragglers of M67, and convective mixing of additional hydrogen to the cores of the 3 $M_\odot$ stragglers of NGC 7789 would alleviate the age restrictions, and allow main-sequence mass loss to accomodate the lower-mass stragglers of NGC 7789, and some anomalous giants of both clusters.

Three clusters, M39, NGC 2567, and NGC 6192, exhibit no unusual features and are well-described by standard stellar evolution. Two of these, M39 and NGC 2567, are perhaps too young (age 0.2-0.4 Gyr) for unusual features characteristic of main-sequence mass loss to have developed. Stars that are losing mass slowly may not have formed a noticeable gap, and stars with rapid mass-loss rates would be indistinguishable from normal main-sequence stars. M39 and the older cluster NGC 6192 (age 1.3 Gyr) are both relatively sparse; it is possible that mass-losing stars were relocated to the cluster halo during dynamical relaxation, where they were easily removed from the cluster by gravitational interactions with passing stars. Blue stragglers, which may be the only obvious clue that main-sequence mass loss is occurring, would be more likely to be absent in a sparse cluster.

Several constraints gleaned from comparing synthesized clusters with actual young disk clusters suggest changes in some of the trial assumptions regarding initial and target masses and mass-loss rates for models of mass-losing main-sequence stars. To simultaneously produce the populated, evolved main-sequence turnoff, account for the relatively unevolved blue stragglers, and populate the giant branch, all during a time less than or equal to the age of the most massive "normal" blue straggler in the cluster will require that: 1) A significant fraction of the turnoff stars must have initial masses in excess of 2 $M_\odot$, and perhaps larger than 3 $M_\odot$. This implies that stars beyond the blue edge of the pulsation instability strip, well into the late-B spectral type range, may also undergo main-sequence mass loss. While some of these stars

populate the turnoff, others with slower mass-loss rates would be required to populate the giant branch. This dual role of A through late-B stars may also require a flatter initial mass function, particularly since derivations of the initial mass function from observed luminosity functions will have underestimated the contribution of 2-3 $M_\odot$ stars. 2) The final or "target" mass of the majority of mass-losing stars is the mass at the apparent turnoff of the young clusters, 1.2 to 1.4 $M_\odot$, near the red edge of the pulsation-instability strip. Stars with higher mass-loss rates are not precluded from progressing further down the main sequence, but enough stars must be left behind to populate the turnoff. If the Sun is to be considered a candidate for main-sequence mass loss, its rapid mass loss and low final mass may have been exceptional. 3) The mass-loss timescales of the stars forming the apparent turnoff must be comparable to the main-sequence evolution timescales. Such timescales can be quite short, e.g., the lifetime of a 3 $M_\odot$ star is ~0.3 Gyr; hence the required mass-loss rates may approach 10^{-8} $M_\odot$/yr.

More definitive tests for main-sequence mass loss in young clusters may exist in the dynamical evolution, giant branch morphology, and red-giant/main-sequence luminosity functions. Barbaro and Pigatto (1984) find that red-giant luminosity distributions of clusters younger than 2 or 3 Gyr fail statistical tests for agreement with theoretical distributions; the distributions are instead similar to those of even younger clusters. Barbaro and Pigatto suggest that consistency might be restored if overshooting from the convective cores in stars of 1.3-2.2 $M_\odot$ is included in evolution calculations. Alternatively, the clusters may actually be younger than estimated due to earlier main-sequence mass loss from turnoff stars; also, hydrogen-burning at higher mass with a larger convective core may mimic the effects of prior convective overshoot in giants. Fainter main-sequence photometry would improve statistics relevant to the luminosity function for F and G stars, and allow better comparisons between the observed and expected numbers of giants, given stellar distributions along the main-sequence near the

turnoff. Dynamical evolution is more difficult to model for disk clusters than for globular clusters, since the crossing time is comparable to the relaxation time (King 1980), and since disk clusters are more easily disrupted. Evidence of mass segregation, presumedly due to dynamical relaxation, has been found in M67 (Mathieu and Latham 1986) and NGC 7789 (Twarog and Tyson 1985). Dynamical evolution modeling of disk clusters has the potential for further constraining the mass-loss timescales and upper- and lower-mass limits for the operation of main-sequence mass loss.

E. Topics for Further Investigation

The output of the evolution calculations conducted for the purpose of cluster synthesis has not been fully utilized. It would be interesting, for example, to examine the changes with time of the convective core size, composition gradients, and moments of inertia of the models with main-sequence mass loss, and to investigate the dependences on initial mass and mass-loss timescale. Since ^{3}He is produced at high interior temperatures in regions which are subsequently exposed following mass loss, it would be interesting to examine the stellar surface ^{3}He abundance as a function of time, initial mass, and mass-loss timescale. This ^{3}He may have relevance in nucleosynthetic processes during post main-sequence evolution, particularly for s-process nucleosynthesis as ^{3}He readily absorbs neutrons. Since evolution calculations were carried out well into first dredge-up, the dependence of the C/N ratio on stellar luminosity, initial mass, and mass-loss timescale during giant-branch ascent is readily obtainable. For radially pulsating stars,

$$P\sqrt{\rho} = Q$$

where P is the pulsation period, ρ is the mean density, and Q is the characteristic pulsation constant. The change in mean density with time determines dP/dt. Since dP/dt is an observable quantity for pulsating δ Scuti variables which may have relevance to the main-sequence mass loss mechanism, it might be interesting to calculate dP/dt as a function of time for the mass-losing models. The

sign as well as the magnitude of dP/dt vary with mass-loss timescale.

As mentioned earlier, to properly synthesize HR diagrams of Population I clusters will require evolution calculations with mass loss from stars of higher initial mass, and either slower mass-loss timescales or larger target mass. Evolution calculations with lower Z would be useful in synthesizing HR diagrams for comparison to those of globular clusters.

Additional literature surveys could also be conducted to check for deficiencies of red giants, to obtain statistics on masses and frequencies of blue stragglers, and to estimate the amount of flattening of the IMF required to simultaneously account for blue stragglers, main-sequence turnoff stars, and red giants in terms of the main-sequence mass loss hypothesis.

IV. GALACTIC CHEMICAL EVOLUTION

A. Introduction

Simple closed galactic chemical evolution models incorporating early main-sequence stellar mass loss were evolved for disk ages 5, 10 and 15 Gyr in order to quantify expected differences in stellar distributions with spectral type and metallicity, and to ascertain effects of altered timescales for stellar returns. Stars with initial mass between 3.0 $M_\odot$ and a metallicity-dependent lower mass M_L (0.8 $M_\odot \leq M_L \leq 1.4$ $M_\odot$) are assumed to lose mass promptly after formation to become stars of mass M_L. In galactic chemical evolution models without main-sequence mass loss, stars of 1-3 $M_\odot$ return processed material after intermediate timescales characteristic of their main-sequence lifetimes; in models with main-sequence mass loss, mass-losing stars return unprocessed material on a short timescale, and then lock the remaining mass into long-lived low mass main-sequence stars.

Because the postulated mass loss converts stars of spectral types A and F into late F or early G type stars, they may have considerable relevance to the familiar G-dwarf problem (van den Bergh 1962, Schmidt 1963, Bond 1981). A variety of modifications to the "closed box" model of chemical evolution can account for the observed deficiency of low metallicity dwarfs, and are discussed in numerous review articles (e.g., see Pagel and Patchett 1975; Tinsley 1980; Twarog 1985; Gusten 1986; and Pagel 1986). The most popular method of avoiding the G-dwarf problem has been to invoke infall (Lynden-Bell 1975; Chiosi 1980; Vader and de Jong 1981; Lacey and Fall 1983; Clayton 1985). The upper limit on the current infall rate deduced from X-ray observations (Cox and Smith 1976) and high velocity cloud statistics (Oort 1970) is $\leq$ 1-2 $M_\odot/pc^2/Gyr$. Present infall rates of this magnitude that have exponentially decreased with long timescales, typically ~3-5 Gyr, are required to eliminate the G-dwarf problem. Twarog (1985) emphasizes that the critical parameter is the ratio of the infall rate to star formation rate; the necessary infall rates are

perhaps 1/3 to 1/2 of the star formation rate, yet the source of this infalling gas is controversial, and the evidence for the presence of any infalling gas is inconclusive.

Attempts to match other observational constraints, such as radial disk metallicity gradients (see e.g., Twarog 1985 and Rana and Wilkinson 1986), the age-metallicity relation, and the apparent constancy of the star formation rate with time (Twarog 1980b), as well as to develop a consistent picture of disk formation have motivated other refinements of the simple model. A few of these pertinent to the G-dwarf problem are listed below: Larson (1986) satisfies constraints in the solar neighborhood by invoking bimodal star formation and requiring that all unseen disk matter be in the form of stellar remnants. Gusten and Mezger (1983), motivated by explaining the disk metallicity gradient, combine bimodal star formation with infall. Wyse and Silk (1987) require bimodal star formation plus a finite initial disk metallicity 1/10 $Z_\odot$ to account for the age-metallicity relation and dwarf metallicity distribution. In the extreme spheroid to thick disk to thin disk transition described by Gilmore and Wyse (1986), the G-dwarf problem is resolved by enriching the thin disk to 0.04 $Z_\odot$ with thick-disk ejecta. Rana and Wilkinson's (1986) model with finite initial disk metallicity 1/4 $Z_\odot$ and 45% of the initial disk mass contained in remnants satisfies the constraints of the G-dwarf distribution, the age-metallicity relation, and the disk metallicity gradient.

Interestingly, recent observations have suggested that the G-dwarf problem may not exist after all. Pagel (1986) notes that G and K giants in Baade's window toward the Galactic center have a broad metallicity distribution in good agreement with the simple closed model. Beers (1987) also finds no deficiency of stars with [Fe/H] $\leq$ -2.6 relative to predictions of the simple model in a sample of 134 low-metallicity F0 to G5 main-sequence stars and giants.

The models we present here are not intended to reproduce stellar distributions in the solar neighborhood, but rather to isolate and understand the effects of including main-sequence mass loss. To this

end, we have simplified assumptions and constraints as much as possible, and have not attempted to include the dependences of quantities such as the star formation rate, IMF, or stellar yield on time, gas density or metallicity. The elimination of the instantaneous recycling approximation for intermediate- and low-mass stars, and the binning of main-sequence stars according to effective temperature and spectral type highlight changes in stellar distributions expected with the inclusion of main-sequence mass loss.

B. Modeling

The models were calculated using the galactic chemical evolution equations of Tinsley (1980), modified to include the effects of main-sequence mass loss. The solar neighborhood is modeled as a two-dimensional annulus in the Galactic disk about the Galactic center passing through the Sun. The differential equations to be solved are

$$\frac{dM_g}{dt} = -\Psi + E_g + f$$

$$\frac{d(Z_g M_g)}{dt} = -Z_g \Psi + E_z + Z_f f$$

where M_g is the gas density in the solar neighborhood, Ψ is the star formation rate, E_g is the gas return rate from stars, f is the gas infall or outflow rate, Z_g is the gas metallicity in the solar neighborhood, E_z is the metal return rate from stars, and Z_f is the metallicity of infalling or outflowing gas. The gas and metal return rates are given by

$$E_g = \int_{m_{turnoff}}^{+\infty} (m - w_m)\, \Psi(t - \tau_m)\, \phi(m)\, dm$$

$$E_z = \int_{m_{turnoff}}^{+\infty} \left[(m - w_m - mp_{zm})\, Z_g(t - \tau_m) + mp_{zm}\right] \Psi(t - \tau_m)\, \phi(m)\, dm$$

where m is the stellar mass, w_m is the remnant mass, τ_m is the main-sequence lifetime of a star of mass m, p_{zm} is the fraction of the mass of a star of mass m that is processed into new metals and returned, and $\phi(m)$ is the initial mass function (IMF). The initial mass function is normalized such that

$$N \int m\, \phi(m)\, dm = 1$$

where N is the normalization constant.

The four assumptions of a "simple" model are, according to Tinsley (1980): 1) the solar neighborhood is a closed system, i.e., f=0; 2) all of the initial mass consists of metal-free gas; 3) the IMF is constant in time; and 4) the gas is chemically homogeneous at all times. The initial gas density in the solar neighborhood used in our models is 50 $M_\odot/pc^2$; this value is in agreement with a recent determination by Kuijken and Gilmore (1988) of the present matter density in the solar neighborhood. Stars are formed with initial masses between 0.7 and 50 $M_\odot$, with constant star formation rate and Salpeter (1955) initial mass function $\phi(m) = m^{-2.35}$. The stellar yields of new metals per generation are constant with time and stellar metallicity, and are based upon a linear fit in mass to the yields of Chiosi and Caimmi (1979) for stars of 10 to 100 $M_\odot$. Only stars with initial mass greater than 18 $M_\odot$ contribute to the production of new metals.

The instantaneous recycling approximation applies to stars of initial mass greater than 3.0 $M_\odot$. Table 9 lists the stellar main-sequence lifetimes used for stars of initial mass less than 3.0 $M_\odot$. The main-sequence lifetimes are those of the models of VandenBerg (1985) for 0.7 to 3.0 $M_\odot$ stars with Z = 0.0169, 0.01, 0.006, 0.003, and 0.0017, and initial Y = 0.25. The main-sequence lifetimes listed in Table 9 are either those labeled "T" (turnoff) in VandenBerg's tables for stars without convective cores, or those labeled "R" (reddest point in the post-main sequence loop) for stars with convective cores. These data were extrapolated to maximum Z = 0.03 and minimum Z = 0.0003.

Table 9. Main-sequence lifetimes in Gyr of 0.7-3.0 $M_\odot$ dwarfs with Y = 0.25, $-3.5 \le \log Z \le -1.52$, and $\alpha = 1.6$ based on the stellar models of VandenBerg (1985). Lifetimes for log Z = -1.52 and -3.50 are extrapolated linearly in log Z from values at intermediate Z

	log Z						
Mass ($M_\odot$)	-1.52	-1.77	-2.00	-2.22	-2.52	-2.77	-3.50
3.00	0.34	0.31	0.27	0.25	0.22	0.21	0.15
2.80	0.41	0.38	0.33	0.29	0.26	0.25	0.18
2.60	0.50	0.46	0.40	0.35	0.32	0.30	0.21
2.40	0.62	0.58	0.49	0.44	0.39	0.36	0.25
2.20	0.80	0.73	0.62	0.54	0.48	0.45	0.30
2.00	1.1	0.97	0.81	0.71	0.62	0.58	0.38
1.85	1.3	1.2	1.0	0.87	0.76	0.70	0.46
1.70	1.7	1.5	1.3	1.1	0.96	0.88	0.57
1.60	2.0	1.8	1.5	1.3	1.1	1.0	0.66
1.50	2.5	2.2	1.8	1.6	1.4	1.2	0.78
1.40	3.4	2.8	2.3	1.9	1.6	1.5	0.86
1.30	4.1	3.6	2.9	2.4	2.0	1.7	1.0
1.20	5.3	4.7	3.7	3.1	2.2	2.8	1.9
1.10	5.1	4.9	3.8	3.3	3.9	3.9	3.3
1.00	10	8.9	7.9	7.1	6.1	5.4	3.8
0.90	18	17	12	10	8.6	8.2	4.6
0.80	31	28	21	17	14	13	7.3
0.70	45	38	32	29	25	23	16

Lifetimes are interpolated from the table using bicubic splines. We adopt Tinsley's (1980) assumption that stars of mass greater than 4.0 $M_\odot$ leave 1.4 $M_\odot$ remnants, and stars of mass between 0.7 and 4.0 $M_\odot$ leave 0.7 $M_\odot$ remnants.

The dwarfs remaining on the main sequence at the final Galactic disk age are sorted into four effective temperature bins, (log T_{eff} = 3.88-3.82, 3.82-3.78, 3.78-3.74, and 3.74-3.70) for later analysis. Effective temperatures of dwarfs of various masses and metallicities, again from the models of VandenBerg (1985), are given in Table 10. The effective temperature of a model dwarf of a given mass depends upon its age, mixing length and Y abundance, as well as its metallicity. The VandenBerg models have initial Y = 0.25, and mixing length α=1.6; to roughly account for stellar age, the effective temperature listed is for stellar age 5 Gyr for long-lived stars ($M \le 0.9$-$1.0\ M_\odot$), and at half the main-sequence lifetime of short-lived stars, following the example of Tinsley (1980). The data are again extrapolated to maximum Z = 0.03 and minimum Z = 0.0003. Effective temperatures for intermediate mass and Z are interpolated from the table using bicubic splines.

Since for a given effective temperature, the spectral type of a star can vary by as much as half of a spectral class over the range of metallicity considered in these models, it is necessary when binning stars by spectral type to account for the dependence upon metallicity as well as effective temperature. The effective temperature-metallicity-spectral type relation adopted is that of Grenon (1976) for F5-K4 dwarfs, extrapolated to spectral type F0. We prepared a lookup table (Table 11) for use in the galactic chemical evolution code by reading from Grenon's curves of constant spectral type plotted as a function of Z and T_{eff}. The spectral types so obtained agree well at solar metallicities with the empirical effective temperature-spectral type relation of Habets and Heintze (1981) for Population I stars.

For the models including main-sequence mass loss, all stars between 3.0 $M_\odot$ and a metallicity-dependent lower mass M_L are assumed to lose mass instantaneously to form stars with mass, lifetime,

Table 10. Log T_{eff} (K) for 0.7-3.0 $M_\odot$ dwarfs with Y = 0.25, $-3.5 \leq \log Z \leq -1.52$, and $\alpha = 1.6$ based on the models of VandenBerg (1985). Temperatures for log Z = -1.52 and -3.50 are extrapolated linearly in log Z from values at intermediate Z

	log Z						
Mass ($M_\odot$)	-1.52	-1.77	-2.00	-2.22	-2.52	-2.77	-3.50
3.00	4.045	4.068	4.103	4.132	4.163	4.184	4.274
2.80	4.024	4.048	4.083	4.113	4.145	4.166	4.258
2.60	4.000	4.025	4.061	4.092	4.125	4.147	4.242
2.40	3.975	4.000	4.037	4.068	4.103	4.125	4.222
2.20	3.947	3.973	4.011	4.043	4.078	4.101	4.200
2.00	3.916	3.942	3.981	4.014	4.050	4.073	4.175
1.85	3.891	3.917	3.956	3.989	4.026	4.050	4.152
1.70	3.862	3.890	3.928	3.962	4.000	4.024	4.127
1.60	3.842	3.870	3.908	3.942	3.980	4.005	4.109
1.50	3.823	3.852	3.887	3.922	3.960	3.984	4.087
1.40	3.806	3.834	3.866	3.900	3.938	3.960	4.059
1.30	3.788	3.816	3.843	3.873	3.911	3.932	4.022
1.20	3.775	3.800	3.823	3.847	3.878	3.902	3.977
1.10	3.760	3.782	3.801	3.822	3.848	3.868	3.933
1.00	3.747	3.762	3.787	3.800	3.823	3.838	3.895
0.90	3.714	3.729	3.758	3.781	3.802	3.815	3.883
0.80	3.667	3.684	3.715	3.748	3.770	3.783	3.864
0.70	3.615	3.636	3.665	3.695	3.723	3.738	3.820

Table 11. Spectral type as a function of metallicity and effective temperature based upon plot by Grenon (1976) and extrapolated to spectral types F0-F4

	Log ($Z/Z_\odot$)														
Log T_{eff}(K)	0.25	0.125	0.00	-0.125	-0.25	-0.50	-0.75	-1.00	-1.25	-1.50	-1.70	-2.00
3.67	—	—	—	—	—	—	—	—	—	—	K0	K0
3.68	—	—	—	—	—	—	—	—	K0	K0	K0	G9
3.69	—	—	—	—	—	—	K0	G9	G8	G8	G8	G8
3.70	—	—	—	—	K0	G9	G8	G7	G6	G6	G5	G5
3.71	—	—	K0	G9	G8	G8	G7	G6	G5	G5	G4	G4
3.72	K0	G9	G8	G8	G7	G6	G5	G4	G3	G3	G2	G2
3.73	G8	G8	G7	G6	G5	G4	G3	G2	G2	G2	G1	G1
3.74	G7	G6	G5	G4	G3	G2	G2	G1	G0	G0	G0	G0
3.75	G5	G4	G3	G2	G2	G1	G0	F9	F9	F9	F8	F8
3.76	G3	G3	G2	G1	G1	G0	F9	F8	F8	F8	F7	F7
3.77	G2	G2	G1	G0	G0	F9	F8	F7	F7	F7	F7	F7
3.78	G1	G0	F9	F9	F9	F7	F7	F6	F6	F6	F6	F6
3.79	G0	F9	F8	F7	F7	F6	F5	F5	F5	F5	F5	F5
3.80	F9	F8	F7	F7	F6	F5	F5	F5	F4	F4	F4	F4
3.81	F8	F7	F6	F5	F5	F5	F4	F4	F3	F3	F3	F3
3.82	F7	F6	F5	F4	F4	F4	F3	F3	F3	F2	F2	F2
3.83	F6	F5	F4	F3	F3	F3	F2	F2	F2	F2	F1	F1
3.84	F5	F4	F3	F2	F2	F2	F1	F1	F1	F0	F0	F0
3.85	F4	F3	F2	F1	F1	F1	F0	F0	F0	—	—	—
3.86	F3	F2	F1	F0	F0	F0	—	—	—	—	—	—
3.87	F2	F1	F0	—	—	—	—	—	—	—	—	—
3.88	F1	F0	—	—	—	—	—	—	—	—	—	—
3.89	F0	—	—	—	—	—	—	—	—	—	—	—

and effective temperature characteristic of a star of initial mass M_L. These assumptions are simplistic and represent extreme conditions, but were chosen to unambiguously highlight the effects of including main-sequence mass loss. The upper mass cutoff for mass loss, 3.0 $M_\odot$, may be too high for most clusters; the mass at which the blue edge of the Cepheid pulsation-instability strip intersects the main sequence varies between 2.0 and 3.0 $M_\odot$ depending upon the Y and Z abundance of stars in the cluster. Also, slowly rotating stars, "blue stragglers", or chemically peculiar stars in the instability strip may not have high mass-loss rates. Finally, not all stars in a cluster will cease losing mass at exactly the same final mass, M_L. Mass loss may cease when a star leaves the pulsation instability strip, spins down sufficiently, and/or develops a substantial envelope convection zone.

Assuming that main-sequence stars lose mass until their surface convection zones contain about 2% of the star's mass (as would be the case if the Sun were such a star), and recognizing that convection zone depth correlates with effective temperature (Cox and Guili 1968) and that increased opacity deepens the convection zone, we can estimate the mass M_L at which a star ceases losing significant amounts of mass a a function of metallicity (WBS 1987). Using VandenBerg's (1985) models, we find that the linear relationship $M_L = 16.4\ Z + 0.73\ M_\odot$ adequately approximates the mass of zero-age stars with effective temperatures equal to that of a zero-age solar-metallicity 1 $M_\odot$ model, as a function of stellar metallicity. Since the above assumptions regarding the termination of main-sequence mass loss are qualitative, and since the slope of the above M_L-Z relation steepens somewhat for slightly-evolved stars, we have adopted the relation $M_L = 20\ Z + 0.8\ M_\odot$ in our models as an heuristic estimate of final main-sequence mass.

While we have included the effects of metallicity on stellar main-sequence lifetimes, we have ignored two additional effects–the reduction in stellar lifetime due to early burning at higher luminosity by stars experiencing main-sequence mass loss, and possible helium enrichment during the lifetime of the disk. Stellar evolution models

(Guzik, Willson and Brunish 1987; Guzik and Willson 1988) show that, for stars of fixed initial composition and initial mass ≤ 2.0 $M_\odot$ evolving toward a final mass of 1 $M_\odot$ with e-folding time 2 x 10^8 yr, the main-sequence lifetime is reduced by ≤ 25% from the main-sequence lifetime of a constant 1 $M_\odot$ star. Further quantification of stellar main-sequence lifetimes in the chemical evolution models would be premature, as the actual mass-loss timescales and the lower and upper mass limits for main-sequence mass loss have not been established. At a given stellar age, the effective temperature of a mass-losing star will also be slightly different than for a star of the same mass that did not undergo mass loss. Models with a short-lived mass-loss phase do follow the empirical main sequence closely as they evolve toward later spectral type, so their effective temperature and luminosity are characteristic of a normal main-sequence star.

Regarding the effect of Y abundance on main-sequence lifetimes, an increase in stellar Y abundance from 0.20 to 0.30 at fixed Z reduces the lifetime of 0.7 to 1.2 $M_\odot$ stars by slightly less than 50% (VandenBerg 1983), while the Z increase considered in our chemical evolution models (0.0003 to 0.029) increases lifetimes by a factor of 3 to 4 at fixed Y (see Table 9). The Y abundance also affects stellar effective temperatures. However, the evidence for correlations in Y enrichment with increasing Z is inconclusive, and is consistent with localized variations in Y uncorrelated with Z (Boesgaard and Steigman 1985). Adding the effects of Z-abundance on lifetimes is relevant, given the proposed dependence of the final main-sequence mass on metallicity, but including effects of enrichment in Y at this point would only increase the difficulty in isolating potential causes for differences in the models.

Models with present Galactic disk ages of 5, 10 and 15 Gyr were evolved, both with and without main-sequence mass loss, using a time step of 0.01 Gyr and a stellar mass increment of 0.01 $M_\odot$. All models have initial gas metallicity Z = 0.0003 (the lowest metallicity included in main-sequence lifetime and effective temperature Tables 9 and 10).

The models were normalized such that for the given disk age, $M_{gas}/M_{total} = 0.120 \pm 0.005$ and $Z_{final} = 0.0290 \pm 0.0002$, by adjusting the star formation rate and yield in new metals per stellar generation. For these models,

$$\text{Yield} = F\ N \int m_z\, \phi(m)\ dm\ \Psi\ \Delta t$$

where F is a yield multiplication factor, N is the IMF normalization, m_Z is the mass of new metals ejected from a star of mass m, $\phi(m) = m^{-2.35}$, Ψ is the star formation rate, Δt is the time step used in the model, and the integral is over the masses of stars that return new metals, i.e. stars of 18-50 $M_\odot$. An adjustment in the star formation rate also affects the yield; F is adjusted to compensate for changes in star formation rate as well as to attain the desired gas metallicity at the present disk age.

C. Results

In this section we describe the characteristics of models for the solar neighborhood both with and without main-sequence mass loss at terminal (i.e. present) ages 5 Gyr, 10 Gyr and 15 Gyr. Table 12 compares the star formation rates and multiplication factors for the yield in new metals per stellar generation necessary to normalize the models with and without main-sequence mass loss to the same final gas mass and metallicity. Figures 34, 35, and 36 compare the gas mass versus time, the log of the gas metallicity versus time, and the gas return rate versus time, respectively, of the 5 Gyr models with and without main-sequence mass loss. The corresponding plots for the 10 and 15 Gyr models are qualitatively similar.

The models with main-sequence mass loss differ from those without such mass loss, in principle, only due to returns from mass-losing stars between 3.0 $M_\odot$ and M_L. Without main-sequence mass loss, these stars return the difference of their initial and remnant mass to the interstellar medium over a range of timescales equal to their main-sequence lifetimes. With main-sequence mass loss, these

Table 12. Star formation rates and yield multiplication factors used for model normalization

		Star Formation Rate ($M_\odot/pc^2/Gyr$)		Yield Multiplication Factor	
	Model	A	B	A	B
Galactic Age (Gyr)	5.00	19.5	19.5	0.61	0.56
	10.00	10.4	9.7	0.57	0.57
	15.00	7.2	6.8	0.54	0.61

A No main-sequence mass loss.
B With main-sequence mass loss.

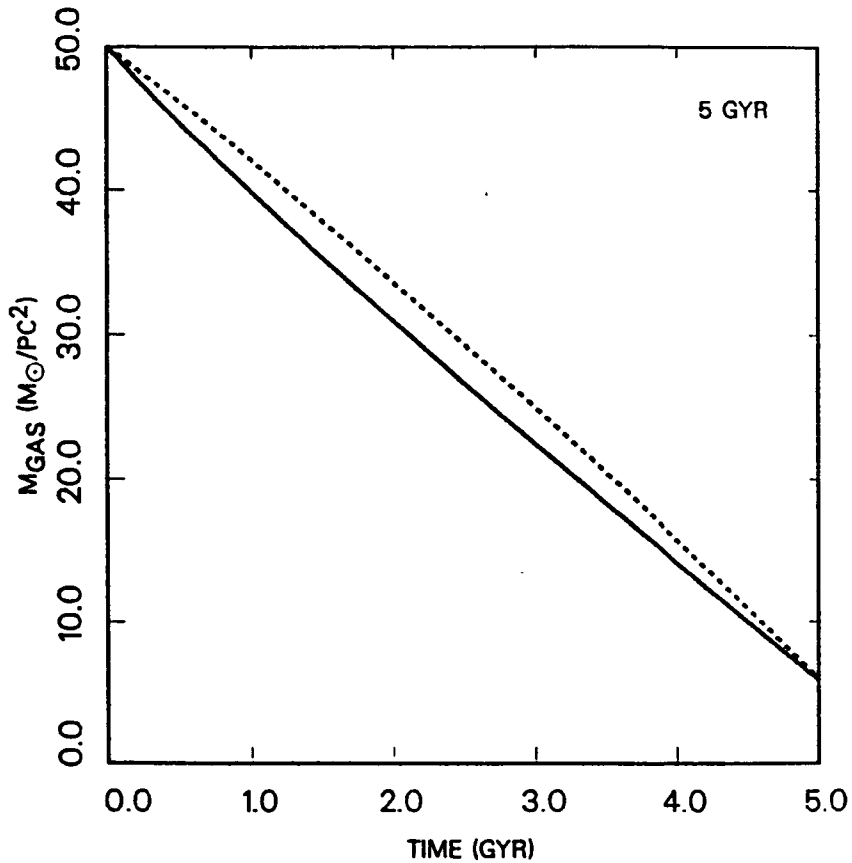

Figure 34. Gas density vs. time compared for 5 Gyr disk age models with (dashed line) and without (solid line) main-sequence mass loss

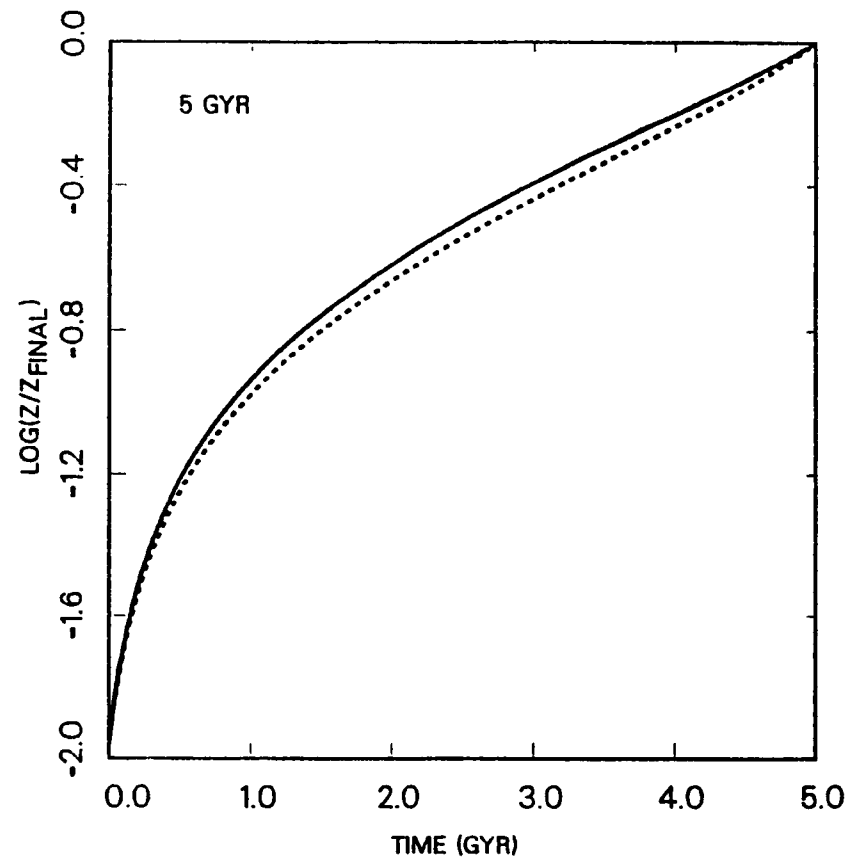

Figure 35. Gas metallicity vs. time compared for 5 Gyr disk age models with (dashed line) and without (solid line) main-sequence mass loss (Z_{final} = 0.029)

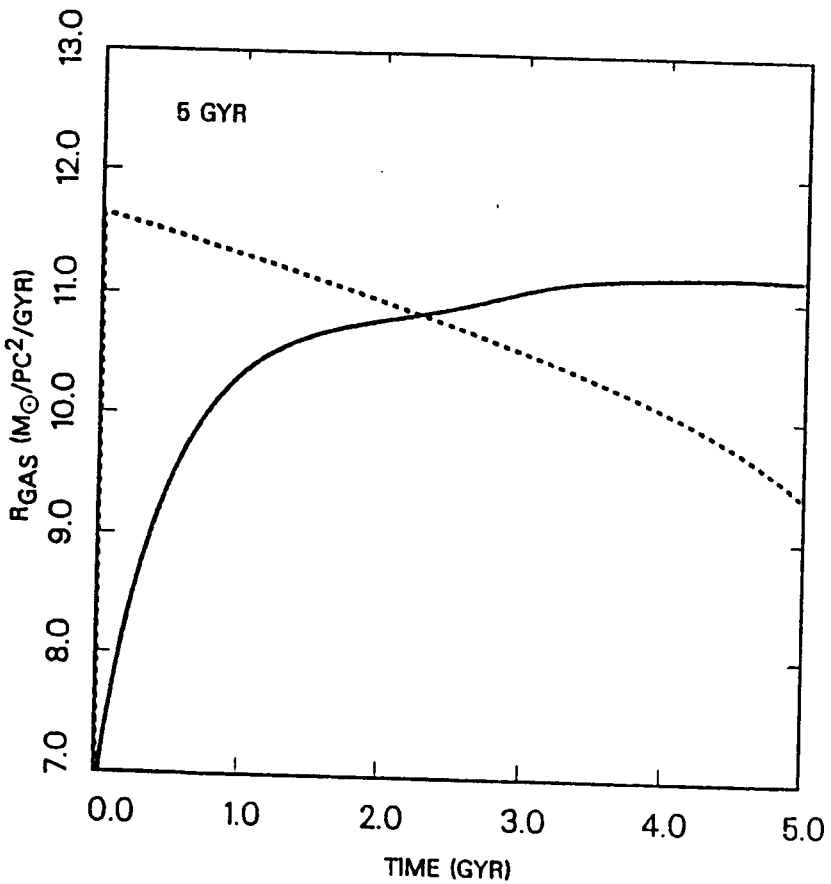

Figure 36. Gas return rate vs. time compared for 5 Gyr disk age models with (dashed line) and without (solid line) main-sequence mass loss

stars return the difference of their initial mass and M_L instantaneously, but the difference of M_L and their remnant mass after a longer time, namely the main-sequence lifetime of a star of mass M_L. All models are constrained to have the same initial and final gas fraction and gas metallicity, but at about half the final disk age, the amount of free gas can be as much as 10% larger (Figure 34) for the 5 Gyr disk model, (9% and 5% for the 10 and 15 Gyr age models, respectively), and the gas metallicity 10% lower (Figure 35) (9% and 6% for 10 and 15 Gyr age models, respectively) in the models with main-sequence mass loss due to the prompt returns of less-enriched gas from the mass-losing stars.

The gas return rate vs. time increases in models without main-sequence mass loss (Figure 36), since this is partially a cumulative quantity, but decreases in models with mass loss. This occurs because M_L is increasing with gas metallicity, implying a narrower mass range for main-sequence mass loss, and because stars of mass M_L generally have main-sequence lifetimes longer than the disk age. The gas return rate in models with main-sequence mass loss begins to increase at late times for disk ages 10 and 15 Gyr as low-mass stars formed early in the lifetime of the disk begin to leave the main sequence.

For the 5 Gyr models, the net returns from each model balance over time so that the same star formation rate can be used for either case. For the 10 and 15 Gyr models, a 6-7% lower star formation rate is required in the models with mass loss to compensate in the gas/star normalization for the gas locked in stars of mass M_L over long timescales, even though returns from low-metallicity stars begin to appear at late times for the 10 and 15 Gyr models. However, the general impression is that the star formation rate is quite insensitive to the mass loss experienced by intermediate-mass stars. This result is a simple consequence of the fact that, with the Salpeter initial mass function and the low-mass cutoff of 0.7 $M_\odot$ used here, the gas involved in mass loss is a relatively small fraction of the total. Apparently, a large change in the mass function or the low-mass cutoff would be required to alter this result.

Since only stars of initial mass greater than 18 $M_\odot$ return new metals, the amount of new metals ejected per stellar generation depends only upon the star formation rate and yield, both of which are fixed in any onemodel. In the model without mass loss, the gas ejection rate increases with time due to the death of relatively long-lived stars; those leaving the main-sequence return relatively unenriched gas characteristic of the gas metallicity at the time they were formed. Since these stars become stars of mass M_L in the model with mass loss, and do not return metal-poor gas before age 5 Gyr, the yield must be decreased to attain the same final gas metallicity as in the model without mass loss. For the 10 Gyr models, the reduced star formation rate of the model with mass loss effectively reduces the yield by the necessary amount. For the 15 Gyr model, the effect of the reduced star formation rate in the model with mass loss is stronger than the dilution effect in the model without mass loss, so the yield must be larger in the model without mass loss. However, in all cases the differences are relatively small (0-13%; see Table 12).

Figure 37 show the quantity $1\text{-}M_{gas}$ (or the mass of stars plus remnants) and the cumulative mass of stars remaining on the main sequence at the final disk age versus log Z_{gas} for disk ages 5, 10 and 15 Gyr. The y-axis is labeled "S" for mass of stars and/or stellar remnants, as opposed to gas. All curves are normalized by dividing by 0.88 M_{total}. For the models including main-sequence mass loss, 30% to 60% more stars by mass remain on the main sequence at the current disk age, since stars of mass between 3.0 $M_\odot$ and M_L lose mass to become long-lived stars of mass M_L. The largest effect is for disk age 10 Gyr, since by age 15 Gyr stars of mass M_L begin to leave the main sequence.

Figure 38 shows the cumulative mass of stars that remain on the main sequence at the final disk age versus log Z_{gas}, sorted into four effective-temperature bins and normalized by dividing by 0.88 M_{total} as before. Without the added complication of the metallicity-dependent conversion from T_{eff} to spectral type, these figures are useful for highlighting changes in metallicity distributions with the inclusion of

Figure 37. $1\text{-}M_{gas}$ vs. metallicity for model without main-sequence mass loss (thick solid line), and the cumulative mass of stars remaining on the main sequence at final disk ages 5 Gyr (upper left), 10 Gyr (upper right) and 15 Gyr (lower left) for models with (dashed line) and without (thin solid line) main-sequence mass loss vs. gas metallicity. All curves are normalized by dividing by 0.88 M_{total}, where M_{total} is the total mass density in the solar neighborhood, 50 $M_\odot/pc^2$

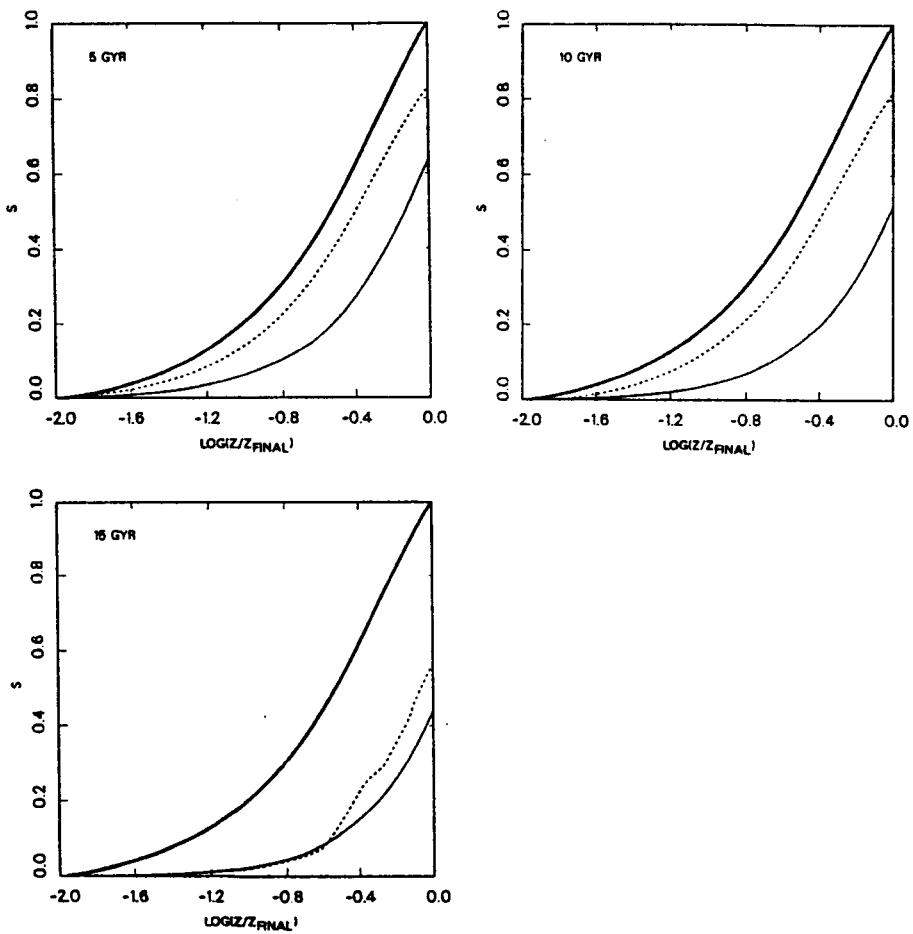

Figure 38. Cumulative mass of stars in log T_{eff} bins 3.82-3.88 (upper left), 3.78-3.82 (upper right), 3.74-3.78 (lower left), 3.70-3.74 (lower right) remaining on the main sequence at the current disk age vs. gas metallicity for models with (thin lines) and without (thick lines) main-sequence mass loss, and for disk ages 5 Gyr (solid lines), 10 Gyr (chain-dashed lines), and 15 Gyr (dotted lines). All curves are normalized by dividing by 0.88 M_{total}, where M_{total} is the total mass density in the solar neighborhood, 50 $M_{\odot}/pc^2$

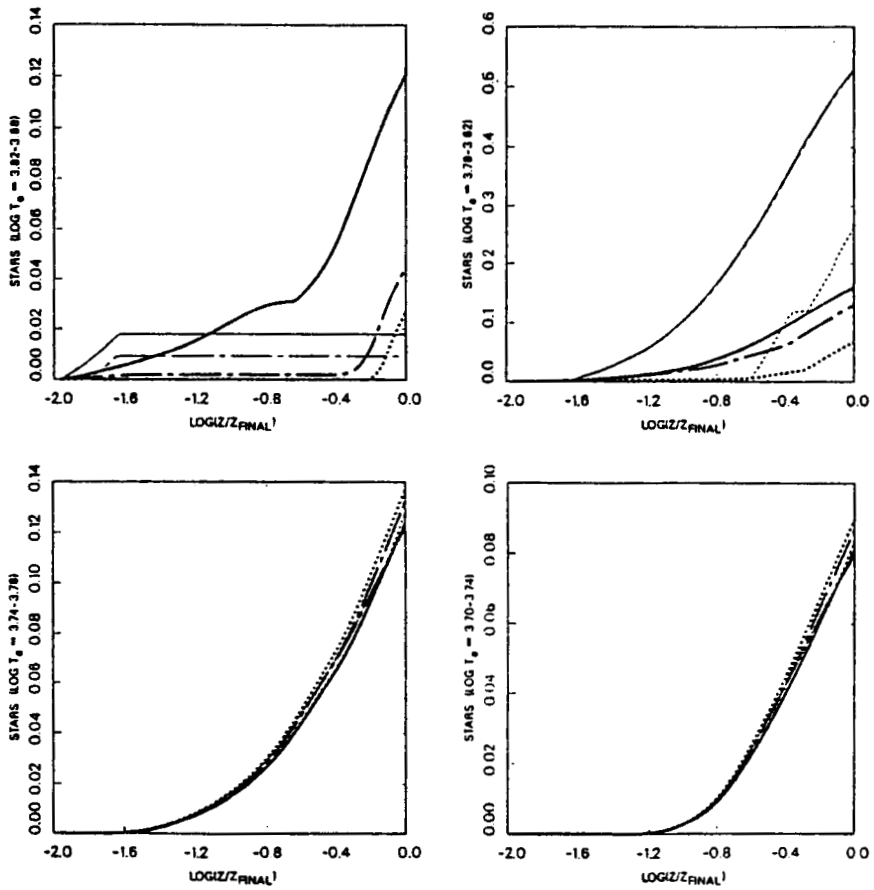

main-sequence mass loss, and for discerning the effects of Z-dependent lifetimes and effective temperatures on the distributions. To understand the features of the plots, it should be remembered that: (1) for a given stellar mass, low-Z stars have higher T_{eff} and shorter main-sequence lifetimes; and (2) for our parametrization of M_L (M_L = 20 Z + 0.8), the mass-losing stars evolve down the main sequence to roughly the same effective temperature (log T_{eff} ~ 3.79). Focusing on the distributions for the models with mass loss and log T_{eff} = 3.82-3.88 (Figure 38, upper left), a few low-Z, high-T_{eff} stars of mass ≤ M_L (~ 0.8 $M_\odot$ for low Z) with main-sequence lifetimes longer than 5 or 10 Gyr are produced, but these stars leave the main sequence by age 15 Gyr. Since the majority of the stars that would have been in this T_{eff} bin lose mass to become stars of lower T_{eff}, the models with main-sequence mass loss show a deficiency of intermediate- and high-Z stars relative to models without mass loss.

Focusing next on the metallicity distributions of stars with log T_{eff} = 3.78-3.82 (Figure 38, upper right), for the models with main-sequence mass loss, a large number of stars lose mass to become stars having effective temperatures in this range. The mass of stars in this bin is larger for the models with mass loss at all metallicities, accumulating to a factor of 3 to 4 by the present disk age. For the 15 Gyr age models, the low-metallicity stars have had time to leave the main sequence, thus reducing the cumulative mass remaining for both models. The "plateau" in the distribution at log Z/Z_{final} ~ -0.4 of the 15 Gyr model with mass loss is due to the increase in M_L, and consequent decrease in the main-sequence lifetime of stars of mass M_L, with increasing Z. At this metallicity, the main-sequence lifetime of a star of mass M_L is comparable to the time remaining in the disk evolution. As M_L increases with increasing Z, the main-sequence lifetime decreases such that stars of this mass leave the main sequence before the end of the disk evolution.

For the two lowest-temperature bins (Figure 38, lower left and right), inclusion of main-sequence mass loss has little effect other than

that attributable to the slightly different star formation rates and yields used to normalize the models to the same final gas fraction and gas metallicity. In reality, not all stars will cease mass loss at the same final mass for a given metallicity, so some stars could be expected to evolve down the main sequence into the log T_{eff} = 3.74-3.78 bin (Figure 38, lower left). No stars with log $Z/Z_{final} \leq -1.6$ are present in the third bin (Figure 38, lower left), and no stars with log $Z/Z_{final} \leq -1.2$ are present in the fourth bin (Figure 38, lower right), due to the low-mass cutoff used for the initial mass function (0.7 $M_{\odot}$). Low-Z stars of mass $\geq$ 0.7 $M_{\odot}$ have log $T_{eff} > 3.78$.

Figures 39, 40 and 41 compare the relative mass of stars remaining on the main sequence at the current disk age, binned by spectral type, for models with and without mass loss, at present disk ages 5, 10 and 15 Gyr, respectively. The results can be understood if one remembers that stars of mass M_L shift to later spectral type with increasing metallicity. Stars of mass M_L are classified as spectral type early-F at low Z, mid-F at intermediate Z, and late-F at high Z. For the 5 Gyr-age models, the early-F stars produced at intermediate and high Z in the model with main-sequence mass loss have become stars of later spectral type, but the majority of early-F stars in both models have not had time to leave the main sequence; thus, the models predict a large deficiency (70%) of early-F stars in the model with mass loss. For the 10 Gyr age model without mass loss, the high-mass early-F stars produced have had time to leave the main sequence; thus the relative deficiency of the model with mass loss becomes only 14%. For disk age 15 Gyr, early-F stars in both models have had time to leave the main sequence; the only early-F stars remaining are those high-mass stars produced at recent times in the model without mass loss.

The A-F stars of low to intermediate Z that have lost mass to become stars of mid-F spectral type produce an excess of these stars in the 5 and 10 Gyr-age models with mass loss. The excess is increased from 87% for the 5 Gyr age model to 117% for the 10 Gyr age model, as some intermediate-Z mid-F stars produced in the model without mass

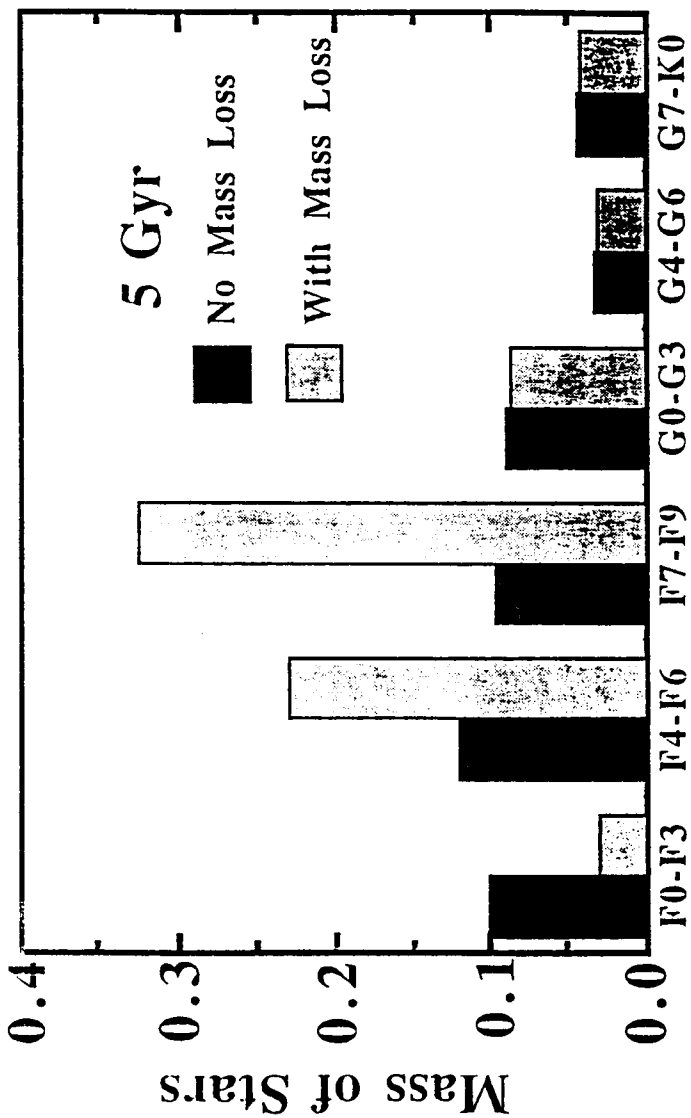

Figure 39. Relative mass of stars remaining on the main-sequence at the current disk age, binned by spectral type, for models with and without mass loss, at present disk age 5 Gyr

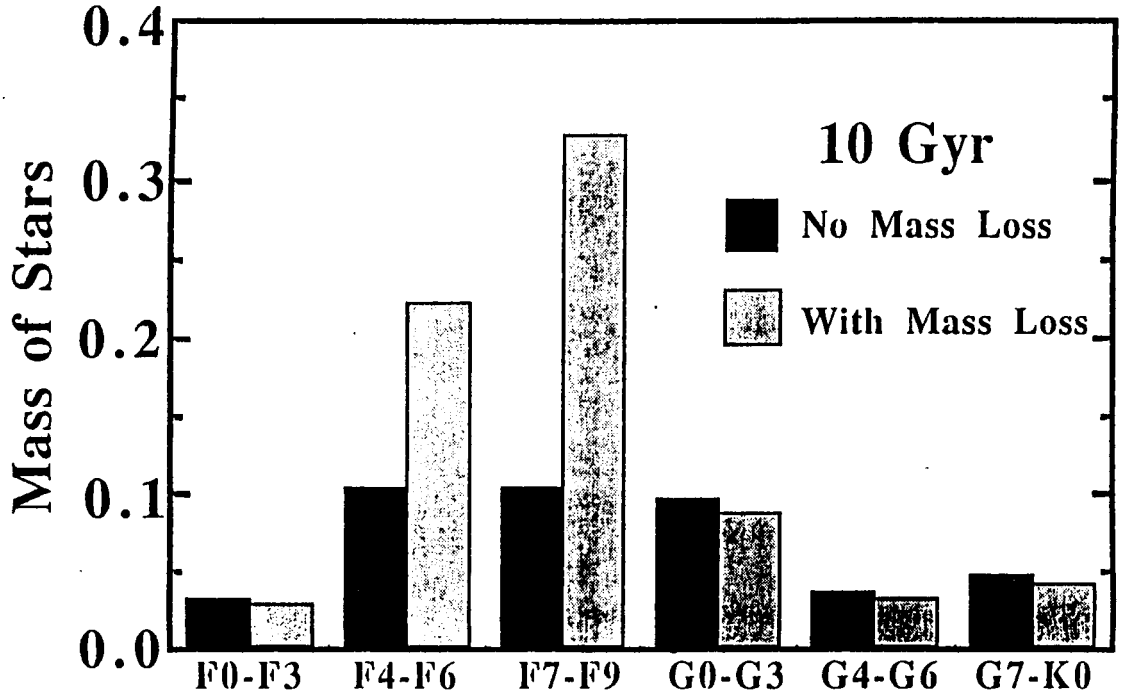

Figure 40. Relative mass of stars remaining on the main-sequence at the current disk age, binned by spectral type, for models with and without mass loss, at present disk age 10 Gyr

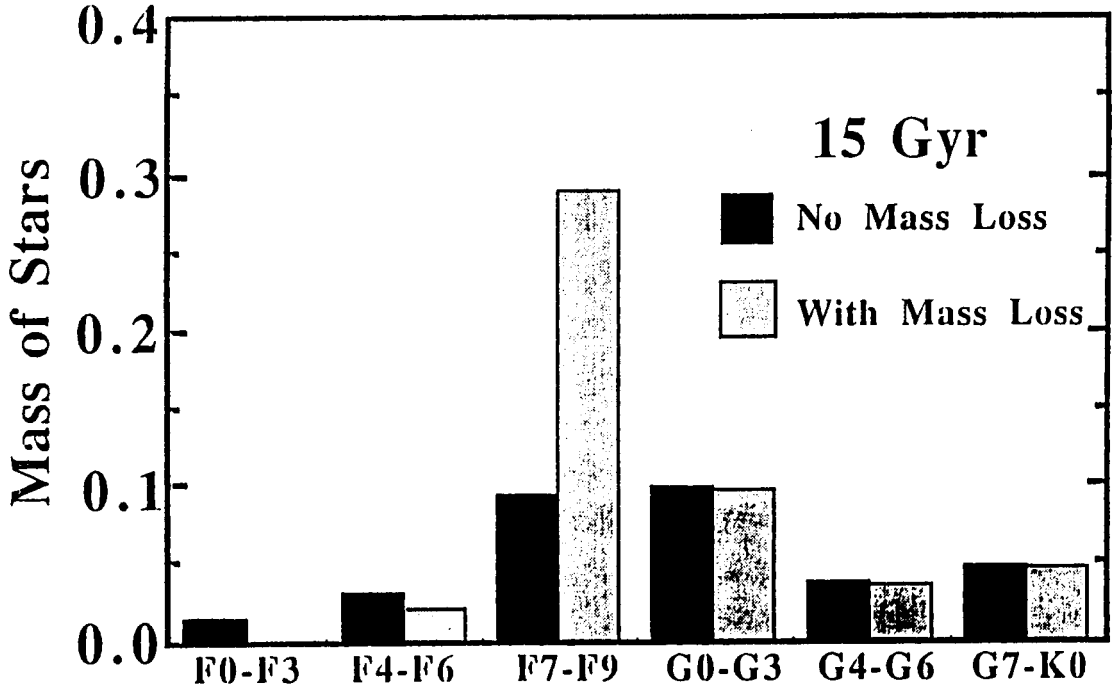

Figure 41. Relative mass of stars remaining on the main-sequence at the current disk age, binned by spectral type, for models with and without mass loss, at present disk age 15 Gyr

loss leave the main sequence. For the 15 Gyr age model, no excess remains, as only low- to intermediate-Z long-lived stars of mass < M_L produced in both models, and some recently produced high-Z stars in the model without mass loss remain on the main sequence.

Considering next the late-F spectral type bins, the models with mass loss produce a consistently large (200-250%) excess of these stars at all final disk ages relative to models without mass loss. The relative excess decreases slightly with increasing disk age, as some late-F stars produced early in the evolution leave the main sequence.

For our parametrization of M_L no stars evolve down the main sequence to become stars of spectral type G. Therefore, the relative masses of stars of these spectral types are changed only slightly. These bins are included mainly to provide some basis for observational comparison with F stars. It should be remembered that the lower-mass cutuff for the IMF used in all models is 0.7 $M_\odot$; thus only G stars with mass ≥ 0.7 $M_\odot$ are included in these histograms. Differences between models with and without mass loss can be attributed to differences in star formation rates and yields used to normalize models to the same final gas fraction and gas metallicity. Generally, the star formation rates of the models without main-sequence mass loss are larger (see Table 12); for the 5 Gyr age models, the star formation rates are the same, but since in the course of evolution the gas metallicity of the model with mass loss is lower than for the corresponding model without mass loss, some would-be G stars shift to the F-star bins.

D. Discussion

Two separate questions can, in principle, be addressed with the model results: 1) What is the predicted present distribution of dwarfs versus spectral type? and 2) What is the predicted present metallicity distribution for dwarfs in a given range of effective temperature? The generalized "G-dwarf" curves which include stars of a large range of masses and spectral types and are obtained assuming instantaneous recycling, dilute or omit effects that may be potentially useful in

discriminating between models. However, very fine binning of observed data by spectral type or metallicity is usually precluded by the size of the sample, and requires more exacting sample corrections. Eventually, confrontation between the observations and models on the above questions should constrain model parameters; some progress has already been made in quantifying the "G-dwarf" problem (van den Bergh 1962; Schmidt 1963; Beers 1987) and determining the time-dependence of the Galactic star formation rate (Twarog 1980b; Scalo 1988) using observations.

The first question above has special relevance to the main-sequence mass loss hypothesis, due to the predicted deficiency of early-F dwarfs and large excess of late F dwarfs. Some observations qualitatively support this prediction. The present-day mass function recently derived by Scalo (1986) exhibits multi-modality, with "bumps" at stellar masses around 1.2 and 3.0 $M_\odot$ and a "dip" for stellar masses that fall within the pulsation instability strip. A period of rapid early main-sequence mass loss as postulated could be the source of this bimodality (WBS 1987). Scalo (1988) suggests that these features are due to two bursts of star formation, one occurring 2×10^8 years ago, such that the present day main-sequence turnoff mass for these stars is 3.0 $M_\odot$, and the second 5×10^9 years ago with corresponding turnoff mass 1.2 $M_\odot$. The ratio of stellar remnants, e.g., white dwarfs, compared to main-sequence stars and the age distribution of white dwarfs offer a way to distinguish between the proposed explanations for features in the mass function, e.g., bimodal star formation (Larson 1986), starbursts (Scalo 1988), and main-sequence mass loss (WBS 1987). Chemical evolution models incorporating either starbursts or bimodal star formation would produce the either the same proportion or an excess of stellar remnants, relative to models with a monotonic star formation rate and initial mass function, while the main-sequence mass loss hypothesis predicts a deficiency of remnants. In addition, the starburst explanation predicts peaks in the age distribution of white dwarfs at 2×10^8 and 5×10^9 years, while the other explanations

in white dwarf ages. Since white dwarfs cool as they age, the white dwarf sequence on the HR diagram is primarily an age sequence; calibrated white dwarf cooling curves would be extremely useful in deciding this question. Unfortunately, this method is at present inconclusive due to the small number of well-observed white dwarfs in clusters, and the uncertainties in determining cluster ages (Shapiro and Teukolsky 1983).

We have counted the main-sequence stars and white dwarfs within 5 and 10 pc of the Sun listed in the *Catalog of Nearby Stars* (Gliese 1969; Gliese and Jahreiss 1979). Incomplete sampling of white dwarfs beyond 5 pc, and small number statistics, especially for A-G dwarfs, preclude using ratios of F-G dwarfs to remnants for distinguishing between models at the present time. This situation may change when a more complete sample of white dwarfs becomes available.

WBS (1987), using a sample of over 20,000 dwarfs from the *Michigan Catalog of Spectral Types* (Houk and Cowley 1975) and correcting for stellar age and volume of space sampled, find a significant deficiency of stars with log $M/M_{\odot}$ between 0.15 and 0.30 ($M = 1.4$ to $2.0\ M_{\odot}$, spectral types A through early-F), though the evidence for an excess of stars of mass $\leq 1.4\ M_{\odot}$ is inconclusive. Böhm-Vitense (1970) showed that a deficiency of stars in this spectral type region is expected, due to the abrupt onset of envelope convection for $T_{eff} \leq$ 8000 K. However, the mass to spectral-type correspondence (Habets and Heintze 1981) accounts for this effect through a change in slope in this region. The severity of the deficiency in the mass function depends upon the mass to spectral-type correspondence, but the gap persists for all but the most contrived choices of this relation within the limits of uncertainty (Willson, Bowen and Titus 1988).

WBS (1987) also find a clear gap along the main sequence in the distribution of eclipsing double-lined spectroscopic binaries from the data of Popper (1980); for these stars, the stellar masses can be determined directly. However, these data suffer from small number statistics and selection effects. More rigorous analysis is in progress

(Willson, Bowen and Titus 1988) to quantify these findings.

With regard to the second question, the distribution of dwarfs of given spectral type with metallicity, the observations that established the existence of the classic G-dwarf problem and provided data to determine the age-metallicity relation are relevant. Schmidt (1963) used the correlation between UV excess (U-B) and [Fe/H] (Wallerstein 1962) to determine the metallicity distribution of 56 late-G dwarfs. Ultraviolet excesses were also used by van den Bergh (1962) to determine the metallicity distribution of 142 F7-G9 nearby and high-velocity stars of luminosity class IV-V. Pagel and Patchett (1975) used the UV excess-[Fe/H] correlation to find the metallicity distributions of G2-G8 dwarfs in four samples: Gliese's (1969) *Catalog of Nearby Stars* (61 stars); the RGO catalog (Wooley et al. 1970) of stars within 25 pc (133 stars); Eggen's (1968) G star photometric catalog (62 stars); and the Yale *Catalog of Bright Stars* (Hoffleit 1964, 76 stars). Bond (1970) obtained Stromgren photometric colors of over 290 F5-G5 stars of luminosity class III-V, and utilized the correlation between (v-b)-(b-y) and [Fe/H] to search for very metal deficient stars.

In deriving the disk age-metallicity relation, Twarog (1980a) obtained uvby and Hβ photometry of 1007 A5-G5 southern dwarfs and giants listed in Volume I of the *Michigan Catalog of Spectral Types* (Houk and Cowley 1975), and combined this with the data of Gronbech and Olsen (1976, 1977) for 2742 stars south of declination +10 degrees from the *Catalog of Bright Stars* (Hoffleit 1964), selecting from each data set the F stars. Twarog (1980b) compares the F star metallicity distribution, corrected for stellar evolution, magnitude-limited volume, and scale height effects, to the metallicity distribution derived by Pagel and Patchett (1975) for G stars in the RGO Catalog (Wooley et al. 1970) to derive the history of the star formation rate in the Galactic disk and constrain the slope of the initial mass function.

Twarog (1980a) emphasizes the advantages of uvby plus Hβ photometry over UBV photometry in measuring effective temperatures, metallicity and surface gravity for field stars, as this system has been

designed to minimize interdependence between these quantities. In the UBV system, the effective temperature index B-V must be corrected for metallicity and interstellar reddening. The Δ(U-B) - [Fe/H] relation is a function of B-V of the star, so errors in UBV photometry introduce correlated errors in [Fe/H]. Hβ photometry is preferable to obtain effective temperatures, as it avoids correlations between age and metallicity caused by random errors in b-y, and avoids correcting b-y for metallicity and reddening. No information can be obtained on the absolute magnitude of a star with UBV photometry, forcing reliance on stellar parallax measurements, while the index (u-v)-(v-b) does provide an indication of absolute magnitude. Twarog (1980b), in determining the age-Z relation and metallicity distribution of F stars, also highlights the necessity of correcting samples for stellar evolution and scale height effects, as well as magnitude-limited volume, and spectral type-effective temperature-metallicity relations.

Since our chemical evolution models were not designed specifically to match constraints in the solar neighborhood, but rather to investigate the effects of including certain modifications to simple models, and since the introduction of some effects, e.g., metallicity dependence, changes results by only about 20% while stellar statistics and corrections imply larger uncertainties in the data, it would not be meaningful to quantitatively compare our results to observations. More complete samples and more rigorous corrections are needed to finely bin dwarfs by metallicity and spectral type in order to effectively constrain models, and in particular to test and refine the main-sequence mass loss hypothesis.

E. Conclusions

Simple "closed-box" models of galactic chemical evolution incorporating early main-sequence mass loss by A-F dwarfs produce a deficiency of early-F dwarfs, a very large enhancement (2 to 2.5 x) in the number of late-F dwarfs, for present disk ages 5 and 10 Gyr, the total mass of mid-F dwarfs remaining on the main sequence also

increases by 90 to 120%, and the mass of early-F dwarfs is diminished by 15 to 70% in models with main-sequence mass loss, as many early-F stars evolve down the main sequence to become stars of later spectral type. The results of these simple models regarding the relative numbers of F and G dwarfs and their metallicity distribution are potentially useful in checking the consistency of the main-sequence mass loss hypothesis with observations.

The models also produce a sizable increase (30 to 60%, depending upon current disk age) in the ratio of main-sequence stars to stars plus remnants relative to models without such stellar mass loss. This result is in direct contrast to some models, including bimodal star formation, which would predict decreases in this ratio (i.e., a greater proportion of stellar remnants) compared to models with a monotonic IMF. Observational data verifying these findings would add credibility to the main-sequence mass loss hypothesis.

The star formation rates and stellar yields necessary to normalize models with and without main-sequence mass loss to the same final gas fraction and gas metallicity differ by only about 10%, as the amount of gas involved in the mass loss is a relatively small amount of the total gas processed or locked into stars. In models with main-sequence mass loss, mass-losing stars return unprocessed material on a short timescale, and then lock the remaining mass into long-lived low mass main-sequence stars. Thus models with main-sequence mass loss have a slightly reduced gas metallicity and slightly increased gas fraction midway through the evolution.

The relative numbers, as well as the character of the metallicity distribution of F and G dwarfs could provide information on such parameters as the Galactic disk age, the percentage of A-F stars experiencing main-sequence mass loss, and the upper and lower mass limits for which such mass loss occurs as a function of metallicity. Binning dwarfs according to spectral type or effective temperature as well as metallicity is important for making comparisons to observations, especially in light of the consequences of main-sequence mass loss

which affect F and early-G, but not late-G dwarf distributions.

F. Topics for Further Investigation

Main-sequence mass loss may affect significantly stellar surface abundances, processing, and yields of light elements. The primordial abundances of ^{3}He, D, and Li are important for constraining cosomological models. The surface abundances of ^{3}He and Li in stars that have experienced main-sequence mass loss are not indicative of the initial abundances; mass-losing main sequence stars may also be responsible for production and returns of substantial amounts of ^{3}He to the interstellar medium, and for returns of material depleted in Li and Be (unless such stars also produce Li and Be). It may be interesting to estimate the contribution of mass-losing stars to the yield of ^{3}He, Li and Be, and to model the chemical evolution history of these elements, with the goal of further constraining the history of the star formation rate, initial mass function, and possibly primordial abundances.

V. REFERENCES

Abbott, D. C. 1982, Ap. J., **259**, 282.

Ando, H. 1981, M. N. R. A. S., **197**, 1139.

Anthony-Twarog, B. J., Twarog, B. A., and McClure, R. D. 1979, Ap. J., **233**, 188.

Bahcall, J. N., Huebner, W. F., Lubow, S. H., Parker, P. D., and Ulrich, R. K. 1982, Rev. Mod. Phys., **54**, 767.

Bame, S. J., Asbridge, J. R., Feldman, W. C., and Gosling, J. T. 1977, J. Geophys. Res., **82**, 1487.

Bania, T. M., Rood, R. T., and Wilson, T. L. 1987, Ap. J., **323**, 30.

Barbaro, G. and Pigatto, L. 1984, Astron. Ap., **136**, 355.

Beers, T. C. 1987, Nearly Normal Galaxies: From the Planck Time to the Present, ed. S. M. Faber (New York: Springer-Verlag), 41.

Bethe, H. A. 1986, Phys. Rev. Lett., **56**, 1305.

Black, D. C. 1972, Geochim. Cosmochim. Acta, **36**, 347.

Boesgaard, A. M. 1987a, P. A. S. P., **99**, 1067.

Boesgaard, A. M. 1987b, Ap. J., **321**, 967.

Boesgaard, A. M. 1976, P. A. S. P., **88**, 353.

Boesgaard, A. M. and Lavery, R. J. 1986, Ap. J., **309**, 762.

Boesgaard, A. M. and Steigman, G. 1985, Ann. Rev. Astron. Ap., **23**, 319.

Boesgaard, A. M. and Tripicco, M. J. 1986, Ap. J. (Letters), **302**, L49.

Boesgaard, A. M., and Steigman, G. 1985, Ann. Rev. Astron. Ap., **23**, 319.

Böhm-Vitense, E. 1970, Astron. Ap., **8**, 283.

Bond, H. E. 1970, Astron. Ap. Suppl. Ser., **22**, 117.

Bond, H. E. 1981, Ap. J., **248**, 606.

Bowen, G. H. 1988, "Effects of Main-Sequence Mass Loss on Solar System Evolution", in preparation.

Breger, M. 1982, Ap. J., **263**, 199.

Brown, J. A. 1987, Ap. J., **317**, 701.

Brunish, W. M. and Truran, J. W. 1982, Ap. J. Suppl. Ser., **49**, 447.

Brunish, W. M. and Truran, J. W. 1982, Ap. J., **256**, 247.

Buser, R. and Kurucz, R. L. 1978, Astron. Ap., **70**, 555.

Caffee, M. W., Hohenberg, C. M, Swindle, T. D., and Goswami, J. N. 1987, Ap. J. (Letters), **313**, L31.

Cameron, L. M. 1985, Astron. Ap., **147**, 47.

Cassinelli, J. P. 1979, Ann. Rev. Astron. Ap., **17**, 275.

Chiosi, C. 1980, Astron. Ap., **83**, 206.

Chiosi, C. and Caimmi, R. 1979, Astron. Ap., **80**, 234.

Christensen-Dalsgaard, J., Gough, D., and Toomre, J. 1985, Science, **229**, 923.

Christian, C. A., Heasley, J. N. and Janes, K. A. 1985, Ap. J., **299**, 683.

Ciardullo, R. B. and Demarque, P. 1977, Transactions Yale University Observatory, 33.

Claria´, J. J. and Lapasset, E. 1986, Astron. J., **91**, 326.

Clayton, D. D. 1968, 1983, Principles of Stellar Evolution and Nucleosynthesis (Chicago: University of Chicago Press), 231, 369.

Clayton, D. D. 1985, Nucleosynthesis: Challenges and New Developments, eds. W. D. Arnett and J. W. Truran (Chicago: University of Chicago Press), 65.

Cox, A. N. and Stewart, J. 1970, Ap. J. Suppl. Ser., **19**, 243.

Cox, A. N., Guzik, J. A., and Kidman, R. B. 1988, Ap. J., submitted.

Cox, D. P. and Smith, B. W. 1976, Ap. J., **203**, 361.

Cox, J. and Guili, T. 1968, Principles of Stellar Structure, Vol. II (New York: Gordon and Breach), Sec. 20.5.

Crawford, D. L. and Barnes, J. V. 1969, Astron. J., **74**, 818.

Crawford, D. L. and Perry, C. L. 1966, Astron. J., **71**, 206.

Davis, R., Jr., Cleveland, B. T., and Rowley, J. K. 1983, Science Underground, eds. M. M. Nieto, W. C. Haxton, C. M. Hoffman, E. W. Kolb, V. D. Sandberg, and J. W. Toevs (New York: American Institute of Physics), 2.

Dearborn, D. S. P., Eggleton, P. P. and Schramm, D. N. 1976, Ap. J., **203**, 455.

Dearborn, D. S. P., Marx, G. and Ruff, I. 1987, Prog. Theor. Phys., **77**, 12.

Dearborn, D. S. P., Schramm, D. N. and Steigman, G. 1986, Ap. J., **302**, 35.

Demarque, P. 1980, Star Clusters, ed. J. E. Hesser, (Dordrecht, Holland: Reidel), 281.

Dziembowski, W. 1979, Lecture Notes in Physics, Nonradial and Nonlinear Stellar Pulsation, **125**, 22.

Eddington, A. S. 1924, M. N. R. A. S., **84**, 332.

Eddington, A. S. 1927, Stars and Atoms (New Haven, Connecticut: Yale University Press), 99.

Eggen, O. J. 1968, Ap. J., **152**, 83.

Eggen, O. J. 1969, Ap. J., **155**, 439.

Eggen, O. J. 1981, Ap. J., **247**, 503.

Eggen, O. J. 1982, Ap. J., **50**, 221.

Faulkner, J. and Gilliland, R. L. 1985, Ap. J., **299**, 994.

Ferland, G. J. 1986, Ap. J. (Letters), **310**, L67.

Fesenkov, V. G. 1949, Soviet Astron. J., **26**, 67.

Fesenkov, V. G. and Idlis, G. M. 1958, The Hertzsprung-Russell Diagram, Proceedings of the 10th International Astronomical Union Symposium held in Moscow, U.S.S.R., August 15-16, 1958, ed. J. L. Greenstein (Paris: IAU), 113.

Fowler, W. A., Caughlan, G. R., and Zimmerman, B. A. 1975, Ann. Rev. Astron. Ap., **13**, 69.

Frogel, J. A. and Twarog, B. A. 1983, Ap. J., **274**, 270.

Geiss, J., Buhler, F., Cerutti, H., Eberhardt, P., and Filleux, Ch. 1972, Apollo 16 Prel. Sci. Rep., NASA SP-315.

Gilmore, G. and Wyse, R. F. G. 1986, Nature, **322**, 806.

Gliese, W. 1969, Veroff Astron. Rechen-Inst. Heidelberg, No. 22.

Gliese, W. and Jahreiss, H. 1979, Astron. Ap. Suppl. Ser., **38**, 423.

Gratton, R. G. 1982, Ap. J., **257**, 640.

Grenon, M. 1976, Abundance Effects in Classification, I.A.U. Symposium 72, eds. B. Hauck and P. C. Keenan (Dordrecht, Holland: Reidel), 75.

Gronbech, B. and Olsen, E. H. 1976, Astron. Ap. Suppl. Ser., **25**, 213.

Gronbech, B. and Olsen, E. H. 1977, Astron. Ap. Suppl. Ser., **27**, 443.

Gunn, J. E. and Kraft, R. P. 1963, Ap. J., **137**, 301.

Gusten, R. 1986, Spectral Evolution of Galaxies, eds. C. Chiosi and A. Renzini (Dordrecht, Holland: Reidel), 449.

Gusten, R. and Mezger, P. G. 1983, Vistas Astron., **26**, 159.

Guzik, J. A. and Struck-Marcell, C. 1988, Astron. J., in press.

Guzik, J. A. and Willson, L. A. 1988, "Cluster H-R Diargrams with Main-Sequence Mass Loss", in preparation.

Guzik, J. A., Willson, L. A., and Brunish, W. M. 1987, Ap. J., **319**, 957.

Habets, G. M. H. J. and Heintze, J. R. W. 1981, Astron. Ap. Suppl. Ser., **46**, 193.

Hall, D. N. B. 1975, Ap. J., **197**, 509.

Hawarden, T. G. 1976, M. N. R. A. S., **174**, 471.

Henyey, L. G. 1960, Astron. J., **65**, 528.

Hirshfeld, A., McClure, R. D., and Twarog, B. A. 1978, The HR Diagram, eds. A. G. Davis Philip and D. S. Hayes (Dordrecht, Holland: Reidel), 163.

Hoffleit, D. 1964, Catalog of Bright Stars (New Haven, Connecticut: Yale University Observatory).

Hoffmeister, C., Richter, G., and Wenzel, W. 1985, Variable Stars (New York: Springer-Verlag), 50.

Houk, N. and Cowley, A. P. (1975). Michigan Catalog of Spectral Types, Vol. 1 (Ann Arbor: University of Michigan).

Hua, X.-M. and Lingenfelter, R. E. 1987, Ap. J., **319**, 555.

Hultqvist, L. 1977, Sol. Phys., **52**, 101.

Iben, I., Jr. 1965, Ap. J., **141**, 993.

Iben, I., Jr. 1975, Ap. J., **196**, 525.

Janes, K. A. 1977, Astron. J., **82**, 35.

Janes, K. A. and Smith, G. H. 1984, Astron. J., **89**, 487.

Johnson, H. L. 1966, Ann. Rev. Astron. Ap., **6**, 193.

King, D. J. 1987, Observatory, **107**, 107.

King, I. R. 1980, Star Clusters, ed. J. E. Hesser (Dordrecht, Holland: Reidel), 139.

Krat, V. 1958, The Hertzsprung-Russell Diagram, Proceedings of the 10th International Astronomical Union Symposium held in Moscow, U.S.S.R., August 15-16, 1958, ed. J. L. Greenstein (Paris: IAU), 121.

Kuijken, K. H. and Gilmore, G. 1988, Bull. A. A. S., **19**, 1108.

Kunth, D. and Sargent, W. L. W. 1983, Ap. J., **273**, 81.

Lacey, C. G. and Fall, S. M. 1983, M. N. R. A. S., **204**, 791.

Lambert, D. L. and Ries, L. M. 1981, Ap. J., **248**, 228.

Larson, R. B. 1986, M. N. R. A. S., **218**, 409.

Lattanzio, J. 1984, M. N. R. A. S., **207**, 309.

Lee, U. and Saio, H. 1986, M. N. R. A. S., **221**, 365.

Lequeux, J., Peimbert, M., Rayo, J. F., Serrano, A., and Torres-Peimbert, S. 1979, Astron. Ap., **80**, 155.

Lynden-Bell, D. 1975, Vistas Astron., **19**, 299.

Maeder, A. 1974, Astron. Ap., **32**, 177.

Maeder, A. 1981, Astron. Ap., **101**, 385.

Masevich, A. G. 1958, The Hertzsprung-Russell Diagram, Proceedings of the 10th International Astronomical Union Symposium held in Moscow, U.S.S.R., August 15-16, 1958, ed. J. L. Greenstein (Paris: IAU), 89.

Mathieu, R. D. and Latham, D. W. 1986, Astron. J., **92**, 1364.

McClure, R. D. 1974, Ap. J., **194**, 355.

McClure, R. D. and Twarog, B. A. 1977, Ap. J., **214**, 111.

McClure, R. D., Forrester, W. T. and Gibson, J. 1974, Ap. J., **189**, 409.

McClure, R. D., Newell, B., and Barnes, J. V. 1978, P. A. S. P., **90**, 170.

McClure, R. D., Twarog, B. A., and Forrester, W. T. 1981, Ap. J., **243**, 841.

Mermilliod, J.-C. 1982, Astron. Ap., **109**, 37.

Michaud, G. 1986, Ap. J., **302**, 650.

Mohan, V. and Sagar, R. 1985, M. N. R. A. S., **213**, 337.

Mustel, E. R. 1958, The Hertzsprung-Russell Diagram, Proceedings of the 10th International Astronomical Union Symposium held in Moscow, U.S.S.R., August 15-16, 1958, ed. J. L. Greenstein (Paris: IAU), 125.

Nissen, P. E. 1984, Observational Tests of the Stellar Evolution Theory, eds. A. Maeder and A. Renzini (Dordrecht, Holland: Reidel), 95.

Nissen, P. E., Twarog, B. A., and Crawford, D. L. 1987, Astron. J., **93**, 634.

Norris, J. and Smith, G. H. 1985, Astron. J., **90**, 2526.

Oort, J. H. 1970, Astron. Ap., **7**, 381.

Osaki, Y. 1974, Ap. J., **189**, 469.

Pagel, B. E. J. 1986, Cosmogonical Processes, eds. W. D. Arnett, C. J. Hansen, J. W. Truran, and S. Tsuruta (Utrecht, Holland: NU Science Press), 66.

Pagel, B. E. J. and Patchett, B. E. 1975, M. N. R. A. S., **172**, 13.

Peimbert, M. 1983, ESO Workshop on Primordial Helium, eds. P. A. Shaver, D. Kunth, and K. Kjar (Garching, West Germany: ESO), 267.

Peterson, R. C., Carney, B. W., and Latham, D. W. 1984, Ap. J., **279**, 237.

Pilachowski, C. A. 1984, Bull. A. A. S., **16**, 997.

Pilachowski, C. A. and Hobbs, L. M. 1988, P.A.S.P., **100**, 336.

Pilachowski, C. A., Booth, J., and Hobbs, L. M. 1987, P. A. S. P., **99**, 1288.

Pilachowski, C. A., Mould, J. R., and Siegel, M. J. 1984, Ap. J. (Letters), **282**, L17.

Popper, D. M. 1980, Ann Rev. Astron. Ap., **18**, 115.

Ramaty, R. 1986, Physics of the Sun, Vol. II, ed. P. A. Sturrock (Dordrecht, Holland: Reidel), 291.

Rana, N. C. and Wilkinson, D. A. 1986, M. N. R. A. S., **218**, 497.

Rood, R. T., Bania, T. M., and Wilson, T. L. 1984, Ap. J., **280**, 629.

Rood, R. T., Steigman, G., and Tinsley, B. M. 1976, Ap. J. (Letters), **207**, L57.

Rosen, S. P. and Gelb, J. M. 1986, Phys. Rev., **D34**, 969.

Rosner, R., Golub, L., and Vaiana, G. S. 1985, Ann. Rev. Astron. Ap., **23**, 413.

Ross, J. E. and Aller, L. H. 1976, Science, **191**, 1223.

Russell, H. N. 1914, Popular Astronomy, **22**, 342.

Ryter, C., Reeves, H., Gradsztajn, E., and Audouze, J. 1970, Astron. Ap., **8**, 389.

Saio, H. and Wheeler, J. C. 1980, Ap. J., **242**, 1176.

Salpeter, E. E. 1955, Ap. J., **121**, 161.

Scalo, J. M. 1986, Fund. Cosmic Phys., **11**, 1.

Scalo, J. M. 1988, Evolution of Galaxies, Proceedings of the 10th IAU Regional Astronomy Meeting, Prague, August 24-29th, 1987, Vol. 4 (Dordrecht, Holland: Reidel), in press.

Scalo, J. M. 1988, Starbursts and Galaxy Evolution, ed. T. Montmerle (Paris: Editions Frontieres), in press.

Scalo, J. M. and Miller, G. E. 1978, Ap. J., **225**, 523.

Schmidt, M. 1963, Ap. J., **137**, 758.

Severnyi, A. B. 1954, Soviet Astron. J., **31**, 362.

Shapiro, S. L. and Teukolsky, S. A. 1983, Black Holes, White Dwarfs, and Neutron Stars (New York: John Wiley and Sons), 82.

Shklovskii, I. K. 1970, 1984, Stars: Their Birth, Life, and Death (Moscow: Nauka), 166.

Sneden, C. and Pilachowski, C. A. 1986, Ap. J., **301**, 860.

Sneden, C., Pilachowski, C. A., and VandenBerg, D. A. 1986, Ap. J., **311**, 826.

Soderblom, D. R. 1983, Ap. J. Suppl. Ser., **53**, 1.

Stellingwerf, R. F. 1979, Lecture Notes in Physics, Nonradial and Nonlinear Stellar Pulsation, **125**, 50-54.

Stothers, R. 1966, M. N. R. A. S., **131**, 253.

Struve, O. and Zebergs, V. 1962, Astronomy of the 20th Century (New York: Macmillan), 258.

Stryker, L. L. and Hrivnak, B. J. 1984, Ap. J., **278**, 215.

Tinsley, B. M. 1980, Fund. Cosmic Phys., **5**, 287.

Twarog, B. A. 1978, Ap. J., **220**, 890.

Twarog, B. A. 1980a, Ap. J. Suppl. Ser., **44**, 1.

Twarog, B. A. 1980b, Ap. J., **242**, 242.

Twarog, B. A. 1983, Ap. J., **267**, 207.

Twarog, B. A. 1985, The Milky Way Galaxy, IAU Symp. No. 106, eds. H. van Woerden, R. J. Allen, and W. B. Burton (Dordrecht, Holland: Reidel), 587.

Twarog, B. A. and Tyson, N. 1985, Astron. J., **90**, 1247.

Usher, P. D. 1963, Observatory, **83**, 184.

Vader, J. P. and de Jong, T. 1981, Astron. Ap., **100**, 124.

van 't Veer, F. 1984, Astron. Ap., **139**, 477.

van den Bergh, S. 1962, Astron. J., **67**, 486.

VandenBerg, D. A. 1983, Ap. J. Suppl. Ser., **51**, 29.

VandenBerg, D. A. 1985, Ap. J. Suppl. Ser., **58**, 711.

VandenBerg, D. A. and Bridges, T. J. 1984, Ap. J., **278**, 679.

Wallerstein, G. 1962, Ap. J. Suppl. Ser., **6**, 407.

Weymann, R. 1963, Ann. Rev. Astron. Ap., **1**, 97.

Willson, L. A., Bowen, G. H., and Struck-Marcell, C. 1987, Comm. Ap., **12**, 17 (WBS).

Willson, L. A., Bowen, G. H., and Titus, T. 1988, "The Gap in the Main-Sequence Mass Function at the Instability Strip", in preparation.

Willson, L. A. and Guzik, J. A. 1988, Bull. A. A. S., **19**, 1022.

Wooley, Sir Richard, Epps, E. A., Penston, M. J., and Pocock, S. B. 1970, Roy. Obs. Ann., No. 5.

Wyse, R. F. G. and Silk, J. 1987, Ap. J. (Letters), **313**, L11.

VI. ACKNOWLEDGEMENTS

I would first like to thank my thesis co-advisors, Dr. Lee Anne Willson and Dr. Curtis Struck-Marcell, who, beyond conscientiously executing their duties as advisors–offering their experience and wisdom concerning directions for my research, reading manuscripts, and writing numerous letters of recommendation, also were excellent role models for interaction in the scientific community and opened doors for new opportunities.

My path toward obtaining a Ph. D. would not have been so smooth without the many people who provided words of encouragement at critical times, most notably Dr. John Basart, Dr. Willet Beavers, Dr. William Kernan, and especially Dr. George Bowen. Discussions with Dr Bowen on solar modeling, and his efforts in writing numerous letters of recommendation are also very much appreciated.

My fiancé Thomas Beach deserves much credit for my accomplishments during the past several years. His support went beyond listening and encouragement, and even beyond addressing specific questions or problems for which I requested his expertise. He was constantly anticipating future problems and needs, and found countless practical ways to improve my efficiency. Tom's high standards of quality, and his perseverance are always an inspiration.

The contagious enthusiasm of David Oesper and other members of the Ames Area Amateur Astronomers was also much appreciated, and helped me to recall my childhood fascination with astronomy. From AAAA members, I acquired much of the basic astronomy knowledge that I had missed by not taking undergraduate astronomy courses.

I would like also to acknowledge my former office-mate John Wallin for his encouragement, perspective, worthwhile discussions, help with submitting this thesis and making graduation deadlines, and especially for his friendship.

The ducks and swans in Lake Laverne on the ISU campus provided welcome diversion, and many hours of entertainment.

The pace of my life would have been much more hectic without research support from the Boeing Corporation for the 1985-86 academic year, ZONTA International Amelia Earhart Fellowships for the 1986-87 and 1987-88 academic years, and additional research support from the ISU Department of Physics. Funds from NASA Astrophysics Theory Program arrived just in time to supplement thesis reproduction costs.

The stellar evolution modeling, i. e., the majority of the work for this thesis, would have been impossible without the computer code and patient, cheerful guidance of Dr. Wendee Brunish at Los Alamos National Laboratory. Many others at Los Alamos provided valuable assistance, especially Dr. Stephen Becker, Dr. Arthur Cox, and Dr. Russell Kidman. I am particularly grateful for the resources that made the stellar evolution modeling possible–extensive Cray time provided by X-Division, and funding for visits, arranged by Dr. Jack Hills, under the X- and T-Division visitors program. I also enjoyed immensely, and gained much-needed experience, working under Dr. Becker (X-2) and Dr. Cox (T-6) as a Graduate Research Assistant during the summer of 1987.